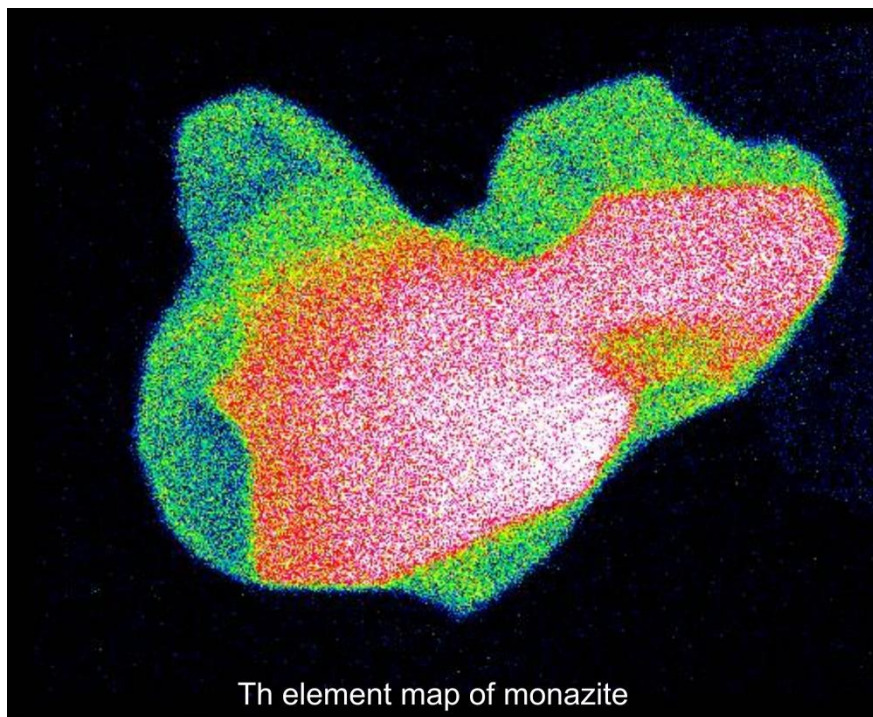


Master Thesis, Department of Geosciences

Sveconorwegian magmatic and metamorphic evolution of southwestern Norway

Ingjerd Ulsaker Høy



50 μm



UNIVERSITY OF OSLO

FACULTY OF MATHEMATICS AND NATURAL SCIENCES

Sveconorwegian magmatic and metamorphic evolution of southwestern Norway

Ingjerd Ulsaker Høy



Master Thesis in Geosciences

Discipline: Geology

Department of Geosciences

Faculty of Mathematics and Natural Sciences

University of Oslo

June 2016

© Ingjerd Ulsaker Høy, 2016

Supervisors: Dr. Trond Slagstad and Prof. Alvar Braathen

This work is published digitally through DUO – Digitale Utgivelser ved UiO

<http://www.duo.uio.no>

It is also catalogued in BIBSYS (<http://www.bibsys.no/english>)

All rights reserved. No part of this publication may be reproduced or transmitted, in any form or by any means, without permission.

Front page: *Th element map of monazite. Monazite was mounted in epoxy and polished to reveal domains in the crystal before a chemical map were produced using a scanning electron microscope (SEM). White indicates high Th concentrations and blue low Th concentrations.*

Abstract

The tectonic evolution of the Late Mesoproterozoic Sveconorwegian Province has traditionally been considered to reflect continent-continent collision, which has been correlated with the Grenville Province in Canada. The metamorphic evolution of southwestern Norway has been described as a regional high-grade metamorphic event that took place between 1035 and 970 Ma, as a result of orogenic thickening, followed by a contact-metamorphic event at c. 930 Ma due to the emplacement of the Rogaland Igneous Complex (RIC). The continent-continent collision model has, however, been questioned based on extensive mapping and new geochronology data from the Sveconorwegian Province. A long-lived accretionary margin, undergoing periodic compression and extension has recently been suggested to better explain the metamorphic and magmatic evolution of the Sveconorwegian Province.

This study evaluates the two tectonic models for the Sveconorwegian Province by detailed geological mapping and U-Pb geochronology from Lysefjorden, Gyadalen and the Kvås-Konsmo area. Undeformed to weakly deformed porphyritic granites and metamorphosed diorites display zircon ages ranging from c. 1050 Ma to 1030 Ma. These ages are compatible with the previously recorded magmatic activity in the Sirdal Magmatic Belt (SMB). The SMB is a recently discovered granitic batholith (c. 1060-1020 Ma). In this study a diorite from the Kvås-Konsmo area was analysed and yield a crystallization age of 991 ± 11 Ma, which is younger than the SMB. Zircon geochronological data from Lysefjorden, Gyadalen and the Kvås-Konsmo area indicate that partial melting and metamorphism was coeval with and possibly related to the emplacement of the SMB. Monazite ages from the Kvås metapelite range from c. 980 to 900 Ma, and it is suggested that these ages reflect heating related to long-lived voluminous magmatism.

In light of the new field and geochronological data it appears that the metamorphic and magmatic evolution of southwestern Norway cannot satisfactorily be explained by crustal thickening and radioactive self-heating as previously suggested. It is therefore proposed that the zircon and monazite ages are a result of magmatically driven UH/UHT metamorphism. And it is proposed that voluminous basaltic underplating can have contributed to the heat that was necessary to cause high-grade metamorphism reflecting long-lived arc magmatism. To be able to explain different pressure estimates in the region, a dome structure formed under the orogen is suggested. The RIC may have formed the core of this dome structure.

Sammendrag

Den tektoniske utviklingen av den senmesoproterozoiske Svekonorvegiske Provinsen har tradisjonelt blitt tolket til å reflektere en kontinent-kontinent kollisjon som har blitt korrelert med Grenvilleprovinsen i Canada. Den metamorfe utviklingen av sørvest Norge har blitt beskrevet som en regional høy-grads metamorfose som foregikk mellom 1035 og 970 Ma, som et resultat av skorpefortykning, etterfulgt av kontaktmetamorfose rundt ca. 930 Ma relatert til intrusjonen av Rogaland Igneous Complex (RIC). Det har imidlertid blitt satt spørsmålstegn med kontinent-kontinent kollisjons-modellen basert på omfattende kartlegging og nye geokronologiske data fra den Svekonorvegiske Provinsen. En langlevd akkresjonsmargin som har gjennomgått perioder med kompresjon og ekstensjon har blitt foreslått for å bedre kunne forklare den metamorfe og magmatiske utviklingen av den Svekonorvegiske Provinsen.

Dette studiet evaluerer de to ulike tektoniske modellene for den Svekonorvegiske Provinsen ved detaljert geologisk kartlegging og U-Pb geokronologi fra Lysefjorden, Gyadalen og Kvås-Konsmo området. Udeformert til svakt deformert porfyrittisk granitt og metamorfosert dioritt viser zirkonaldre som strekker seg fra ca. 1050 Ma til 1030 Ma. Disse aldrene er kompatible med tidligere registrert magmatisk aktivitet i Sirdalbeltet. Sirdalbeltet er en nylig oppdaget granittisk batolitt (ca. 1060-1020 Ma). I dette studiet ble en dioritt fra Kvås-Konsmo området analysert og gav en krystallisasjonsalder på 991 ± 11 Ma, altså yngre enn Sirdalbeltet. Zirkondata fra Lysefjorden, Gyadalen og Kvås-Konsmo området indikerer at partiell oppsmelting og metamorfose kan korreleres med intrusjonen av Sirdalbeltet. Monazittaldre fra Kvås-metapelitten strekker seg fra ca. 980 til 900 Ma, og det er foreslått at disse aldrene representerer en langvarig voluminøs magmatisme.

I lys av nye felt- og geokronologiske data, ser det ut til at den metamorfe og den magmatiske utviklingen av sørvest Norge ikke tilfredsstillende kan forklares med skorpefortykning og radioaktiv selvoppvarming som det tidligere er foreslått. Det er derfor foreslått at zirkon- og monazittaldrene er et resultat av en magmatisk drevet UH/UHT metamorfose. Det er foreslått at voluminøs basaltisk underplating kan ha bidratt til den varmen som var nødvendig for å forårsake høy-grads metamorfose som følge av en langvarig arc magmatisme. For å kunne forklare de ulike trykkestimatene i regionen, har en domestruktur som ble dannet under orogenet blitt foreslått. RIC kan ha dannet kjernen til denne domestrukturen.

Acknowledgements

This thesis is a part of my Master of Science degree in Geology at the Department of Geosciences at the University of Oslo (UIO). It was mainly carried out at the Geological Survey of Norway (NGU) and field- and labwork resulting in this thesis were financed by NGU. Dr. Trond Slagstad (NGU) and Professor Alvar Braathen (UIO) have been the supervisors for this project. I will thank them both for all help and support and for giving me the opportunity to work on this project.

In addition, I will especially thank my main supervisor, Trond Slagstad, for his support, help, feedbacks, never ending patience and for always leaving the door open for questions and discussions for whenever needed.

A big thanks also goes to Nolvann Coint (NGU) and Iain Henderson (NGU) for good advice during fieldwork, for feedbacks and for always lending an ear for questions and discussions whenever needed.

I also want to thank Marianne Floen Stange (NTNU) for good company during our field work in Vest-Agder, and Anette Utgård Granseth (NTNU) for good discussions and feedbacks during the writing of this thesis.

A big thanks also goes to the Mineral Resources group at NGU for having warmly greeted me at NGU. I would also like to thank Benjamin Berge (NGU) and Bengt Johansen (NGU) for preparing thin sections, Øyvind Skår (NGU) and Torkil Røhr (NGU) for helping with the LA-ICP-MS.

Furthermore, I would like to thank my fellow students at NTNU, UNIS and UIO. My five years as a student would not have been the same without you. And finally, I want to thank my family and friends for their never-ending encouragement and support through all those years with hard work.

Ingjerd Ulsaker Høy

Trondheim, May 2016

Table of contents

Abstract.....	I
Sammendrag	II
Acknowledgements	III
Table of contents	IV
List of figures and tables	VII
Abbreviations	IX
1 Introduction.....	1
1.1 Background and aims of the study.....	1
1.2 Description of the study area	2
2 Regional geology.....	4
2.1 Geological setting	4
2.1.1 A four-phase model.....	8
2.1.2 Metamorphism in the Rogaland-Vest Agder Sector	11
2.1.3 Continent-continent collision or a long lived accretionary margin?	11
3 Theory	15
3.1 Uranium-lead geochronology.....	15
3.1.1 U-Th-Pb.....	15
3.1.2 U-Pb Concordia Plots.....	16
3.1.3 Zircon	18
3.1.4 Monazite.....	19
3.2 U-Th-Pb dating methods	19
3.2.1 ID-TIMS	20
3.2.2 SIMS.....	21
3.2.3 LA-ICP-MS	21
3.3 Correction methods.....	23
3.3.1 Data reduction.....	23
3.3.2 Common lead corrections	23
4 Methods	24
4.1 Fieldwork.....	24

4.2 Sample preparation	24
4.2.1 Thin section	24
4.2.2 Mineral separation	24
4.2.3 Scanning Electron Microscope	25
4.3 Geochronological analysis	25
4.3.1 LA-ICP-MS	25
5 Results	27
5.1 Field observations (Kvås-Konsmo)	28
5.1.1 Porphyritic biotite granite	31
5.1.2 Xenolith-rich zone	33
5.1.3 Hornblende biotite granite (HBG)	38
5.2 Zircon geochronology	39
5.2.1 Granites, diorite and amphibolite	39
5.2.2 Migmatites	52
5.2.3 Metapelites	56
5.3 Monazite geochronology	60
5.3.1 IH128061 (metapelite, Kvås)	60
5.3.2 ROG092322 (foliated granitic gneiss, Lysefjorden)	61
5.4 Structures	69
5.4.1 Foliation, lineation and folding	69
5.4.2 Hellevatn outcrop	70
6 Discussion	73
6.1 Magmatic evolution of southwestern Norway	73
6.2 Metamorphic evolution of southwestern Norway	74
6.2.1 Regional high grade metamorphism?	74
6.2.2 1065-1030 Ma (underplating, mafic magmatism, SMB and metamorphism)	75
6.2.3 1000 Ma – 900 Ma (metamorphism and magmatism)	79
6.2.4 Interpretation of the U-Pb geochronology of monazite	80
6.3 Regional variation in metamorphic grade	82
6.4 Structures	83
6.5 Continent-continent collision or a long lived accretionary margin?	86
7 Conclusions	88
8 Further research	89
9 References	90

Appendix	96
Appendix A – Samples	97
Appendix B – Zircon geochronological data	98
Appendix C – Monazite geochronological data.....	116

List of figures and tables

Figures

1.1	Geological map over southwestern Norway with important locations	3
2.1	Precambrian domains within Fennoscandia	5
2.2	Map over southwestern Scandinavia	5
2.3	Geological map over southern Norway	6
2.4	Sketchmap showing metamorphism and magmatism in the Sveconorwegian orogeny	10
2.5	Schematic illustration for the Sveconorwegian evolution	14
3.1	Decay chains for U and Th	16
3.2	Concordia diagrams	17
3.3	Instrument illustration	20
3.4	SIMS	21
3.5	LA-ICP-MS	22
5.1	Geological map over southwestern Norway	29
5.2	Geological map over the Kvås-Konsmo area	30
5.3	Field photographs of granites	32
5.4	Photomicrographs of granites	33
5.5	Field photographs of migmatites	34
5.6	Field photographs of metapelite	35
5.7	Flaser gneiss photographs	36
5.8	Field photographs of amphibolites	37
5.9	Field photographs of HBG	38
5.10	Template of zircon description	39
5.11	Sample IH128056	40
5.12	Sample Ih128058	42
5.13	Sample IH128068	43
5.14	Sample IH128070	45
5.15	Sample IH128074	46
5.16	Sample VAG084396	49
5.17	Sample VAG084397	50
5.18	Sample VAG084399	51
5.19	Sample IH128065 A and B	54
5.20	Sample IH128072	55
5.21	Sample IH128061	58
5.22	Sample ROG092326	59
5.23	Element maps of monazite	63
5.24	Sample IH128061, mnz	64
5.25	Sample IH128061, mnz	65

5.26	Summary mnz IH128061	66
5.27	Summary mnz ROG092322	67
5.28	Sample ROG092322	68
5.29	Field photographs of folding in the Kvås-Konsmo area	70
5.30	Hellevatn outcrop	71
5.31	Stereonet	71
5.32	Hellevatn outcrop observations	72
5.33	Tectonic evolution of the Hellevatn outcrop	72
6.1	Schematic cross section for the Gyadalen transect	77
6.2	Summary of magmatic and metamorphic geochronology data	78
6.3	Schematic emplacement model of the Sirdal Magmatic Belt	85
6.4	Illustration of the geological evolution of the Knaben zone	85
6.5	Schematic illustration of magmatic processes in southwestern Norway	87

Tables

5.1	Mineral abbreviations	27
5.2	Geochronological summary of the analysed samples	28

Abbreviations

BKSK	Bjerkreim-Sokndal Layered Intrusion
BSE	Backscatter electron image
CL	Cathodoluminescent image
HAOM	High-alumina orthopyroxene megacryst
HBG	Hornblende biotite granite
ID-TIMS	Isotope Dilution Thermal Ionization Mass Spectrometry
LA-ICP-MS	Laser Ablation Inductively Coupled Plasma Mass Spectrometer
LREE	Light rare earth element
MZ	Mylonite Zone
NGU	Norges Geologiske Undersøkelse (Norwegian geological Survey)
PZ	Protogine Zone
RIC	Rogaland Igneous Complex
SEM	Scanning Electron Microscope
SFDZ	Sveconorwegian Frontal Deformation Zone
SIMS	Secondary Ion Mass Spectrometry
SMB	Sirdal Magmatic Belt (Sirdalbeltet)
SSD	Southwest Scandinavian Domain
TIB	Transscandinavian Igneous Belt

1 Introduction

1.1 Background and aims of the study

This thesis is essentially a regional geological study, one that aims to gain a better understanding of the metamorphic and the magmatic evolution of southwestern Norway. Geological mapping and U-Pb geochronology forms the basis of this study. Data were collected from Lysefjorden, Gyadalen and the Kvås-Konsmo area (**Figure 1.1**). An approximately 50 km² area in the Kvås-Konsmo area was mapped and samples were taken. Samples from Lysefjorden and Gyadalen were also analysed to be able to compare the result on a regional scale. The samples were analysed using a Laser Ablation Inductively Plasma Coupled Mass Spectrometer (LA-ICP-MS) at the Geological Survey of Norway (NGU) to constrain the timing of metamorphism and magmatism.

The tectonic evolution of the Sveconorwegian Province is debated but has traditionally been considered to reflect a continent-continent collision which has been linked to the Grenville Province in Canada. The metamorphic evolution of southwestern Norway has been described as a regional high-grade metamorphic event that took place between 1035 and 970 Ma which was followed by a contact-metamorphic event at ca. 930 Ma due to the emplacement of the Rogaland Igneous Complex (**Bingen et al., 2008b**). The continent-continent collision model has, however, been questioned (e.g., **Coint et al., 2015; Slagstad et al., 2013a**) based on extensive mapping, new observations and new geochronology data from the Sveconorwegian Province. **Slagstad et al. (2013a)** argues that the observed geological features are incompatible with processes related to a continent-continent collision and require that the southwestern Baltican margin remained active throughout the Sveconorwegian orogeny. They therefore suggest that a long-lived accretionary margin, undergoing periodic compression and extension could better explain the metamorphic and magmatic evolution of the Sveconorwegian Province.

This thesis evaluates the two different models for forming the Sveconorwegian Province. The aim of the fieldwork is to obtain field- and geochronological data which can test these two models. Geological mapping has been important to be able to get a good understanding of the field relationships when interpreting the geochronology data. If southwestern Norway was formed by a continent-continent collision it would be expected to find regional metamorphism due to crustal thickening and radioactive self-heating. If southwestern Norway was formed by

a long-lived accretionary margin the metamorphism could potentially be magmatically driven and it would be expected to find intrusive contacts and a link between the geochronology of the metamorphism and the magmatism.

This study provides new geochronology- and field data which contribute to the discussion of the metamorphic and magmatic evolution of southwestern Norway and the results can be of potential value for future research and understanding of the Sveconorwegian orogeny.

1.2 Description of the study area

The study area is located in the southernmost part of the Sveconorwegian Province, in the Rogaland Vest-Agder Sector. The study area is situated inside and outside the Sirdal Magmatic Belt (SMB) which is a recently discovered granitic batholith (**Slagstad et al., 2013a**). Fieldwork was carried out in an approximately 50 km² area located between two small villages called Kvås and Konsmo, which is situated on the Municipal boundary between Lyngdal, Hægebostad and Audnedal in the Vest-Agder County. Lysefjorden and Gyadalen are located in the Rogaland County, west for the Sirdal Magmatic Belt. Gyadalen is a valley stretching from Helleland to Tonstad (**Figure 1.1**) while Lysefjorden is a fjord stretching east-west from Forsand to Lysebotn (**Figure 1.1**).

The landscape between Kvås and Konsmo is dominated by forests, marshes, lakes and small hills. The outcrops are good near the lakes and in the road cuts, but in the forest they are covered with mosses and lichens making the observations difficult. The water level in Sundsvatnet is low making it a good place for observing different rock types. Some places the granitic landscape was too steep to map.

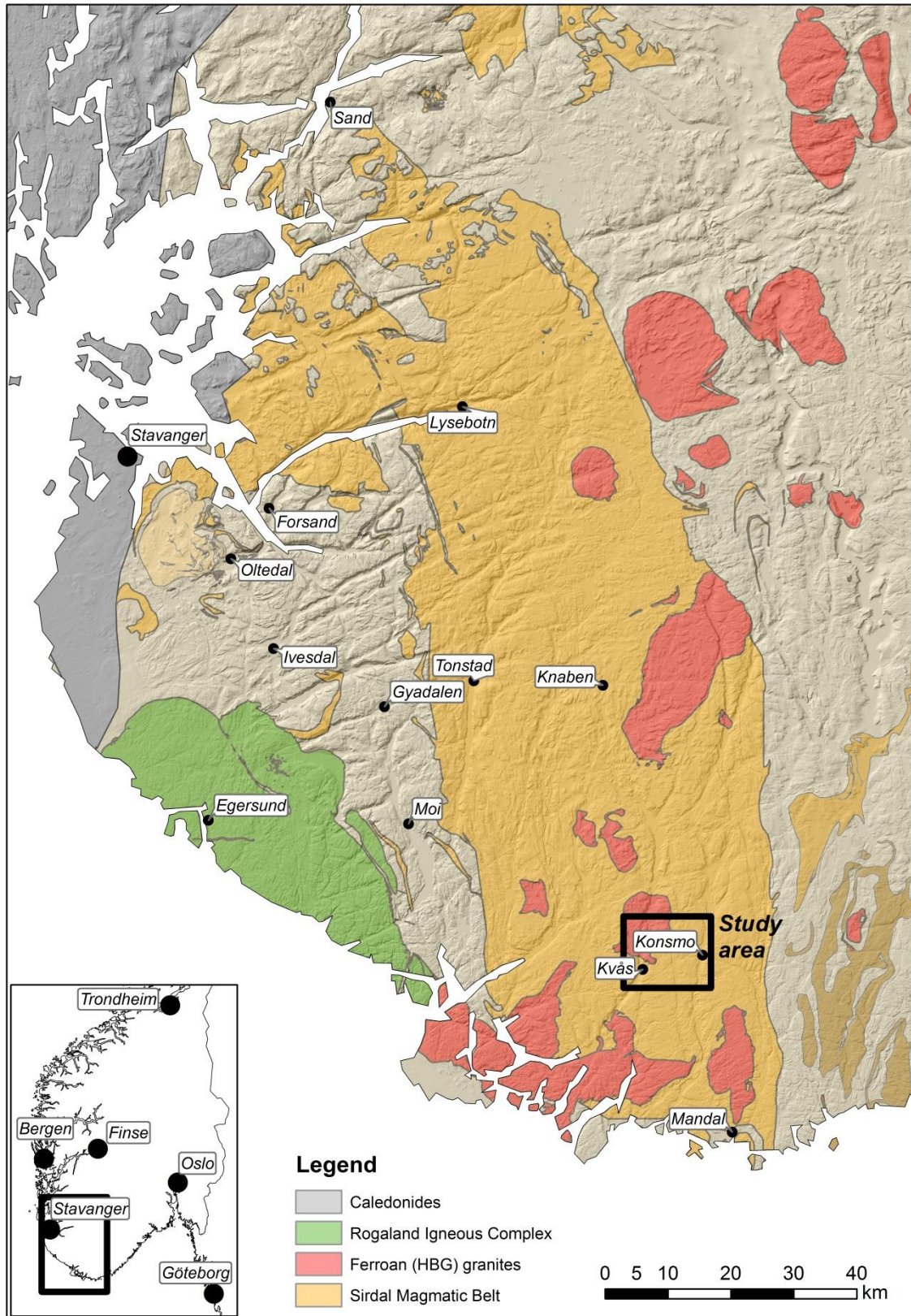


Figure 1.1: Simplified geological map of southwestern Norway. The square marks the study area where detailed geological mapping was carried out. Important localities are also marked on the map.

2 Regional geology

2.1 Geological setting

The Sveconorwegian Province is situated along the western margin of Fennoscandia (Fennoscandian Shield) (**Gorbatshev and Bogdanova, 1993**). Fennoscandia represents the northwestern part of Baltica and is divided into several domains (**Figure 2.1**); Archaean cratonic fragments in the northeast, Svecofennian, Transscandinavian Igneous Belt (TIB) and the Southwest Scandinavian Domain (SSD). Svecofennian generally refers to the 2.0-1.8 Ga Svecofennian orogenic period of continental growth and accretion within Fennoscandia (**Roberts and Slagstad, 2015**). The TIB is a series of batholiths that extend from the northwestern Norwegian coast, through central Sweden to the southeastern Swedish coastline. The batholiths mainly consist of coarse monzodiorites to granites with an alkali-calcic signature which formed between 1850 and 1660 Ma. The formation of the TIB has been widely debated, but most of the models involve a convergent margin (**Högdahl et al., 2004; Roberts and Slagstad, 2015**). The SSD comprises southern Norway and southwestern Sweden and is separated from the Svecofennian domain by the TIB, the Caledonian nappes and two Sveconorwegian shear zones; the Protogine Zone (PZ) and the Sveconorwegian Frontal Deformation Zone (SFDZ) (**Figure 2.2, 2.3**). The PZ marks the boundary between reworked (Eastern Segment) and relatively undeformed TIB crust (**Roberts and Slagstad, 2015**). The SFDZ marks the easternmost limit of Sveconorwegian deformation along discrete shear zones (**Bingen et al., 2008b**). At the end of the Mesoproterozoic, most of the geology of the SSD was reworked during the Sveconorwegian orogeny (1.1-0.9 Ga), producing the c. 600 km wide Sveconorwegian orogenic belt (**Bingen et al., 2008**). The protoliths were most likely from Gothian (i.e. 1.75-1.5 Ga) and/or Mesoproterozoic time (**Andersen, 2005; and references therein**).

At present the subdivision of the SSD is not consistent and varies from author to author. **Bingen et al. (2008a)** divide the Sveconorwegian Belt southeast of the Caledonian front into five units that are separated by crustal scale shear zones. These are the Eastern Segment, Idefjorden, Kongsberg, Bamble and Telemarkia Terranes. The use of the term terrane is also controversial. According to **Andersen (2005)** a terrane is a *“fault-bounded crustal blocks which have distinct lithologic and stratigraphic successions and which have geologic histories different from neighbouring terranes”*. Andersen points out that the knowledge is

insufficient at the present stage to use the term “terrane”, he therefore suggests to use a non-genetic nomenclature such as “blocks” instead.

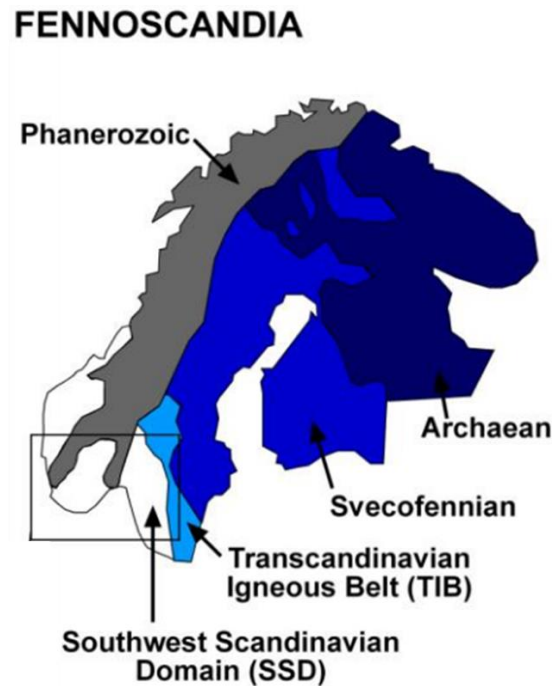


Figure 2.1: Precambrian domains within Fennoscandia. Map from: **Roberts (2010)**.

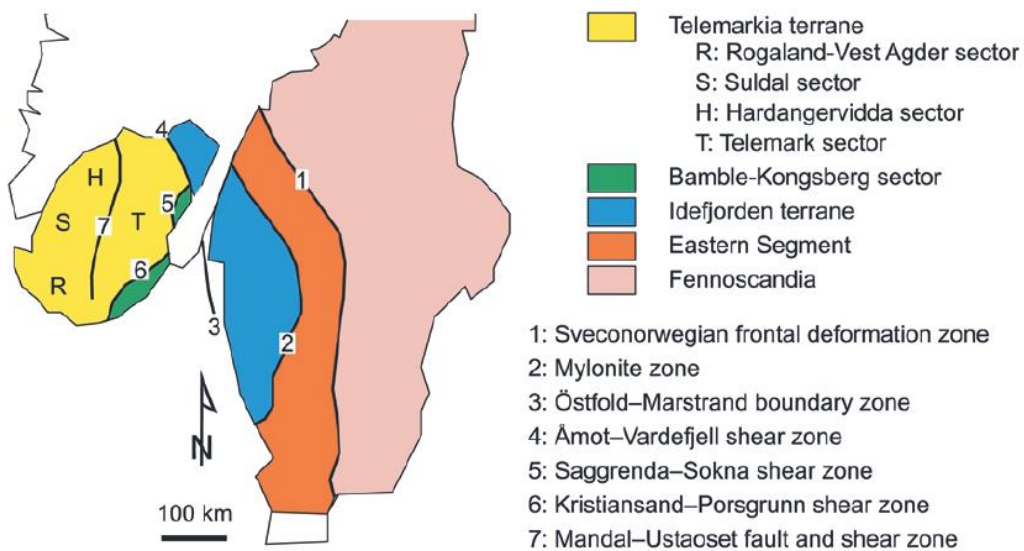


Figure 2.2: Map of southwestern Scandinavia showing the Sveconorwegian lithotectonic domains and shear zones Map from: **Bingen et al. (2005)**.

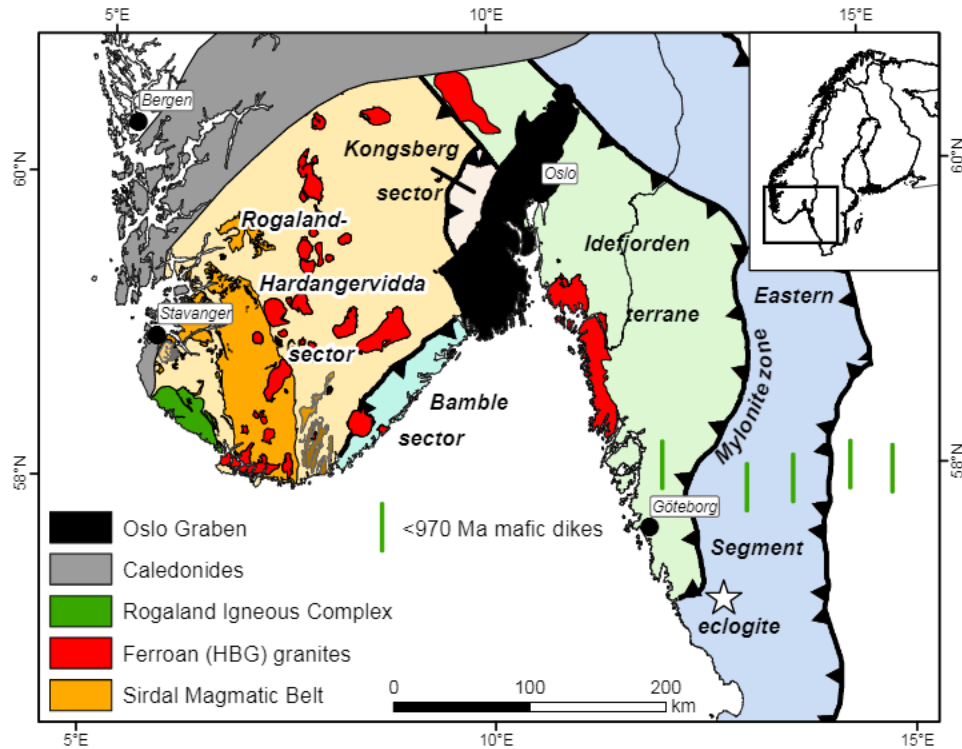


Figure 2.3: Geologic map over southern Norway. Here the Telemark, Hardangervidda, Suldal and Rogaland-Vest Agder sectors have been merged into Rogaland-Hardangervidda sector. Map from: *Slagstad & Roberts, unpublished*.

The Eastern Segment lies to the west of the TIB and is a 50-100 km wide belt that mainly consists of 1.80-1.64 Ga granitic gneisses with a high-pressure metamorphic overprint, which has been dated to 0.97 Ga (Möller, 1998; Möller et al., 2015). The granitic gneisses are intruded by 1560 Ma mafic dykes, 1460-1380 Ma granitic dykes and plutons and 1250-1200 Ma granite plutons (Söderlund et al., 2002). The granitic gneisses can be traced eastward across the SFDZ into the TIB and are also similar in composition to the TIB rocks, they are therefore considered to be an extension of the TIB which was reworked prior to and during the Sveconorwegian orogeny (Bingen et al., 2008b; Möller, 1998). Eclogite-facies metamorphism is found south of Lake Vänern. Zircon inclusions in an eclogite-facies garnet give an age of 972 ± 14 Ma and is considered as the best estimate of the maximum age of the eclogitization (Johansson et al., 2001).

To the west of the Eastern Segment lies the Idefjorden Terrane which comprises greenschist- to amphibolite-facies tholeiitic to calc-alkaline magmatic suites and metagreywacke sequences (1660-1520 Ma). The lithologies show a younging trend towards the west (Bingen

et al., 2005; and references therein). Separating the Eastern Segment from the overlying Idefjorden Terrane is the Mylonite Zone (MZ). The Mylonite Zone is an arcuate terrane boundary with complex kinematics. The dominating deformation is interpreted as SE-directed backthrusting occurring at c. 970 Ma (**Viola et al., 2011**).

The Kongsberg and Bamble terranes are two small terranes which are made up of metasedimentary rocks, plutonic and volcanic rocks. Most of the rocks were formed around c. 1.55 to 1.45 Ga (**Roberts and Slagstad, 2015**). **Bingen et al. (2005)** consider the Bamble and Kongsberg Terranes to be a collision zone between the Telemarkia and the Idefjorden terranes. The Bamble and Kongsberg terranes consist of rocks that are similar in age and composition to the Telemarkia Terrane, but it is questioned if the Idefjorden were involved in the collision due to no record of metamorphism of this age in the Idefjorden Terrane (**Roberts and Slagstad, 2015**).

The Telemarkia Terrane is divided into four sectors by **Bingen et al. (2005)** for descriptive purposes; Telemark, Hardangervidda, Suldal and Rogaland-Vest Agder Sectors. The nomenclature and the division vary from author to author. The Telemark, Hardangervidda, Suldal and Rogaland-Vest Agder sectors have been merged into Rogaland-Hardangervidda sector by **Slagstad & Roberts (unpublished) (Figure 2.3)**. The Telemarkia Terrane have been called Hardangervidda-Rogaland and Telemark blocks by **Andersen (2005)**. The boundaries between the sectors are generally transitional, except along the N-S trending Mandal-Ustaoset Fault and Shear Zone (**Bingen et al., 2008b**). The Telemarkia Terrane is characterized by 1520-1480 Ma volcanic and plutonic suites overlain by metasedimentary sequences which are older than c. 1350 Ma. Between 1280 and 1130 Ma these rocks were intruded and overlain by magmatic and sedimentary rocks (**Bingen et al., 2003; Brewer et al., 2004**). During the Sveconorwegian orogeny the Telemarkia Terrane experienced several episodes of voluminous plutonism (**Coint et al., 2015; Slagstad et al., 2013a**).

The Hardangervidda sector consists of amphibolite-facies gneisses which are interpreted to be pre-Sveconorwegian (**Bingen et al., 2008b**). The geology of the Suldal sector can be divided into the “basement” and the nappes of Caledonian age. The basement formed in several Proterozoic events which have ages between 1540 and 1210 Ma. Some granitoid intrusions in the Suldal sector are of Sveconorwegian age (**Roberts, 2010; and references therein**).

The central part of the Telemark sector is made up of supracrustal rocks where original stratigraphic textures can be seen. The metamorphic grade increases northeast-wards to

amphibolite-facies, whereas the central parts of the sector only contain lower-grade metamorphic rocks. Amphibolite-facies rocks can also be found in the southern parts of the sector. This metamorphism is dated to c. 913 Ma and attests to a late Sveconorwegian metamorphism (**Bingen et al., 2008b; and references therein**). The Rogaland-Vest Agder sector is characterized by amphibolite- to granulite-facies metamorphism (**Bingen et al., 2008b**) (described in more detail in 2.1.2). The hornblende biotite granite (HBG) suite and the Rogaland Igneous Complex (RIC) is the youngest documented magmatism in the Sveconorwegian Province which have intruded various parts of the Province (**Figure 2.3**). The HBG-suite has been dated to 990-920 Ma (**Vander Auwera et al., 2011**) and the RIC has been dated to 950- 920 Ma (**Bybee et al., 2014; Vander Auwera et al., 2011**). The RIC is composed of three anorthosites (Egersund-Ogna, Håland-Helleren and Åna-Sira), Bjerkreim-Sokndal Intrusion (BKSK), two smaller leuconoritic bodies (Hidra, Garsaknatt) and a small volume of mafic rocks ranging in composition from high-Al gabbros to jotunites (hypersthene-bearing monzodiorites). All of the anorthosites in the RIC have megacrysts of plagioclase and orthopyroxene. Due to a high aluminium content in the opx megacrysts they are termed high-alumina orthopyroxene megacrysts (HAOM) (**Charlier et al., 2010**). The HBG-suite is hydrous whereas the RIC is anhydrous (**Vander Auwera et al., 2003**), and based on these data **Vander Auwera et al. (2003)** suggested that the parent magmas of the RIC and the HBG-suite formed from partial melting of two different sources: *“a lower crustal anhydrous, gabbro-noritic source for the RIC and a hydrous, undepleted to slightly depleted potassic mafic source for the HBG-suite”*. Due to their ferroan composition it has been suggested that they are extension related (**Vander Auwera et al., 2011**).

Research on the Sveconorwegian orogen has essentially been based on petrological, geochemical, isotopic or geochronological data. Few structural and kinematic studies across the orogen are available. The structural and tectonic evolution of the Sveconorwegian orogen is therefore not well understood (**Viola et al., 2011**).

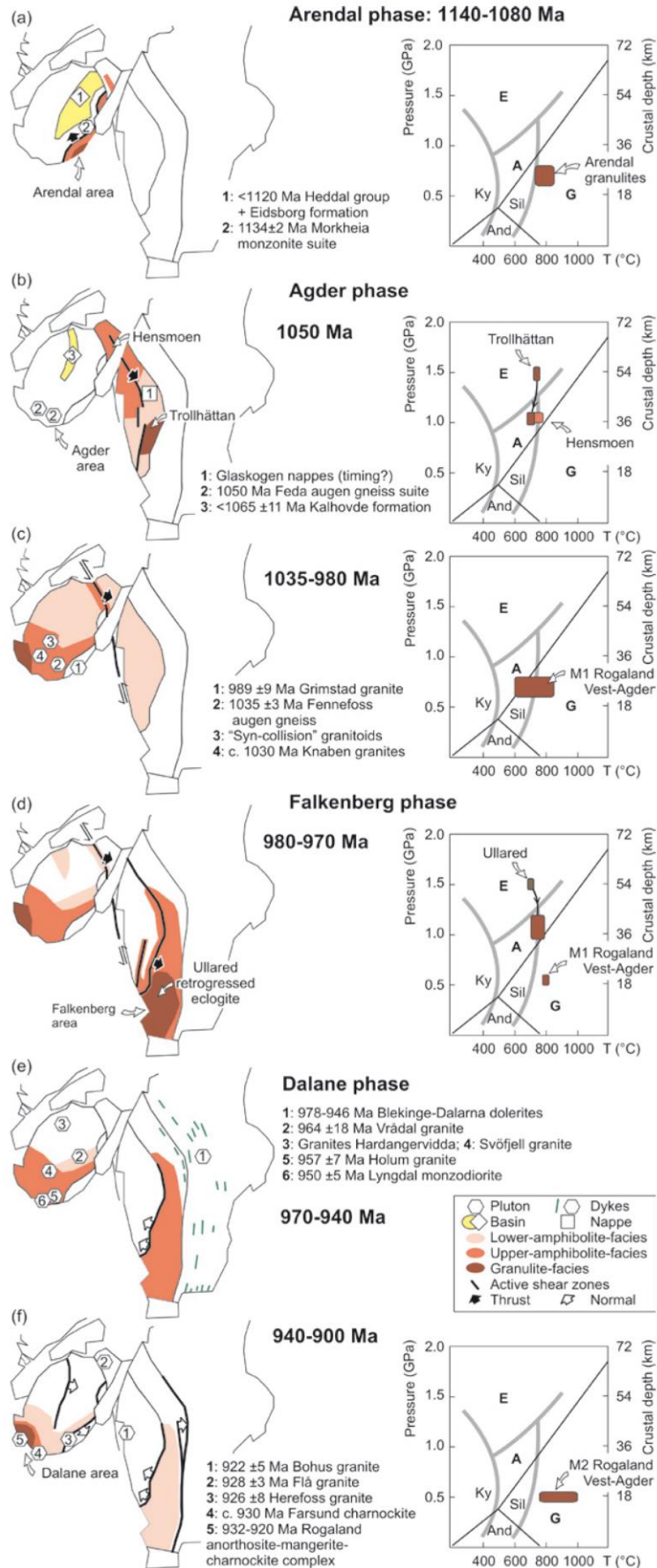
2.1.1 A four-phase model

The tectonic evolution of the Sveconorwegian Province is debated but has traditionally been considered to reflect a continent-continent collision which has been linked to the Grenville Province in Canada. **Bingen et al. (2008b)** suggested a four-phase model (**Figure 2.4**) for the continent-continent collision between Fennoscandia and another continent, possibly Amazonia. The four phases are the Arendal phase, the Agder phase, the Falkenberg phase and the Dalane phase. The Arendal phase (1140-1080 Ma) is described as a northwest-directed

subduction of an oceanic basin resulting in collision between the Telemarkia and the Idefjorden Terranes. This caused the formation of the Bamble and Kongberg wedges. The period between 1080 Ma and 1050 was characterized by tectonic inactivity in the Sveconorwegian Province (**Bingen et al., 2008b**). The Agder phase (1050-980 Ma) is said to be the main Sveconorwegian orogenic event, which is interpreted as resulting from a continent-continent collision between Fennoscandia and another large continent, suggested to be Amazonia. This caused crustal thickening, deformation and metamorphism in the Idefjorden and Telemarkia Terranes. The metamorphism related to this stage varies from lower amphibolite facies to high-pressure granulite facies and is interpreted to be a result of underthrusting and burial of the Idefjorden Terrane (**Bingen et al., 2008b**). The Falkenberg phase (980-970 Ma) is described as a major compressional event that resulted in high-pressure granulite and eclogite facies metamorphism in the Eastern Segment. In the Rogaland-Vest Agder Sector, the Falkenberg phase has also been interpreted as the transition between convergence and divergence. A late Sveconorwegian gravitational collapse took place between c. 970 and 900 Ma during the Dalane phase. This phase was characterized by voluminous post-collisional magmatism, which peaked at 930-920 Ma with intrusion of the Rogaland Igneous Complex and the large Bohus and Flå plutons in the Idefjorden Terrane. The source of the magmatism and the high-temperature metamorphism is suggested to be related to upwelling of hot lithospheric mantle close to the base of the crust at the end of the Sveconorwegian orogenic cycle (**Bingen et al., 2008b**).

Figure 2.4 (Facing page): Sketchmap showing the distribution of metamorphism, magmatic rocks and sedimentary basins during the Sveconorwegian orogeny. For each time slice the metamorphism is also illustrated in a pressure-temperature diagram. **(a)** Arendal phase: 1140-1080 Ma. **(b), (c)** Agder phase: 1050-980 Ma. **(d)** Falkenberg phase: 980-970 Ma. **(e), (f)** Dalanes phase: 970-900 Ma. Illustration from **Bingen et al. (2008b)**.

2 Regional geology



2.1.2 Metamorphism in the Rogaland-Vest Agder Sector

Bingen et al. (2008a) describe the Rogaland-Vest Agder Sector as having been through two main metamorphic phases, M1 and M2. The first one (M1), they describe as a regional high-grade metamorphic event between 1030 and 970 Ma which they link to orogenic thickening of the Rogaland- Vest Agder sector (during the Agder phase). They describe this event to be associated with strong deformation of the rocks. **Bingen et al. (2008a)** suggest that the crust was ductile after 970 Ma during gravitational collapse of the orogen. Based on U-Pb dating from Ivesdalen in Rogaland County (**Figure 1.1**), **Drüppel et al. (2013)** suggested that UHT-metamorphism occurred during regional Sveconorwegian metamorphism at c. 1010 Ma (M1) prior to the emplacement of the Rogaland Igneous Complex. The second phase (M2), they describe as a younger contact-metamorphic event due to the emplacement of the RIC at c. 930 Ma (during the Dalane phase). The metamorphism in the Rogaland-Vest Agder sector is described by **Bingen and van Breemen (1998b)** as increasing westwards and indicated by four isograds: clinopyroxene-in, orthopyroxene-in, osumilite-in and pigeonite-in. The N-S trending opx-isograd is according to **Bingen et al. (2006)** related to the 1030-970 Ma regional metamorphism, while the cpx-isograd is related to metamorphism due to the emplacement of the RIC. The osumilite-in and the pigeonite-in isograds are parallel to the contact of the RIC (**Bingen et al., 2008b**).

2.1.3 Continent-continent collision or a long lived accretionary margin?

Slagstad et al. (2013a) documented that areas previously mapped as granitic gneisses were weakly to undeformed and unmetamorphosed granites. This revealed a large granite batholith that was previously unknown. **Slagstad et al. (2013a)** named this large granitoid belt, the Sirdal Magmatic Belt (SMB). They describe the belt as a “*N-S trending belt that consists of mostly porphyritic granitoids with a calc-alkaline magnesian geochemistry*”. The SMB-granites are enriched in large ion lithophile elements which are typical for subduction zone magmas. Calc-alkaline magmatism in the Sveconorwegian orogen was first described by **Bingen (1989)** and termed, the “*Feda augen gneiss*”. It was described as a porphyritic granitoid belt. In a study by **Bingen and van Breemen (1998a)** the granitoid was dated and yielded an age of 1051 Ma. At first they interpreted the Feda augen gneiss to reflect a short-lived subduction prior to continent-continent collision, but later they interpreted it to be orogenic granitoids (**Bingen et al., 2006**). Based on observations around Tonstad where the granitic unit is only weakly foliated and is similar to the SMB granites, the Feda augen gneiss is considered a part of the much larger SMB by **Coint et al. (2015)**. Based on zircon dating,

Slagstad et al. (2013a) suggested that the magmatism in the SMB was continuous from ca 1060 to 1020 Ma, indicating long-lived magmatism that started c. 25 Myr before the documented metamorphism. **Coint et al. (2015)** suggest that the intensity of the magmatic activity may have varied, but with intensity peaks at c. 1050 and 1035 Ma. Xenolith-rich zones are characteristic for the SMB, and have previously been mapped as banded gneisses (**Falkum, 1982**). **Coint et al. (2015)** points out that these are zones that are rich in xenoliths with different lithologies; migmatites, granitic gneisses, amphibolites and metapelites rather than banded gneisses. They suggest that these zones represent pre-Sveconorwegian bedrock and contact zones between different intrusive bodies in the batholith.

Based on extensive mapping and new geochronological data **Slagstad et al. (2013a)** have questioned the traditional continent-continent collisional model and argue that the observed geological features are incompatible with processes related to continent-continent collision and require that the southwestern Baltican margin remained active throughout the Sveconorwegian orogeny. They suggest that a long-lived accretionary margin, undergoing periodic compression and extension could better explain the metamorphic and magmatic evolution of the Sveconorwegian Province (**Figure 2.5**). **Slagstad et al. (2013a)** divide the Sveconorwegian orogeny into three time periods; (1) 1060-1020 Ma, (2) 1020-990 Ma and (3) 990-920 Ma (**Figure 2.5**).

Age data (**Slagstad et al., 2013a**) showed that the magmatism in the SMB was continuous from c. 1060 to 1020 Ma (1). **Coint et al. (2015)** refer to a study by **Weaver et al. (1990)** where they document that emplacement of large granite batholit, similar to the SMB is characteristic of Andean-type accretionary orogens. **Slagstad et al. (2013a)** question if it is possible to have long-lived magmatism in a continent-continent collision and if a Himalaya-style collision setting is able to produce the heat that is needed to form the SMB. **Slagstad et al. (2013b)** refer to a study by **Drüppel et al. (2013)** where they documented that Sveconorwegian-age UHT metamorphism in southwestern Norway involved temperatures of c. 1000°C at pressures around 7.5 kbar. **Slagstad et al. (2013b)** argue that such PT conditions cannot be produced in a continent-continent collision. **Coint et al. (2015)** suggest that the UHT metamorphism may be correlated to heat from magmatism, which is related to formation of the SMB and the RIC. **Slagstad et al. (2013a)** also point out that the metamorphic ages varies across the Province. High-grade metamorphism at 1035-970 Ma was geographically restricted to the Rogaland-Vest-Agder Sector, while in the Telemark Sector only low-grade metamorphism was documented at this time (**Bingen et al., 2008a**). **Slagstad**

et al. (2013a) point out that the limited geographical distribution of high-grade Sveconorwegian metamorphism is not consistent with the development of an orogenic plateau. In **Coint et al. (2015)** they discuss if the ‘opx-in isograd’ really exists. Based on detailed mapping in the Gyadalen transect they concluded that the metamorphic isograd in that area was an intrusive contact between the SMB and older, metamorphic rocks and not a metamorphic isograd.

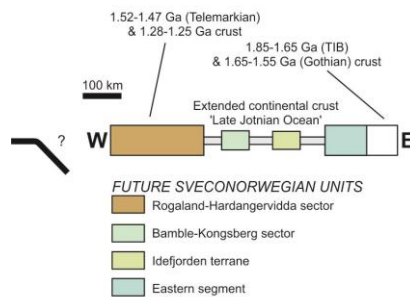
The 1020-990 Ma period (2) was characterized by a pause in the magmatism. **Slagstad et al. (2013a)** suggests that this could be caused by a flattening of the subducting slab, e.g. as a result of subduction of an oceanic plateau.

The 990-920 Ma period (3) was dominated by the formation of the HBG-suite and the RIC. **Slagstad et al. (2013a)** argue that the geographically widespread ferroan granite magmatism has been formed over a much larger period of time than what is usual for post-collisional magmatism. They therefore suggested that the magmatism between c. 990 and 920 Ma could be “*a result of delamination or convective thinning of the thickened mantle root to the SMB arc, and partial melting of dehydrated lower crust, which may have resisted earlier eclogitization and delamination on account of its dry nature*”. A study by **Bybee et al. (2014)** supports the theory of a long-lived Andean-type arc system. Based on Nd and Pb isotopic geochronology and geochemistry of orthopyroxene megacrysts from the RIC they suggest that they are formed from a mantle source near the Moho in an Andean-type arc setting. Sm-Nd dating of the orthopyroxene megacrysts gives an age of 1041 ± 17 Ma, which is similar in age to the SMB. They suggest that the opx-megacrysts represent cumulates from the crystallizing basaltic magma that may have ponded at the MOHO and eventually given rise to the anorthosites (949-920 Ma).

The Sveconorwegian orogen has traditionally been correlated with the Grenville orogen in North America and Canada, which formed during the assembly of the supercontinent Rodinia (**Gower et al., 1990; Karlstrom and Williams, 1998**). Recent studies in the eastern Grenville Province by **Gower et al. (2008)** have, however, questioned this. They argue that the Sveconorwegian Province may not be a direct continuation of the Grenville Province based on structural evidence. In the eastern part of the Grenville Province the geology is characterized by dextral, strike-slip movement which deviate from the frontal-thrust ramp tectonics that are characteristic for the western part of the Grenville province (**Gower et al., 2008**).

Slagstad and Roberts (in prep.) point out that the new theory of an active SW Baltican margin throughout Sveconorwegian orogenesis argues against a direct continuation with the Grenville Province, and suggests that the Late Mesoproterozoic Laurentia-Baltica margin may have been tectonically much more diverse than previously suggested. They also suggest that the margin could have been similar to the modern-day continental margins such as the south Asian margin.

Pre-Sveconorwegian configuration



Sveconorwegian evolution

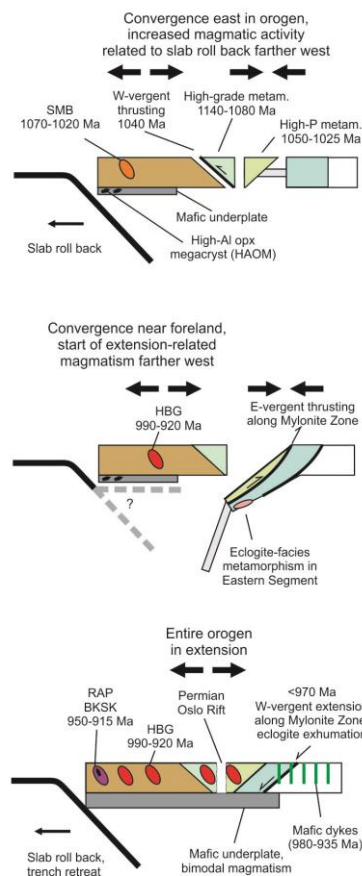


Figure 2.5: Schematic illustration for the Sveconorwegian evolution. Illustration from *Slagstad (unpublished)*.

3 Theory

A fundamental part of this thesis is U-Pb geochronology of zircon and monazite by Laser Ablation Inductively Coupled Plasma Mass Spectrometry (LA-ICP-MS). In this chapter a short presentation of the most important aspects of the method will be introduced.

3.1 Uranium-lead geochronology

3.1.1 U-Th-Pb

The decay of uranium and thorium to stable lead isotopes is the basis for several important methods of dating. U ($Z = 90$) and Th ($Z = 92$) have similar chemical properties because of similar electron configurations (**Faure and Mensing, 2005**). Uranium occurs in nature as radioactive ^{238}U , ^{235}U and ^{234}U . Thorium occurs mainly as ^{232}Th . Lead exists as radiogenic ^{206}Pb , ^{207}Pb and ^{208}Pb and non-radiogenic ^{204}Pb (**Passarelli et al., 2009**). Uranium and thorium do not decay directly to lead, but through a chain of intermediate daughter isotopes (**Figure 3.1**) where alpha and beta particles are emitted. The half-lives of the parent isotopes are much longer than the daughter isotopes. The half-life of ^{238}U is 4.47 Ga (**Jaffey et al., 1971**) and 0.7 Ga for ^{235}U (**Mattinson, 2010**). The decay of ^{238}U , ^{235}U and ^{232}Th to ^{206}Pb , ^{207}Pb and ^{208}Pb is summarized in the following equations (3.1, 3.2, 3.3), where ^4He is an alpha particle, β^- is beta radiation (electron) and Q is the energy that is liberated during the process (million electron volts) (**Schoene, 2014**).



Uranium and thorium can occur as trace elements in major phases or they can be concentrated in accessory minerals such as zircon (ZrSiO_4), which concentrates more U than Th, and monazite ($[\text{La,Ce,Th}]\text{PO}_4$), which concentrates more Th than U. In this study zircon and monazite were used for U-Pb dating; these will therefore be described in details later in this chapter. Both zircon and monazite have high closure temperatures (T_c) > 900 °C. The closure temperature is the temperature of the mineral when there is no longer any significant diffusion of the parent or daughter isotopes out of the system and out to the surroundings. The closure temperature is a function of diffusivity, cooling rate, and effective diffusion radius (**Dodson,**

1973). Not only zircons and monazite are used for U-Pb dating; apatite, xenotime, titanite, rutile, baddeleyite, allanite and perovskite are also used (Passarelli et al., 2009).

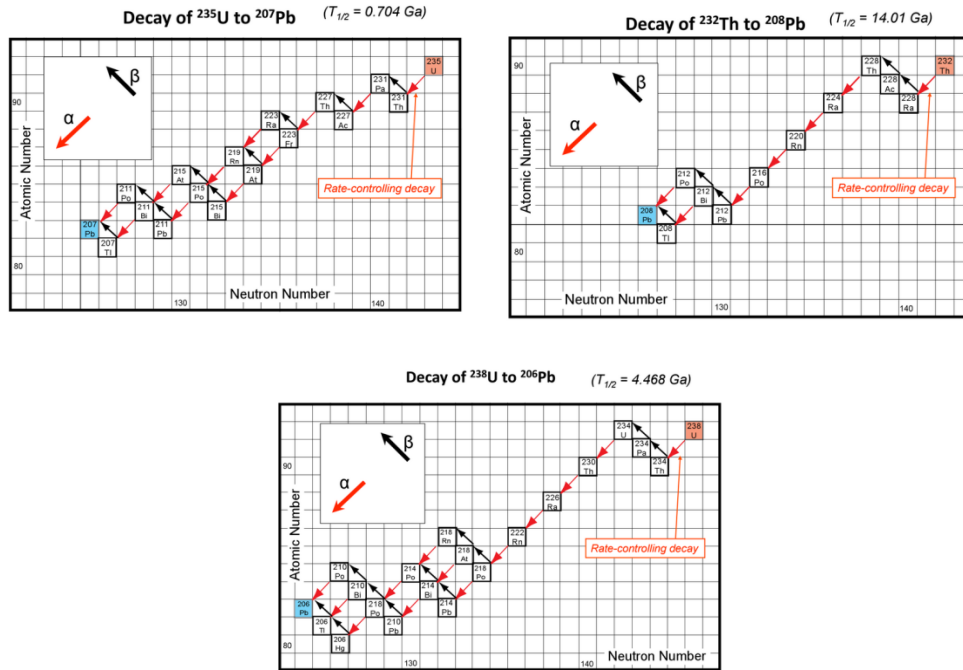


Figure 3.1: The figure shows the decay chains for ^{235}U , ^{232}Th and ^{238}U . Figures from **Kylander-Clark and Cottle (2014)**.

3.1.2 U-Pb Concordia Plots

When the isotope data are collected from the LA-ICP-MS, the data are plotted in a concordia diagram and ages can be calculated. The two most used U-Pb concordia plots are the Conventional diagram (**Wetherill, 1956**) ($x = ^{207}\text{Pb}/^{235}\text{U}$, $y = ^{206}\text{Pb}/^{238}\text{U}$, $z = ^{204}\text{Pb}/^{238}\text{U}$) (often called a Concordia plot) and the Tera-Wasserburg diagram (**Tera and Wasserburg, 1972**) ($x = ^{238}\text{U}/^{206}\text{Pb}$, $y = ^{207}\text{Pb}/^{206}\text{Pb}$, $z = ^{204}\text{Pb}/^{206}\text{Pb}$) (z are used if 3-dimensional concordia plots are used). The two diagrams have advantages and disadvantages. The Tera-Wasserburg plot has advantages in visualization. High common lead values can be seen by a vertical trend of the data. If the data show a horizontal array this can be a sign of fractionation. A disadvantage of the Tera-Wasserburg diagram is that it is difficult to show data with a large range of U/Pb ages, and impossible to show a zero-age point (**Ludwig, 2003**).

Figure 3.2 is illustrating how the concordia diagram works. The **Wetherill (1956)** concordia diagram plots $^{206}\text{Pb}/^{238}\text{U}$ versus $^{207}\text{Pb}/^{235}\text{U}$. Both these ratios are proportional with time. The curve in the diagram is called the concordia; all natural samples with coherent U-Pb systems must develop along this curve ($^{238}\text{U} - ^{206}\text{Pb}$ age is equal to the $^{235}\text{U} - ^{207}\text{Pb}$ age). ^{235}U decays

faster than ^{238}U due to a smaller decay constant, resulting in the characteristic concave downward shape of the concordia. A zircon does not always plot on the concordia, but can also be plotted on a line called the discordia. A zircon will plot on this line if the system is not closed and the zircon loses Pb. **Figure 3.2** is illustrating examples of zircons that have lost different amount of lead at one event at 2.5 Ga. If one zircon lost all of its lead, the zircon will be reset and plot at 0 and then continue evolving on the concordia line. The rest of the zircons will continue evolving on different concordia – curves (dashed). The discordia will intercept the concordia curve at two places; one yielding the total age of the rock (3.5 Ga), and the other yielding the age of the lead loss (1 Ga since lead loss at 2.5 Ga) (**Schoene, 2014; Winter, 2001**).

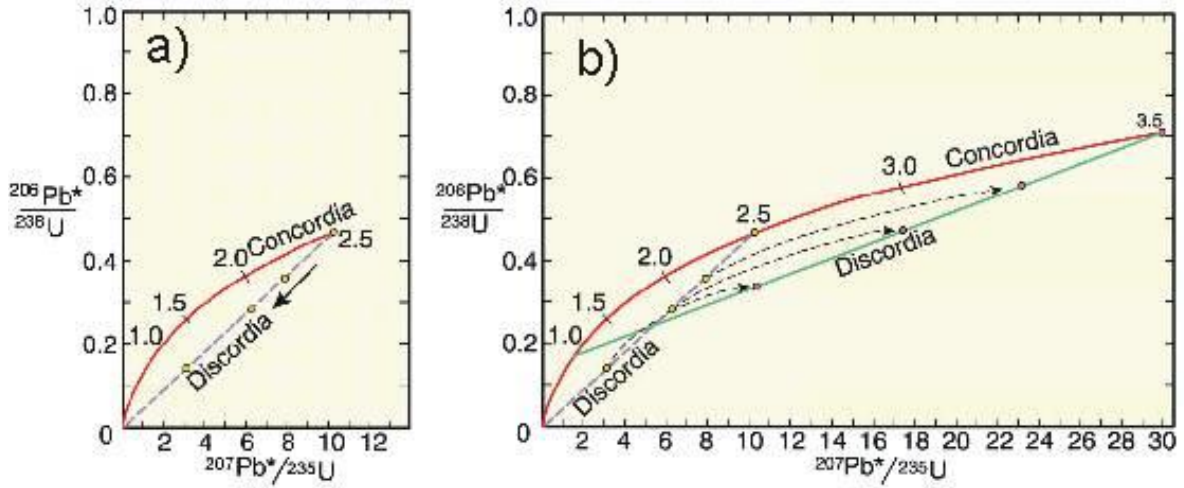


Figure 3.2: Concordia diagram that is illustrating the lead development of a 3.5 Ga old rock that have been exposed by a single episode of Pb loss. **(a)** Radiogenic ^{206}Pb and ^{207}Pb are evolving along the concordia diagram for the first 2.5 Ga, where lead loss occurred. The zircons are losing variable amount of lead. **(b)** The evolution of the Pb system is continued for 1 Ga. The undepleted zircons are following the concordia curve, while the depleted zircons are following separate Concordia- curves (dashed) to their new positions. The discordia is intersecting the concordia at two places; one yielding the total age of the rock (3.5 Ga), and the other yielding the age of the lead loss (1 Ga since lead loss at 2.5 Ga). Diagrams from **Winter (2001)**.

The equations used to plot a concordia diagram are as followed:

$$\frac{^{206}\text{Pb}}{^{238}\text{U}} = (e^{\lambda_{238}t} - 1) \quad (3.4)$$

$$\frac{^{207}\text{Pb}}{^{235}\text{U}} = (e^{\lambda_{235}t} - 1) \quad (3.5)$$

λ is the decay constant and t is the time. The decay constant for ^{235}U is $1.54 \times 10^{-10} \text{ y}^{-1}$ and for ^{238}U it is $9.72 \times 10^{-10} \text{ y}^{-1}$ (**Faure and Mensing, 2005**). To produce a Tera-Wasserburg plot, two equations are used (**Schoene, 2014**):

$$\frac{^{207}\text{Pb}}{^{206}\text{Pb}} = \frac{1}{137.88} \frac{(e^{\lambda_{235}t} - 1)}{(e^{\lambda_{238}t} - 1)} \quad (3.6)$$

$$\frac{^{238}\text{U}}{^{206}\text{Pb}} = \frac{1}{(e^{\lambda_{238}t} - 1)} \quad (3.7)$$

In equation (3.6), $1/137.88$ is the ratio of $^{235}\text{U}/^{238}\text{U}$ at present time, t is the time since formation of the zircon and λ_{235} and λ_{238} are the decay constants of ^{235}U and ^{238}U . The decay constants are; λ_{235} : $1.54 \times 10^{-10} \text{ y}^{-1}$ and λ_{238} : $9.72 \times 10^{-10} \text{ y}^{-1}$ (**Faure and Mensing, 2005**).

The $^{206}\text{Pb}/^{238}\text{U}$ age is often preferred for young rocks while $^{207}\text{Pb}/^{235}\text{U}$ age is often preferred for older samples. This has to do with the uncertainties of the ages. The uncertainties will be larger for the $^{206}\text{Pb}/^{238}\text{U}$ for older samples while the uncertainties will be larger for $^{207}\text{Pb}/^{235}\text{U}$ for younger samples.

3.1.3 Zircon

Zircon (ZrSiO_4) is the most common mineral used as a geochronometer. It is a common accessory mineral in nature and it can be found in sedimentary, igneous, and metamorphic rocks. They can contain minor and trace elements which are very useful in geochronology. Trace elements can provide insight into the petrological context of the isotopic dates (**Hanchar and Hoskin, 2003**). Zircon is very resistant to chemical and physical weathering and has a slow diffusion rate that makes them resistant to resetting (**Hanchar and Hoskin, 2003**). The mineral structure of zircon excludes Pb^{2+} because they have large ionic radius and lower charge compared to Zr^{4+} , U^{4+} and Th^{4+} . Zircon therefore has low Pb content when formed and high U/Pb and Th/Pb ratios. Smaller grains of zircon usually loose more Pb due to diffusion than big grains due to the high surface/volume ratio. Pb loss mainly happen in hot fluid-rich environments (**Schoene, 2014**). Zircon formed in different geological environments generally has characteristic internal structures. The internal structures can be revealed using cathodoluminescent images (CL). Cracks and inclusion are usually best seen in backscatter electron images (BSE). Magmatic zircon is commonly subhedral to euhedral. Zircon from volcanic rocks usually produces prismatic to acicular shapes. Oscillatory zonation is often well developed in magmatic zircon and common in granites. Sector zoning can also be seen in magmatic zircons which are produced when the environment is unstable and the growth

velocity of crystal facies is changing. The zircon can record geological events as rims in the grain. The core of the zircon is often unaffected and can preserve the chemical characteristics of the original rock. Metamorphic zircons are often anhedral to euhedral. Internal structures that are common in metamorphic zircon are patchy zoning, weakly zoning, sector zoning or no zoning (**Wu and Zheng, 2004**).

3.1.4 Monazite

Monazite ($[\text{La,Ce,Th}]\text{PO}_4$), is a Light Rare Earth Element (LREE) phosphate which can be found in several magmatic rocks. It can also be found in pelitic schists and gneisses, and because it is relatively resistant to weathering it can also be found in several sedimentary rocks. Monazite also occurs as inclusions in several host minerals including feldspar, mica, quartz and garnet. Monazite has been increasingly used as a geochronometer during the last years and has the ability to contain large amounts of Th and U, generating a very high ratio of radiogenic Pb to common Pb (**Loehn, 2011**). All the radiogenic Pb which is present in monazite is derived from the decay of U and Th, the age can therefore be calculated based on the concentrations of U, Th and Pb. Analysing monazite can be a good way to get information on metamorphic events because monazite can be zoned preserving multiple age/or compositional domains in one single grain (**Slagstad, 2006**). But in some cases the zonation can be misleading because monazite can have a complex zonation, but be quite uniform in age (**Bosse et al., 2009**).

3.2 U-Th-Pb dating methods

There are different methods for U-Th-Pb geochronology, ID-TIMS, SIMS and LA-ICP-MS are some examples (**Figure 3.3**). All three methods have advantages and disadvantages depending on how they are used. The choice of analytical method depends on the amount of sample that are analysed, which instrument is available, the concentration of the elements and the purpose of the study (**Faure and Mensing, 2005**). In this study a LA-ICP-MS was used to date zircon and monazite.

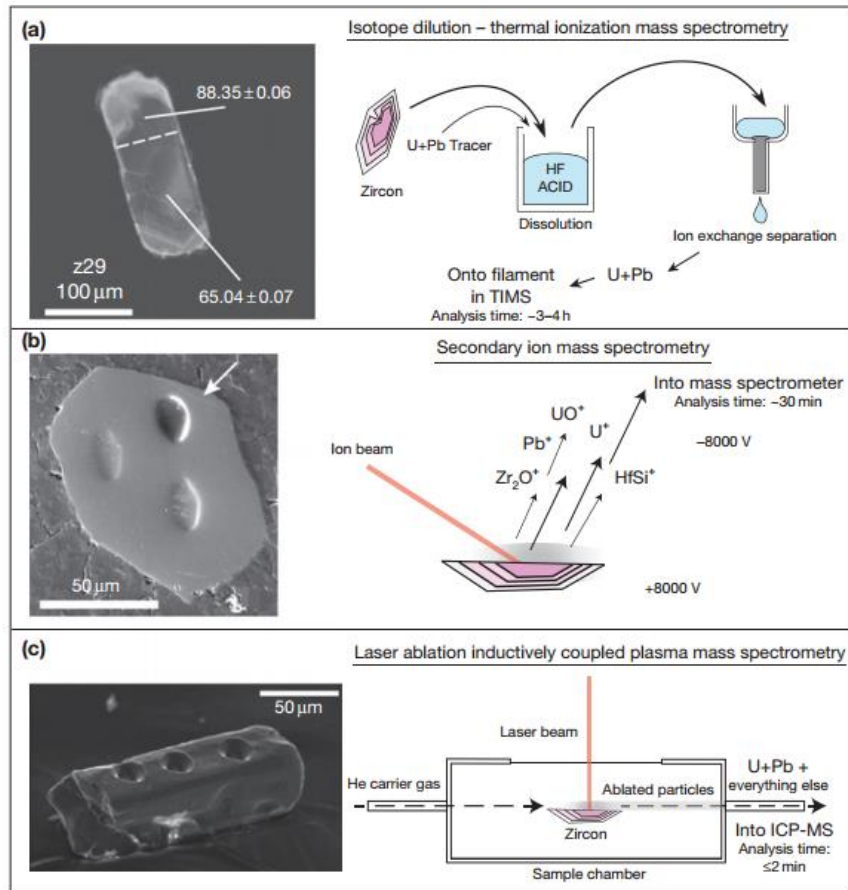


Figure 3.3: Short illustration of how the three instruments are working. (a) ID-TIMS. (b) SIMS (c) LA-ICP-MS. Figure from *Schoene (2014)*.

3.2.1 ID-TIMS

In Isotope Dilution Thermal Ionization Mass Spectrometry (ID-TIMS) (**Figure 3.3a**) a homogenous mixture is made by dissolving the sample in acid with a known amount of tracer with a known isotopic ratio. The sample is placed on a metal filament and heated to ionize the elements of interest, which are then accelerated into a magnetic sector mass spectrometer (**Schoene, 2013**). In the mass spectrometer the known tracer composition is subtracted from the sample, and the isotopic composition of the sample can be calculated. The Isotope dilution analytical method is a widely used method in geochronology due to its many advantages. It is a very accurate and precise method that can measure low concentrations of many elements and it is possible to measure small amounts of material (**Faure and Mensing, 2005**).

3.2.2 SIMS

In Secondary Ion Mass Spectrometry (SIMS) (**Figure 3.4**) a beam of high-energy primary ions is focused onto a polished surface. The primary beam can be composed of positively charged ions or negatively charged ions. If the beam is composed of negative ions the generation of positive ions is favoured, opposite with a positive charged beam. When the beam hits the surface of the sample the atoms in the sample are ionized to produce secondary ions. These are then analysed by a mass spectrometer. The beam is usually small, around 10 to 50 μm in diameter, making it a good method for analysing small domains in a zircon or in other minerals. SIMS is also a good method to measure the chemical and isotopic composition of solid materials. SIMS can also be coupled with other instruments making it possible to get Cathode Luminescence- and Backscatter Electron images as well (**Mueller and Vervoort, 2012**).

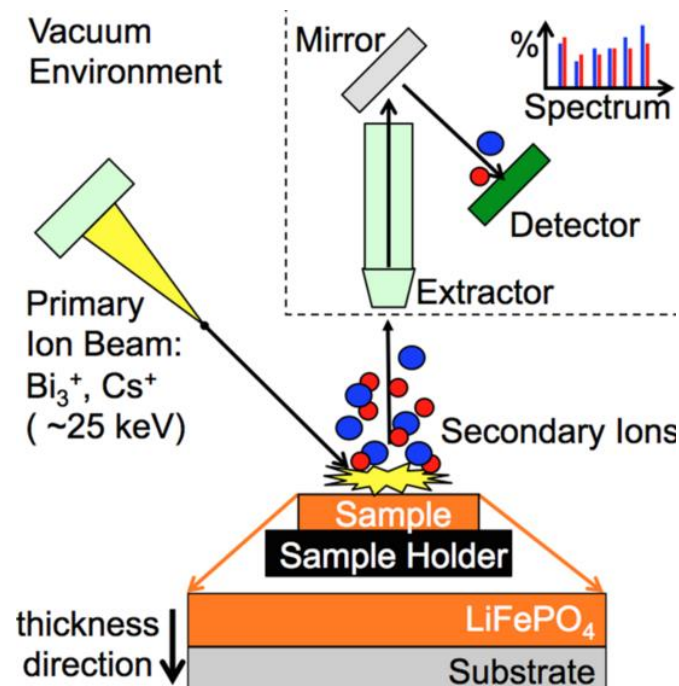


Figure 3.4: Components of SIMS. An ion gun fires ions at a sample producing secondary ions. These are then analysed by a mass spectrometer. Figure from **ChiuHuang et al. (2014)**.

3.2.3 LA-ICP-MS

There are several different types of ICPMS. In this study a Laser Ablation Inductively Coupled Plasma Mass Spectrometer was used. In a LA-ICP-MS the zircons or other minerals are ablated with a laser (**Figure 3.5**). The ablated material is then transported by a He gas stream to the plasma. Argon is often used as plasma. The energy from the Inductively

Coupled Plasma source (ICP) converts the atoms of the elements in the sample to positive ions by removing an electron from its orbital. As a consequence elements that prefer to form negative ions (Cl, I, F, etc.) are difficult to determine with the ICPMS. When the ions are formed they are transported to the mass spectrometer. In the mass spectrometer the ions are separated by their mass-to-charge ratio. After passing through the mass spectrometer the ions reach the detector where the ions hit the surface of the detector and are converted to electrons and counted (**Wolf, 2005**).

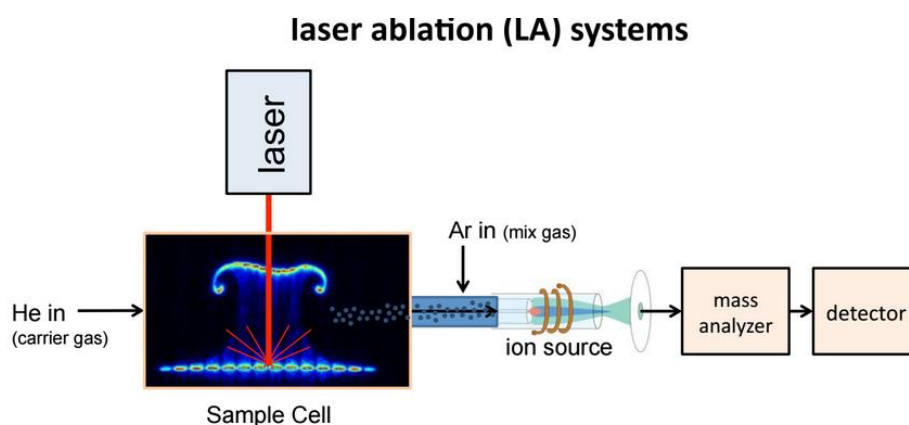


Figure 3.5: The figure shows an illustration of the main parts of a LA-ICP-MS. The laser is ablating the sample. He gas is transporting the material into the plasma (Ar). The ions produced are then transported into the mass-spectrometer (mass analyzer) before they reach the detector. Figure from **Kylander-Clark and Cottle (2014)**.

There are several parameters that can affect the precision and accuracy of the data using a Laser Ablation ICP-MS. Examples of such parameters are laser wavelength, pulse duration, laser beam profile, spot size and composition of ambient gas (**Hanchar & Hoskin, 2003**). Depending on the use of the instrument and purpose of the research it is several advantages and disadvantages using LA-ICP-MS. The main assets of the instrument are that it is quickly operated, the instrument is relatively cheap, local analysis is possible, the diameter of the beam can be regulated, almost any sample can be analysed and it is relatively sensitive. The main disadvantage using the instrument is that fractionation can occur due to “large” spot size (**Oishi & Fukuda, 2004**). The main reasons for choosing LA-ICP-MS in this study were that it is a rather cheap method, the instrument is accessible and the measurements take relative short time. Moreover it is possible to date rims and cores of both zircons and monazite.

3.3 Correction methods

3.3.1 Data reduction

The data acquired from the laser are reduced and the U-Th-Pb isotope ratios calculated using the GLITTER software. During the laser sampling the data are corrected both for U-Pb and Th-Pb fractions and for instrumental mass discrimination (mass bias). This provides accurate ages. It is also common to apply statistical models to increase the precision of an age interpretation and account for scatter in the dataset (**Van Achterbergh et al., 2001**). Isotope results are often presented with the mean squared weighted deviation (MSWD). MSWD is calculated using the following equation:

$$\frac{1}{v} * \sum_{i=1}^n \frac{(x_i - \bar{x})^2}{\sigma_i^2} \quad (3.8)$$

Where v is the degrees of freedom ($n-1$), x_i is the observed data, \bar{x} is the theoretical or expected data, and σ^2 is the variance of the observed data (**Horstwood, 2008**).

A MSWD value of approximately 1 indicates that the scatter in the data can be explained by analytical uncertainties alone, $\text{MSWD} \ll 1$ indicates that analytical uncertainties have been overestimated, and values greater than 1 can indicate either that the uncertainties have been underestimated and/or scatter due to non-analytical causes e.g. real geological differences. To assess the quality of a result for a population of data or a single data point, an uncertainty usually expressed at the level of 2 sigma (data point) or 95% confidence (population) is required (**Horstwood, 2008**).

3.3.2 Common lead corrections

Common lead is according to **Andersen (2002)**, “*lead of nonradiogenic origin that is incorporated into a mineral during its initial formation, in subsequent recrystallization processes or by contamination during analysis*”. Common lead can be a source of error in U-Pb geochronology (**Andersen, 2002**). In this study common lead correction was not used. Former studies have experienced that common lead corrections using LA-ICP-MS data does not work well because of ^{204}Hg interference. Mercury is often present in the Ar gas, but also often in parts of the ICPMS instrument contributing to the 204 signal intensity (**Kosler and Sylvester, 2003**). The ^{204}Pb were measured making it possible to exclude the common lead affected data from further calculations.

4 Methods

The methods that were used in the study are introduced in this chapter. Fieldwork was important to study the geology in detail, record field relationship and to collect samples for analysis. Mineral separation was performed before dating the zircons and monazites using a Laser Ablation Inductively Coupled Plasma Mass Spectrometer (LA-ICP-MS).

4.1 Fieldwork

Geological fieldwork was carried out on the municipal boundary between Lyngdal, Hægebostad and Audnedal in Vest-Agder County during the period 10.06.2015 to 30.06.2015. An area of approximately 50 km² was mapped. One outcrop containing several geological structures was studied in some detail.

The mapping was plotted on black and white topographic maps (1:10,000) with colour pencils. A handheld GPS was used to find the exact positions and to precisely locate where samples were collected. A geological hammer, compass and a digital camera were used to take samples, measure and to document the observations. A handheld SM20 magnetic susceptibility-meter was helpful for distinguishing between different granites in the field area.

During one week in October (19.10.2015 to 23.10.2015) several additional localities were studied to obtain greater regional control. Among these were the Lysefjorden locality and the Gyadalen transect where the ROG092322, ROG092326 and the VAG- samples were taken.

4.2 Sample preparation

A total of 13 samples were selected for geochronological analysis of zircon and two samples were selected for geochronological analysis of monazite. The geochronological analyses were done using the LA-ICP-MS at the Geological Survey of Norway (NGU), Trondheim.

4.2.1 Thin section

All the samples were submitted to the thin section lab at the Geological Survey of Norway (NGU) in Trondheim where thin sections were prepared. The thin sections were 30 µm thick and used for petrographic description.

4.2.2 Mineral separation

A jaw crusher was used to crush the rock samples. Then the material was split, one part was sent to the geochemistry lab, the rest of the material was sieved. The zircons were separated

from the <250 µm material by a combination of Wilfley-table washing, magnet, heavy liquid separation (diiodomethane, 3.325 g mL⁻¹) and magnetic-separation with a Frantz isodynamic separator. The Frantz separates the magnetic and the nonmagnetic minerals into two different cups using different angles and magnetic forces. The zircons from the nonmagnetic cup were then handpicked using a tweezers under a binocular microscope. Around 25-35 zircons were picked from each sample if feasible. Selected crystals were mounted in epoxy, and then polished to approximately half the thickness using a 6 µm diamond paste. Monazite were also picked from some of the samples and mounted into epoxy to be used for U-Pb dating.

4.2.3 Scanning Electron Microscope

A Scanning Electron Microscope at the Geological Survey of Norway (NGU), Trondheim, was used to take pictures of the zircons and monazites. CL-images reveal internal structures in zircon and monazite. This is very helpful to determine where the analysis should be taken. Chemical maps of the monazite grains were also made.

The SEM at NGU is a 1450 Variable pressure (VP) SEM manufactured by LEO Electron Microscopy LTD. It has an X-ray analytical system and accompanying INCA software, suite version 4.09 by Oxford Instruments.

Chemical mapping of the monazite was done by setting up an automapping session within the INCA software. X-rays generated by scanning an electron beam across the monazites were used to produce chemical maps. The process time was set to 2, number of frames was set to 7, map dwell to 4000 µs (c. 3400s time per frame), channels to 2K, Iprobe to 5000 pA and vacuum to 25 Pa.

4.3 Geochronological analysis

4.3.1 LA-ICP-MS

U and Pb isotopes in zircon and monazite were analysed using the Laser Ablation Inductively Coupled Plasma Mass Spectrometer (LA-ICP-MS) at the Geological Survey of Norway (NGU), Trondheim. The LA- ICP-MS at NGU consists of an ELEMENT XR single-collector, high-resolution ICP-MS, coupled to a UP193-FX 193 nm short-pulse excimer laser ablation system from New Wave Research. The isotopes measured were ²⁰²Hg, ²⁰⁴(Hg + Pb), ²⁰⁶Pb, ²⁰⁷Pb, ²⁰⁸Pb, ²³⁸U and ²³²Th. The data were not corrected for common lead, but ²⁰⁴Pb was measured making it possible to exclude analyses with high common lead from further calculations.

Zircon dating

A spot size of 10 μm was used with a repetition rate of 10 Hz and an energy corresponding to a fluence of 4-5 J/cm^2 . The laser was set to ablate single, up to 60 μm long lines. Each analysis had 30 s of background measurement before 30 s of ablation. The ablation was always away from the suction to be able to avoid contamination from other grains.

Calibration of isotopic ratios was performed using GJ-1 (608.5 ± 1.5 Ma) (**Jackson et al., 2004**) as a standard, whereas 91500 (1065.4 ± 0.3 Ma) (**Wiedenbeck et al., 1995**), OS-99-14 (1797 ± 3 Ma) (**Skår, 2002**) and Z-6412 (1160 ± 2 Ma) (**unpublished, GSC Ottawa**) were used for checking precision and accuracy.

The data were reduced and all U-Th-Pb isotope ratios were calculated using the GLITTER software (**Van Achterbergh et al., 2001**). Plotting of isotopic data and age calculations were carried out using Isoplot (**Ludwig, 2003**).

Monazite dating

A spot size of 10 μm was used with a repetition rate of 5 Hz and an energy corresponding to a fluence of 4-5 J/cm^2 . Each analysis had 30 s of background measurement before 30 s of ablation.

Calibration of isotopic ratios was performed using BB-0109 (1137 ± 1 Ma) (**Bingen et al., 2008a**) as a standard, whereas Moacir (504.3 ± 0.2 Ma) (**Gasquet et al., 2010**), BB-0030 (1092 ± 1 Ma) (**Bingen et al., 2008a**), A-276 (1915 ± 4 Ma) (**Salli, 1983**) and BB-9952 (403 ± 5 Ma) (**Bingen, unpublished**) were used for checking precision and accuracy.

The data were reduced and all U-Th-Pb isotope ratios were calculated using the GLITTER software (**Van Achterbergh et al., 2001**). Plotting of isotopic data and age calculations were carried out using Isoplot (**Ludwig, 2003**).

5 Results

The results in this study are based on detailed mapping from the Kvås-Konsmo area and geochronological and petrographic data from samples taken from Lysefjorden, the Kvås-Konsmo area and the Gyadalen transect (**Figure 5.1**). Detailed mapping of the Kvås-Konsmo area was important to be able to combine lab results with the observations done in the field. Samples from Lysefjorden and Gyadalen were used to compare the result on a regional scale and to compare the metamorphism inside and outside the Sirdal Magmatic Belt. A geological map of the Kvås-Konsmo area is shown in **Figure 5.2**. 13 samples were dated using zircon as a geochronometer and two samples were dated using monazite as a geochronometer. Mineral abbreviations used in this thesis are from **Whitney and Evans (2010)** and found in **Table 5.1**. Geochronological data from the analysed samples are presented in **Table 5.2**.

Complete data from all analysis are found in the Appendix.

Abbreviation	Mineral	Abbreviation	Mineral
Ap	Apatite	Ms	Muscovite
Bt	Biotite	Opq	Opaque
Chl	Chlorite	Opx	Orthopyroxene
Cpx	Clinopyroxene	Pl	Plagioclase
Crd	Cordierite	Qz	Quartz
Ep	Epidote	Sil	Sillimanite
Grt	Garnet	Spn	Titanite/Sphene
Hbl	Hornblende	Spl	Spinel
Kfs	K-feldspar	Zrn	Zircon
Mnz	Monazite		

Table 5.1: Mineral abbreviations used in this thesis are from **Whitney and Evans (2010)**.

5 Results

Sample	Locality	East	North	Rocktype	Method	Age (Ma), 2s	*I/M
IH128056	Kvås/Konsmo	396017	6459582	Amphibolite	No zircon found	No zircon found	
IH128058	Kvås/Konsmo	397261	6459640	Diorite	La-ICP-MS of zircon	991 ± 11	I
IH128061	Kvås/Konsmo	395379	6459660	Metapelite	La-ICP-MS of zircon	1024 ± 9	M
IH128061	Kvås/Konsmo	395379	6459660	Metapelite	La-ICP-MS of monazite	~ 980 – 900	M
IH128065a	Kvås/Konsmo	403000	6461183	Migmatite, mesosome	La-ICP-MS of zircon	1464 ± 21	I
IH128065b	Kvås/Konsmo	403000	6461183	Migmatite, leucosome	La-ICP-MS of zircon	1039 ± 17	M
IH128068	Kvås/Konsmo	400453	6465027	Deformed granite	La-ICP-MS of zircon	1045 ± 20	I
IH128070	Kvås/Konsmo	401687	6465410	Folded granite	La-ICP-MS of zircon	1050 ± 39	I
IH128072	Kvås/Konsmo	402995	6461179	Migmatite	La-ICP-MS of zircon	1065 ± 23	M
IH128074	Kvås/Konsmo	398980	6460798	Porphyritic granite	La-ICP-MS of zircon	1043 ± 22	I
ROG092326	Lysefjorden	334213	6532806	Metapelite	La-ICP-MS of zircon	1035 ± 17	M
ROG092322	Lysefjorden	335928	6538186	Foliated granitoid	La-ICP-MS of monazite	1025 ± 16	M
VAG084396	Gyadalen	356101	6502651	Granitic gneiss	La-ICP-MS of zircon	1048 ± 22	I
VAG084396	Gyadalen	356101	6502651	Granitic gneiss	La-ICP-MS of zircon	~ 1017	M
VAG084397	Gyadalen	357625	6503462	Quartz dioritic migmatitic gneiss	La-ICP-MS of zircon	1033 ± 17	I/M
VAG084399	Gyadalen	359379	6504170	Foliated granite	La-ICP-MS of zircon	1037 ± 7	I

Table 5.2: Geochronological summary of the analysed samples from the Kvås-Konsmo area, Lysefjorden and Gyadalen. UTM WGS84 coordinates in zone 32N. * I = igneous age, M = metamorphic age.

5.1 Field observations (Kvås-Konsmo)

The units observed in the Kvås-Konsmo area are divided into porphyritic biotite granite (SMB), xenolith-rich zones and hornblende biotite granite (HBG). The xenolith-rich zones consist of several different rock types including: migmatite, metapelite, flaser gneiss and amphibolite. A geological map of the field area is shown in **Figure 5.2**. This map is the result of detailed geological mapping of the Kvås-Konsmo area. The amount of xenoliths in the

xenolith-rich zone is varied. The areas with the highest xenolith concentration are marked with symbols in the map.

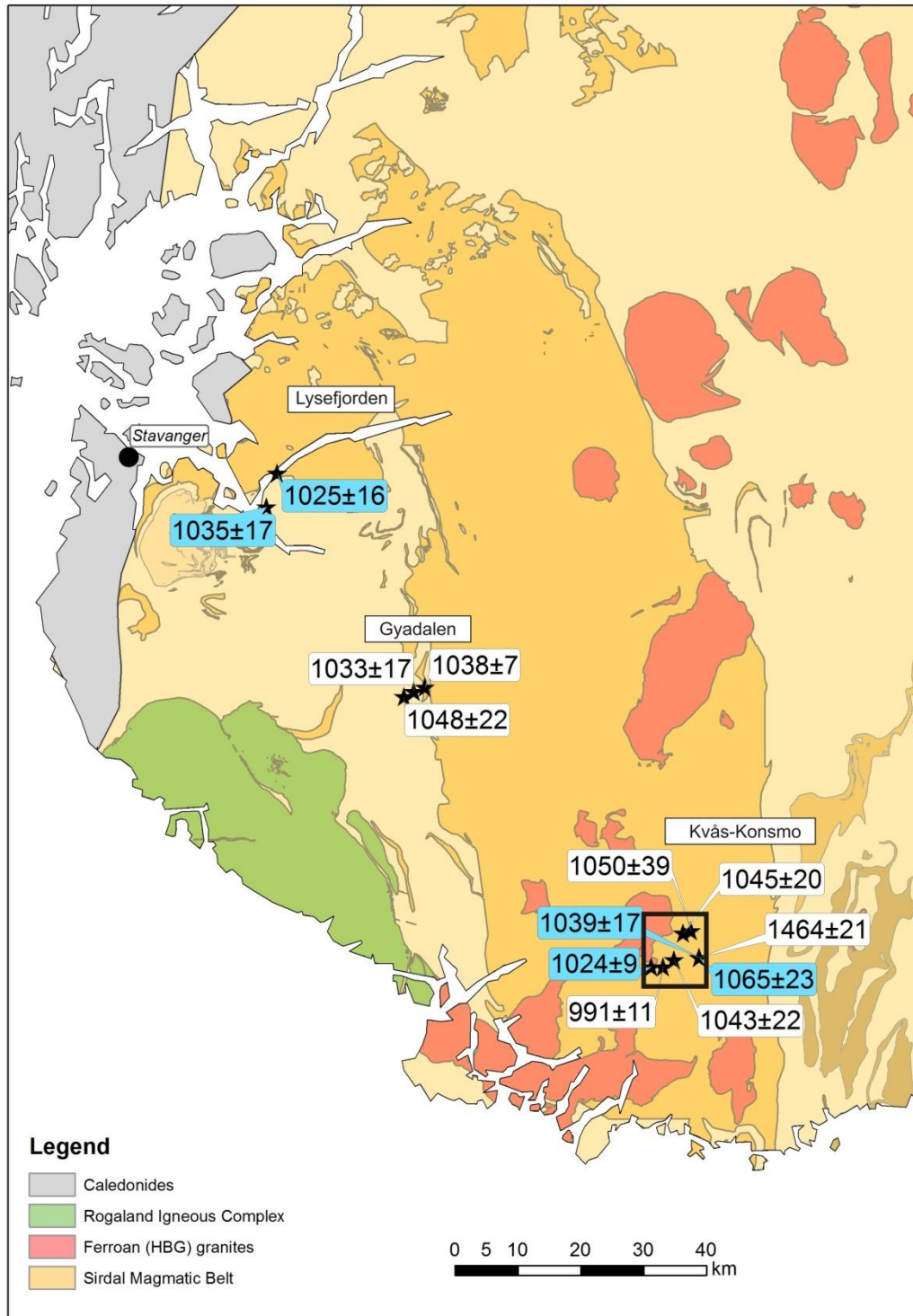


Figure 5.1: Simplified geological map of southwestern Norway. Geochronological data are marked on the map, blue are metamorphic ages, white indicate crystallization ages. The black square marks the study area (Kvås-Konsmo) (Figure 5.2).

5.1.1 Porphyritic biotite granite

Several varieties of granite are found in the Kvås-Konsmo area (**Figure 5.3**), but the most dominant lithology is the porphyritic granite. The porphyritic granite (**Figure 5.3b and c**) is usually medium grained, biotite rich with phenocrysts of K-feldspar. The phenocrysts vary in size, shape and abundance; they are usually 2-3 cm, but some places they can be up to 6 cm. They are stubby to prismatic and can constitute up to 80% of the rock. The granite is mostly undeformed, but a few granites display a lineation defined by alignment of K-feldspar phenocrysts. The granite does not show any significant recrystallization. **Stormoen (2015)** documented from Knaben that mineral lineation without any significant recrystallization is caused by magmatic to submagmatic flow. The main rock forming minerals in the porphyritic biotite granite is K-feldspar, quartz and biotite (**Figure 5.4**). Quartz and K-feldspar occur in similar amount. Myrmekite intergrowth and perthite are also present in several of the samples. Large quartz grains show undulatory extinction and lobate grain boundaries. Accessory phases are apatite, zircon and opaque minerals. Secondary minerals such as chlorite, epidote and sericite are also present.

One variant of the porphyritic granite contains hornblende (**Figure 5.3a**). The granite is usually medium-grained with phenocrysts of K-feldspar. In some cases the granite is foliated and deformed. The texture is igneous, but shows weak evidence of recrystallization. The granite usually has the same amount of hornblende and biotite. The hornblende displays blue to green pleochroism and the biotite displays brown to yellowish pleochroism. Titanite (Spn) and opaque minerals are abundant in these granites. Quartz grains show undulatory extinction and lobate grain boundaries.

Another variant of the granite is coarse-grained, equigranular and contains large quartz crystals (**Figure 5.3g**). This granite does not have K-feldspar phenocrysts or hornblende. The granite is pinkish with smoky quartz phenocrysts. This granite is found as smaller outcrops in several locations in the field area. In other cases the granite appears to be foliated. A similar granite is described in the Knaben-zone by **Stormoen (2015)**.

Granites

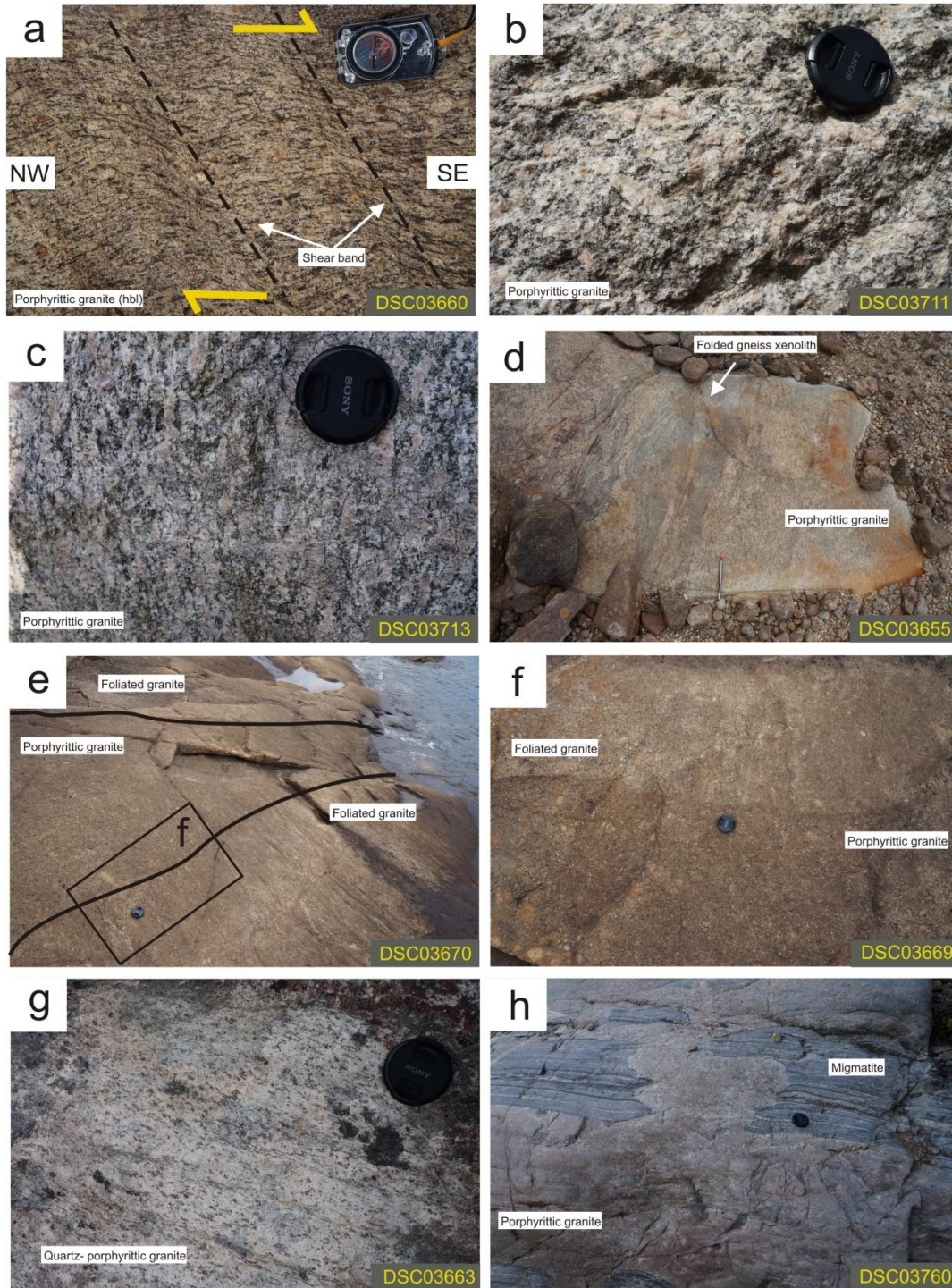


Figure 5.3: Field photographs of granites found in the Kvås-Konsmo area. (a) Porphyritic granite with hornblende. The shear bands indicate a top-to-the-SE movement. (b) Porphyritic biotite granite with K-feldspar phenocrysts. (c) Porphyritic biotite granite with K-feldspar phenocrysts. (d) Folded gneiss xenolith in a porphyritic granite observed in a xenolith-rich zone. (e) Porphyritic granite cutting into an older porphyritic, foliated granite. (f) A closer look at porphyritic granite cutting an older, porphyritic, foliated granite. (g) Quartz-porphyritic granite with a weak foliation. The granite is observed in a xenolith-rich zone. (h) Porphyritic granite cutting into a migmatite.

pinkish migmatite. The migmatites observed in the Kvås-Konsmo area are generally stromatic migmatites which are characterized by a layered structure. The leucosomes and the mesosomes are more or less continuous. The thickness and colour of the leucosomes varies. Alignments of biotite and hornblende in between quartz and plagioclase are typical for the mesosomes. The leucosomes have typically larger grains of K-feldspar and quartz than the mesosomes.

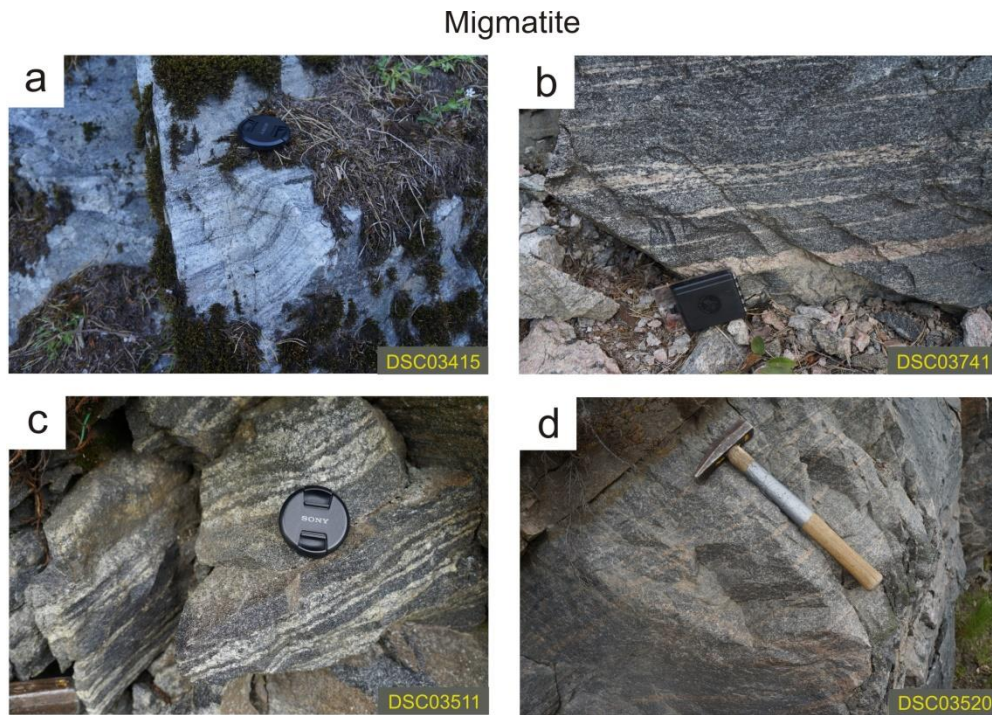


Figure 5.5: Field photographs of migmatites found in the Kvås-Konsmo area. All the migmatites display a stromatic texture. For thin section photos see **Figure 5.19g and h and 5.20c and d**. (a) Fine-grained, grey migmatitic gneiss. (b) Sample no. IH128072 was taken from this outcrop. The leucosomes varies in thickness from 0.1 cm to 5cm. (c) Medium-grained migmatite. The thickness of the leucosomes and mesosomes varies from 0.5 cm to 5cm. (d) Pink leucosomes and grey mesosomes. This migmatite is cut by porphyritic granite.

Metapelite

Metapelite has been observed in xenolith-rich zones at several sites in and outside of the SMB, but are generally restricted to the western part of the SMB, with the exception of the Kvås outcrop. In this study metapelites were studied near Kvås and Lysefjorden. Isoclinal folding is observed in both small-scale and large-scale in the metapelite near Kvås. Such folding indicates high strain deformation. The folding can be seen in a mafic layer in the metapelite, veins of leucosomes and in the metapelite itself (**Figure 5.6**). The metapelites in

Kvås and Lysefjorden have a patch migmatitic structure where the leucosomes are irregular and ranging from a few mm- to several cm-thick and dm-long patches. The foliation in the melanosomes is defined by the alignment of biotite. The leucosomes have a granitic composition with K-feldspar and quartz as the main rock forming minerals. Cordierite, spinel and sillimanite are common in the metapelite from Lysefjorden. Garnet is usually found in the leucosome. For photomicrographs see **Figure 5.21d and 5.22b, c and d**.

Metapelite

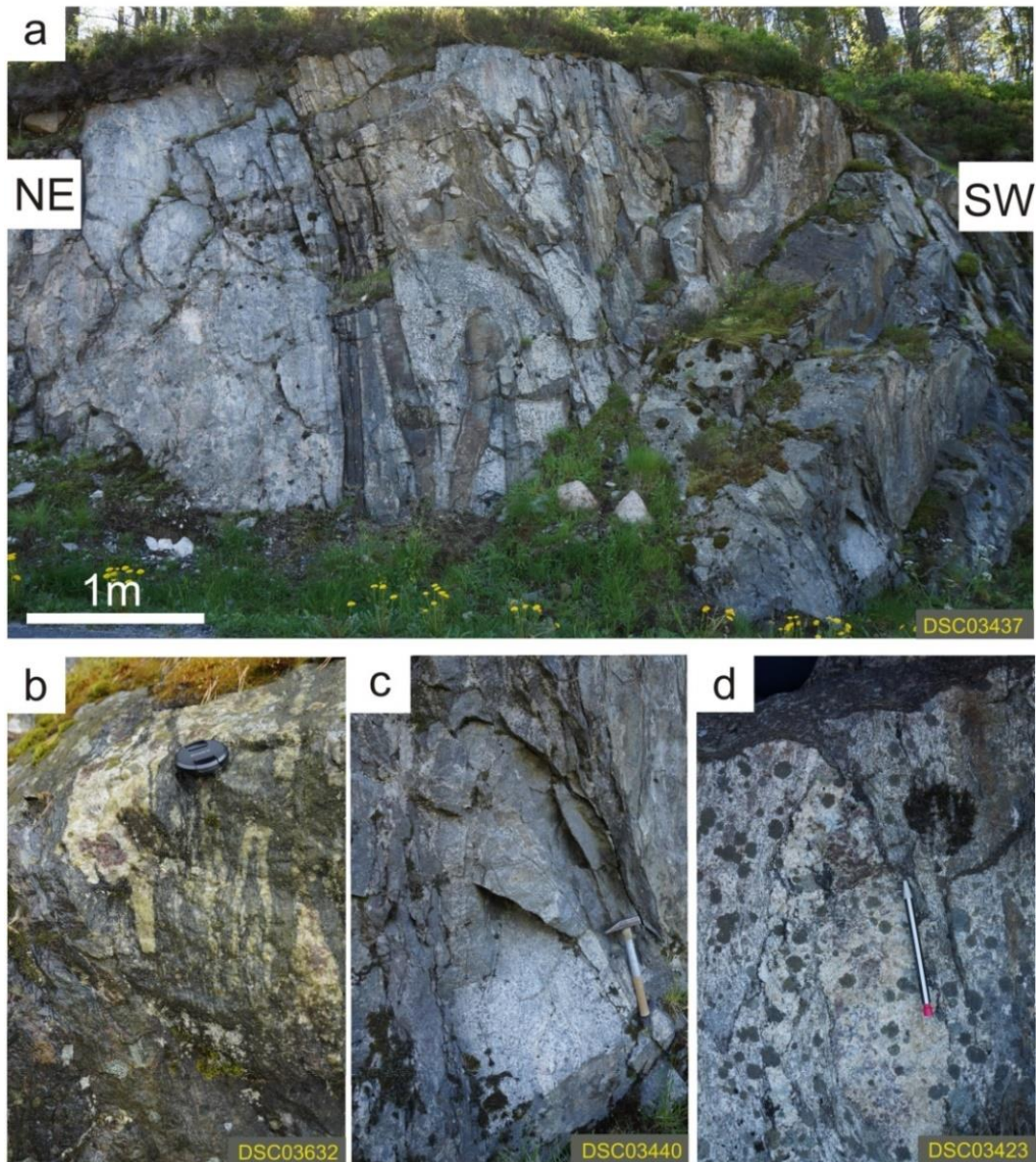


Figure 5.6: Field photographs of metapelite from the Kvås-Konsmo area. (a) Overview of the metapelitic outcrop near Kvås. Note the isoclinal folding of the mafic layer. (b) Folded leucosome with large garnets in metapelite. (c) Folded metapelite. (d) A large leucosome in metapelite with several garnets.

Flaser gneiss

Flaser gneiss has been found several places in the SMB and has been described as one of the most common xenolith lithologies in the Knaben-zone (**Stormoen, 2015**). Rather often flaser gneiss is cut by porphyritic granite with a relative sharp boundary (**Figure 5.7a, b and c**), indicating that the flaser gneiss is older than the porphyritic granite. The flaser gneiss was not dated in this study, but in **Stormoen (2015)** a flaser gneiss located at Knaben was dated and yielded a concordia age of 1253 ± 9 Ma (2σ , MSWD = 5.3). The flaser gneiss is a deformed granite with recrystallized K-feldspar megacrysts in between biotite. K-feldspar, quartz, biotite and hornblende are the main rock forming minerals. Quartz show undulatory extinction and lobate grain boundaries. Zircon, titanite, plagioclase, apatite and opaque minerals are present as accessory phases. Myrmekite and perthite are also present.

Flaser gneiss

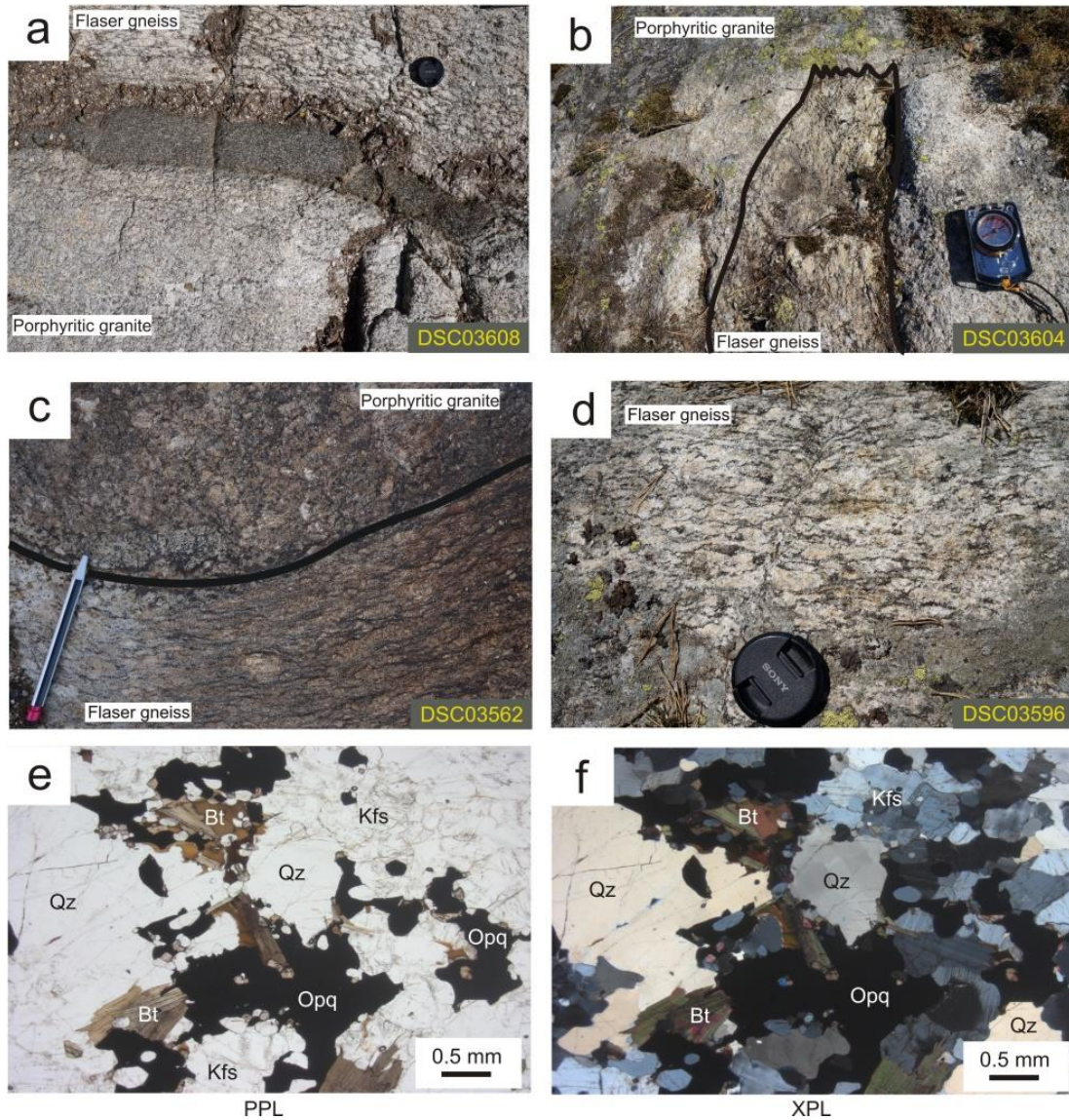


Figure 5.7 (previous page): Examples of flaser gneiss xenoliths in the Kvås-Konsmo area. (a) Amphibolite xenolith between porphyritic granite and flaser gneiss. (b) Flaser gneiss xenolith in porphyritic granite. (c) Flaser gneiss cut by porphyritic granite. (d) Flaser gneiss. (e), (f) The flaser gneiss is similar in composition to the porphyritic granite with hornblende. Quartz, K-feldspar, biotite and hornblende are the main rocks forming minerals. Opaque minerals and titanite (Spn) are also common.

Amphibolite

Amphibolite is the most common xenolith in the Kvås-Konsmo area (**Figure 5.8**). The amphibolites vary in shape, size and number. Most of them are fragments up to 1 meter long. The contact between the amphibolite and the granites and other xenoliths is usually sharp.

The amphibolite is fine-grained, showing nematoblastic to lepidoblastic texture with hornblende and biotite defining the foliation. Plagioclase is the main felsic mineral, apatite and opaque minerals are accessory phases. Chlorite is present as a secondary mineral in amphibolites cut by granites.

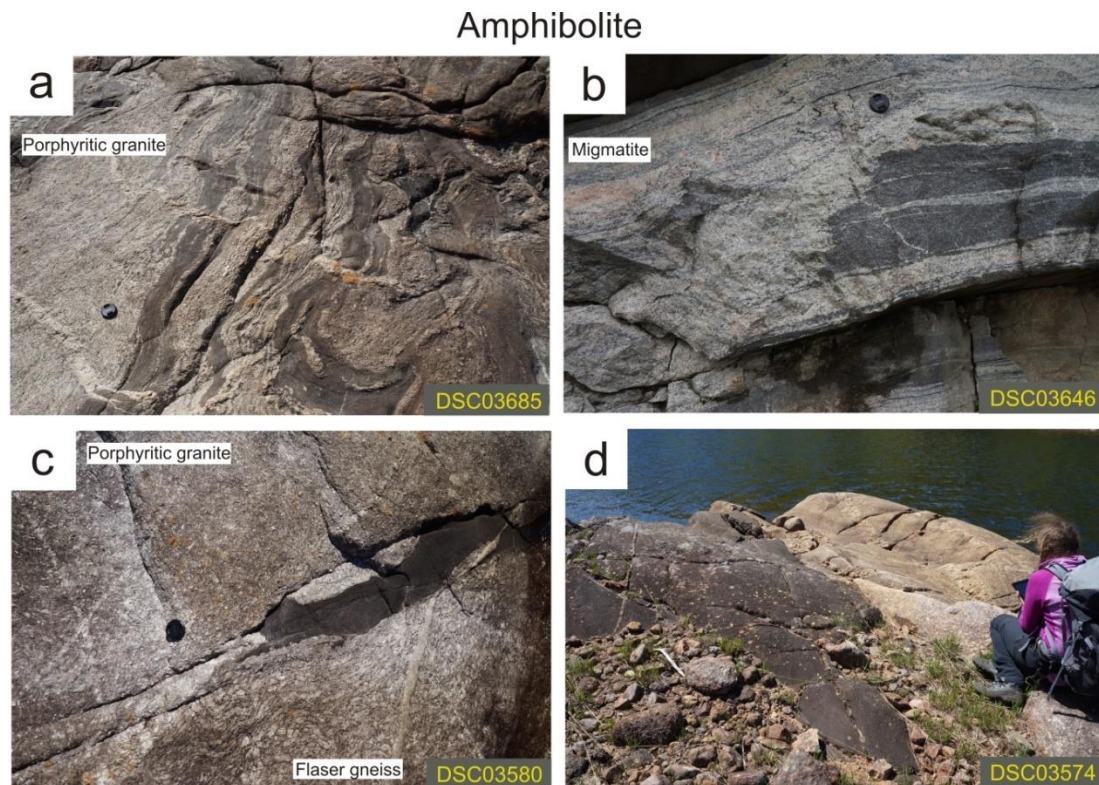


Figure 5.8: Examples of amphibolite xenoliths in the Kvås-Konsmo area. (a) Amphibolite xenoliths folded inside porphyritic granite. (b) Amphibolite xenolith inside migmatite. (c) Amphibolite xenolith between flaser gneiss and porphyritic granite. (d) Amphibolite xenolith in porphyritic granite. This is one of the largest amphibolite xenoliths observed in the Kvås-Konsmo area.

5.1.3 Hornblende biotite granite (HBG)

Plutons of hornblende biotite granite (**Figure 5.9**) are found in the SMB and also in the Kvås-Konsmo area. The granite can be distinguished from SMB-granite by its appearance and also by magnetic susceptibility. The HBG is medium-grained with clusters of biotite and it rarely has K-feldspar phenocrysts. The HBG normally has a higher magnetic susceptibility than the SMB-granite. Near the boundary between the two granites they were difficult to distinguish from each other and the SMB-granite also seems to get higher susceptibility measurements than usual. K-feldspar, quartz, biotite and hornblende are the main rock forming minerals. Zircon, titanite, apatite, plagioclase and opaque minerals are present as accessory phases. Myrmekite and perthite are also present.

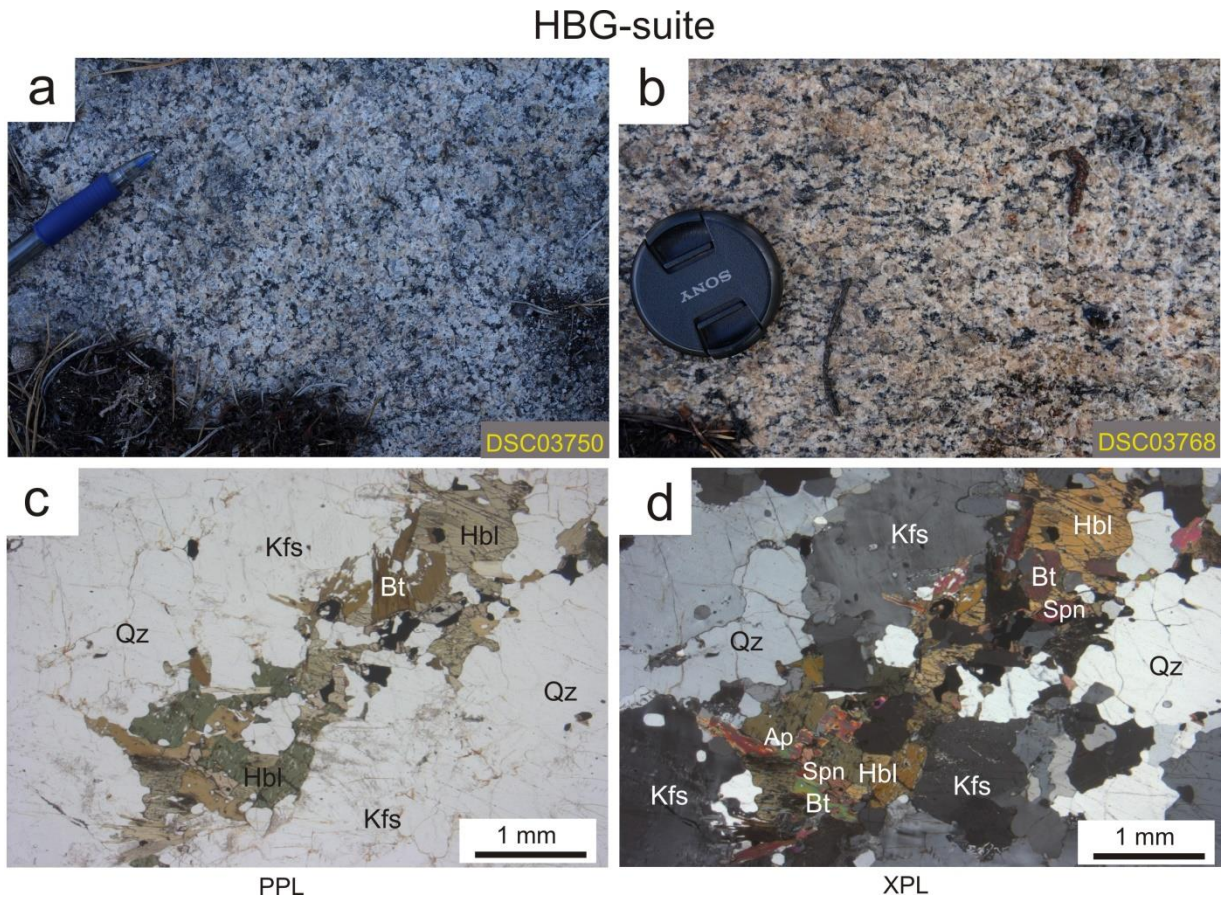


Figure 5.9: (a), (b) Field photographs showing hornblende biotite granite from the Kvås-Konsmo area. Note the distinct clusters of biotite. (c), (d) K-feldspar, quartz, biotite and hornblende are the main rock forming minerals. Titanite (Spn) and opaque minerals are also common.

5.2 Zircon geochronology

13 samples from Gyadalen, Lysefjorden and the Kvås-Konsmo area were analysed using zircon as a geochronometer (1 sample lacked zircon). In this section the samples are presented based on the observations in the field, the petrography and the geochronology data. The samples were divided into three groups: (1) undeformed granite, weakly foliated granite, quartz diorite, (2) migmatites and (3) metapelites. The zircon morphologies are described using **Figure 5.10** as a template.











Crystal shape		Internal structures	
	Prismatic		Oscillatory zoning
	Acicular (~1:10)		Core/rim
	Stubby		Core/mantle
	Euhedral		Embayment core
			Patchy zoning
			Sector zoning

Figure 5.10: Template for describing crystal shape and internal structures of zircon.

5.2.1 Granites, diorite and amphibolite

Undeformed to deformed granite, diorite and amphibolite were dated to obtain a crystallization age and in some cases a possible deformation age of the rock.

Sample IH128056 (amphibolite)

This sample was taken in the road cut between Kvås and Konsmo (32 V 39601, 6459582), from an amphibolite that is cut by granite (**Figure 5.11**). The granite around the amphibolite is medium-grained, pink with up to 2 cm phenocrysts. In the amphibolite small folds of granite are observed; they have a different colour and texture than the granite around. The folded granitic veins are white and grey with 2 mm-large clusters of amphibole. The boundary between the amphibolite and the folds are relative sharp. The amphibolite displays a nematoblastic texture where hornblende and biotite are defining the foliation. Hornblende and plagioclase constitute approximately 85% of the rock. Most of the biotite has been replaced by chlorite. Hornblende has a yellow to olive-green pleochroism. Plagioclase is the main

felsic mineral. Apatite and opaque minerals are accessory phases. Some sauritization of the plagioclase is also present.

Amphibolite (IH128056)

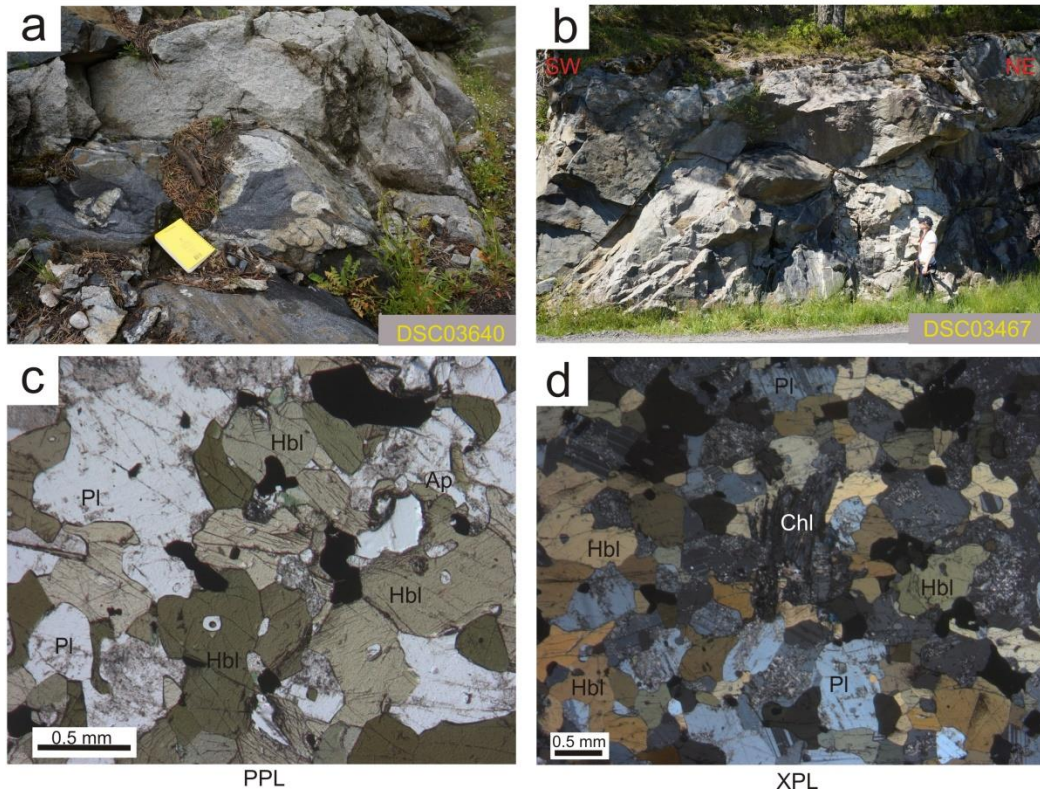


Figure 5.11: Sample IH128056, amphibolite. No zircon was found in this sample. (a) Field photograph showing folded granite in amphibolite. (b) Field photograph of an amphibolite xenolith in porphyritic granite. (c), (d) Photomicrographs of the sample displays nematoblastic texture with hornblende and plagioclase as the main rock forming minerals. Most of the biotite is replaced by chlorite.

Sample IH128058 (diorite)

This sample was taken from a diorite in the road cut between Kvås and Konsmo (32 V 397261, 6459640) in between porphyritic granites (**Figure 5.12**). It is a medium-grained, homogenous diorite with a hypidiomorphic granular texture. A c. 5 mm wide leucocratic vein cuts into the rock. Biotite, hornblende, plagioclase and orthopyroxene are the main rock forming minerals. Hornblende, orthopyroxene and biotite constitute approximately 50% of the rock, while approximately 40% are plagioclase. Hornblende is replacing the orthopyroxene. Zircon, apatite and opaque minerals are present as accessory phases. Zircon is found in biotite, plagioclase, hornblende and opaque minerals.

The zircons are prismatic, colourless to brownish on tape and c. 100-200 μm . The BSE image of the zircons displays several cracks. The grain-parallel, patchy zonation seen in the CL-image can be the result of alteration along these cracks.

Twelve zircons were dated from this sample. A regression line through the geochronological data intercept the concordia curve at $991 \pm 11 \text{ Ma}$ (2σ , MSWD = 0.47). This age is interpreted to represent the crystallization age of the diorite.

Sample IH128068 (deformed porphyritic granite)

This sample was taken by the Sundsvatn Lake (32 V 400453, 6465027) from a porphyritic granite that is cut by several pegmatites. The granite is foliated and seems to be weakly deformed. It has up to 3 cm phenocrysts and clusters of biotite and hornblende (**Figure 5.13**). It is a medium grained granite with an allotriomorphic texture. Quartz, K-feldspar, biotite, hornblende and plagioclase are the main rock forming minerals. Titanite, zircon, apatite and opaque minerals are present as accessory phases. The opaques, hornblende, biotite and titanite constitute approximately 20% of the rock, while the feldspars constitute approximately 50% of the rock. Quartz constitutes c. 30% of the rock. The hornblende displays blue to green pleochroism. The quartz has lobate grain boundaries and displays undulatory extinction.

The zircons are prismatic, colourless to brownish on tape and c. 150 μm . In the CL-images some of the grains have bright cores cut by darker rims; some show an oscillatory zonation while others show a patchy zonation.

Twelve zircons were dated from this sample. A regression line through the geochronological data intercept the concordia curve at $1045 \pm 20 \text{ Ma}$ (2σ , MSWD = 1.06). One of the analyses (no. 10) was excluded from the calculations due to a high common lead content. The Tera-Wasserburg plot has a horizontal array. This can be a result of fractionation; a weighted $^{207}\text{Pb}/^{206}\text{Pb}$ age was therefore calculated. The weighted $^{207}\text{Pb}/^{206}\text{Pb}$ gives an age of $1042 \pm 14 \text{ Ma}$. The same analysis (no. 10) was excluded by Isoplot. The rims in the zircons look metamorphic. Most of them were too small to date, so most of the dated material came from the cores. The age is therefore interpreted to represent the crystallization age of the granite. One important point to consider is that if the crystallization age and the deformation age of the granite are separated only by a few million years the difference will not be resolvable.

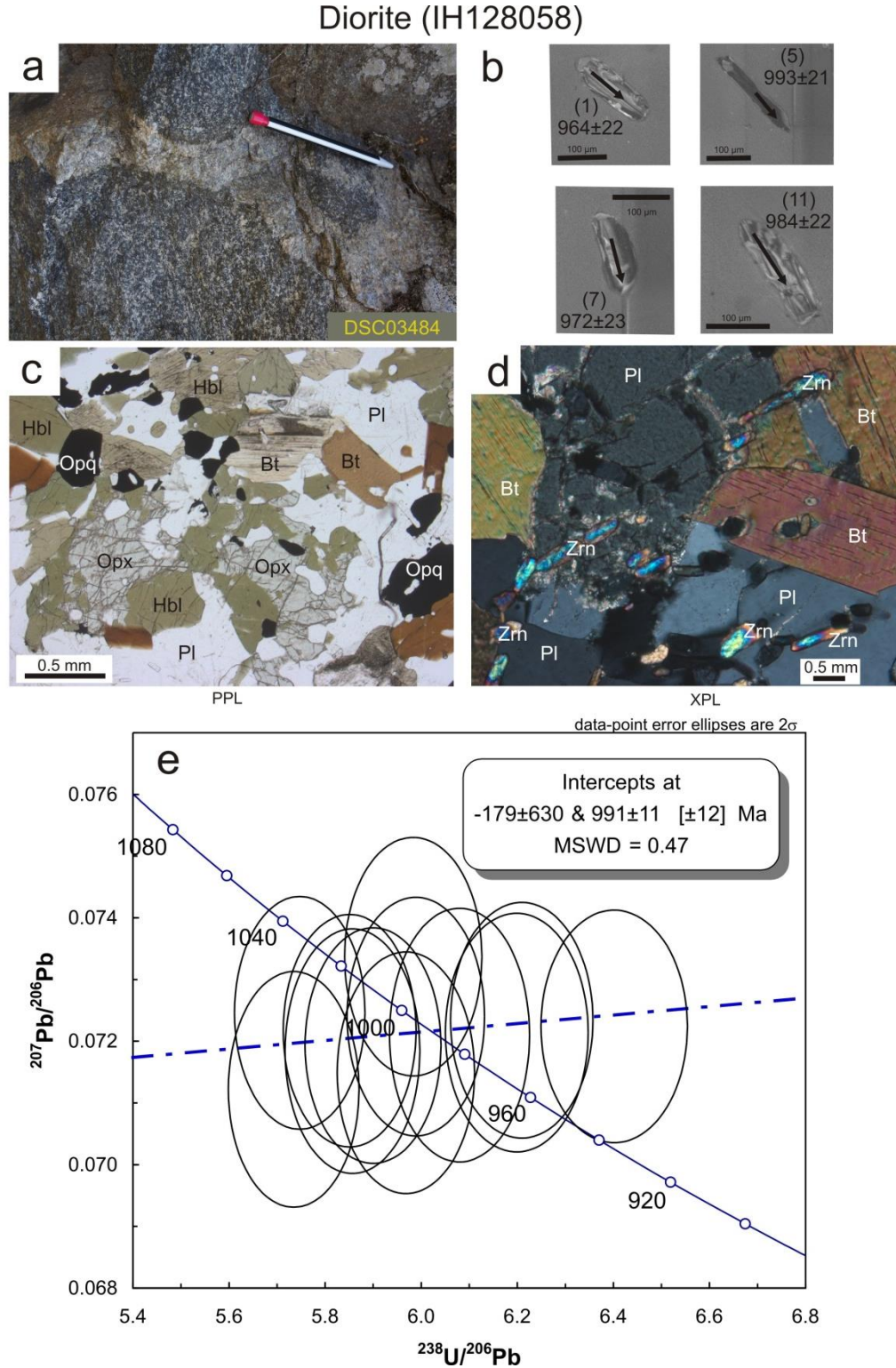


Figure 5.12: Sample IH128058, diorite. (a) Field photograph. A c. 5 mm leucocratic vein cuts into the diorite. (b) Four selected CL-images of dated zircons with arrows showing where the crystals were analysed (c), (d) Photomicrographs. The diorite displays hypidiomorphic granular texture with hornblende, biotite, orthopyroxene and plagioclase as the main rock forming minerals. (e) Tera-Wasserburg plot of the U-Pb data from the sample.

Deformed porphyritic granite (IH128068)

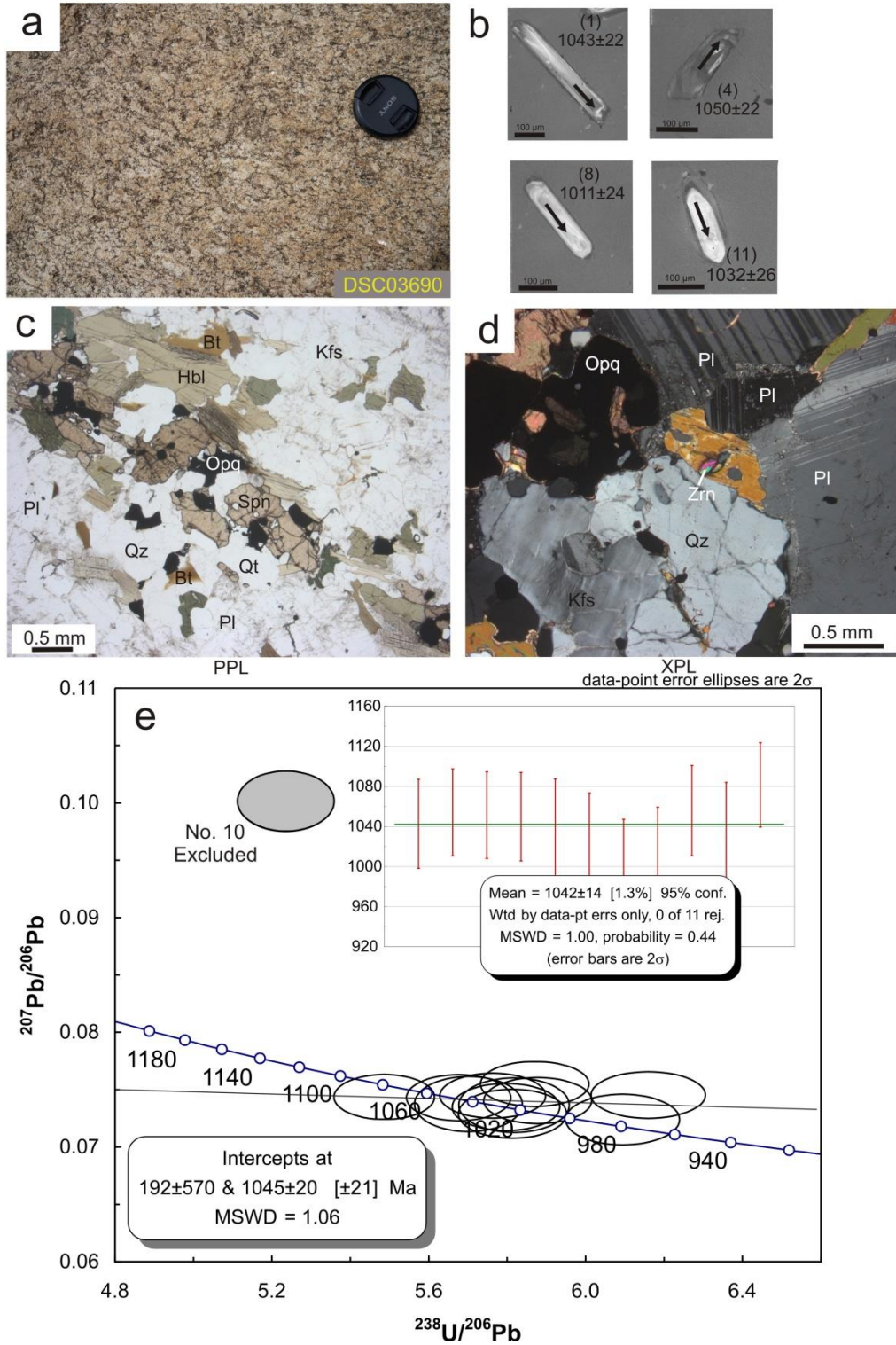


Figure 5.13: Sample IH128068, deformed porphyritic granite. (a) Field photograph. (b) Four selected CL-images of dated zircons with arrows showing where the crystals were analysed. (c), (d) Photomicrographs. The granite displays an allotriomorphic texture. Quartz, biotite, K-feldspar, plagioclase and hornblende are the main rock forming minerals. Opaque minerals and titanite (Spn) are also common. (e) Tera-Wasserburg plot of the U-Pb data and a weighted $^{207}\text{Pb}/^{206}\text{Pb}$ diagram. No. 10 was excluded from the calculations.

Sample IH128070 (folded porphyritic granite)

This sample was taken from a folded porphyritic granite, situated in a xenolith rich zone by Hellevatn Lake (**Figure 5.14**) (32 V 401687, 6465410). A detailed description of the structures in this outcrop is found in **section 5.4.2**. The granite is folded, but it also seems to cut the foliation in the gneiss surrounding the granite. The granite is grey with up to 2 cm phenocrysts. The whole rock was crushed during the mineral separation so no thin sections were available for petrographic description.

The zircons are brownish on tape, stubby to prismatic and c. 100 μm . The CL- images show dark zircons with no rims, some with oscillatory zonation and some with patchy zonation.

Twelve zircons were dated from this granite. The geochronological data are not very good and show high discordance and common lead. Six analyses were excluded to be able to calculate an age (no. 4, 5, 9, 10, 11 and 12). A regression line through the geochronological data intercept the concordia curve at $1050 \pm 39 \text{ Ma}$ (2σ , MSWD = 0.18). This age is interpreted to represent the crystallization age of the granite.

Sample IH128074 (foliated porphyritic granite)

This sample was taken from a foliated porphyritic granite in the road cut between Kvås and Konsmo (32 V 398980, 6460798). The granite is cut by some c. 5 cm-thick pegmatitic veins (**Figure 5.15**). The granite has some phenocryst up to 1 cm, but most of them are recrystallized. It is a medium grained granite with an allotriomorphic texture. K-feldspar, quartz and biotite are the main rock forming minerals. The quartz grains are large, up to 6 mm, and show undulatory extinction and lobate grain boundaries. Zircon, apatite and opaque minerals were present as accessory phases. Myrmekite and perthite are also present.

The zircons are brown on tape, c. 150 μm , stubby to prismatic with some inclusions. The zircons are relative dark in the CL- images, showing a patchy zonation.

Twelve zircons were dated from this granite. Three analyses were excluded due to common lead (no. 3, 4 and 6). The rest of the analyses yield a concordia age of $1043 \pm 22 \text{ Ma}$ (2σ , MSWD = 2.2). This age is interpreted to represent the crystallization age of the granite.

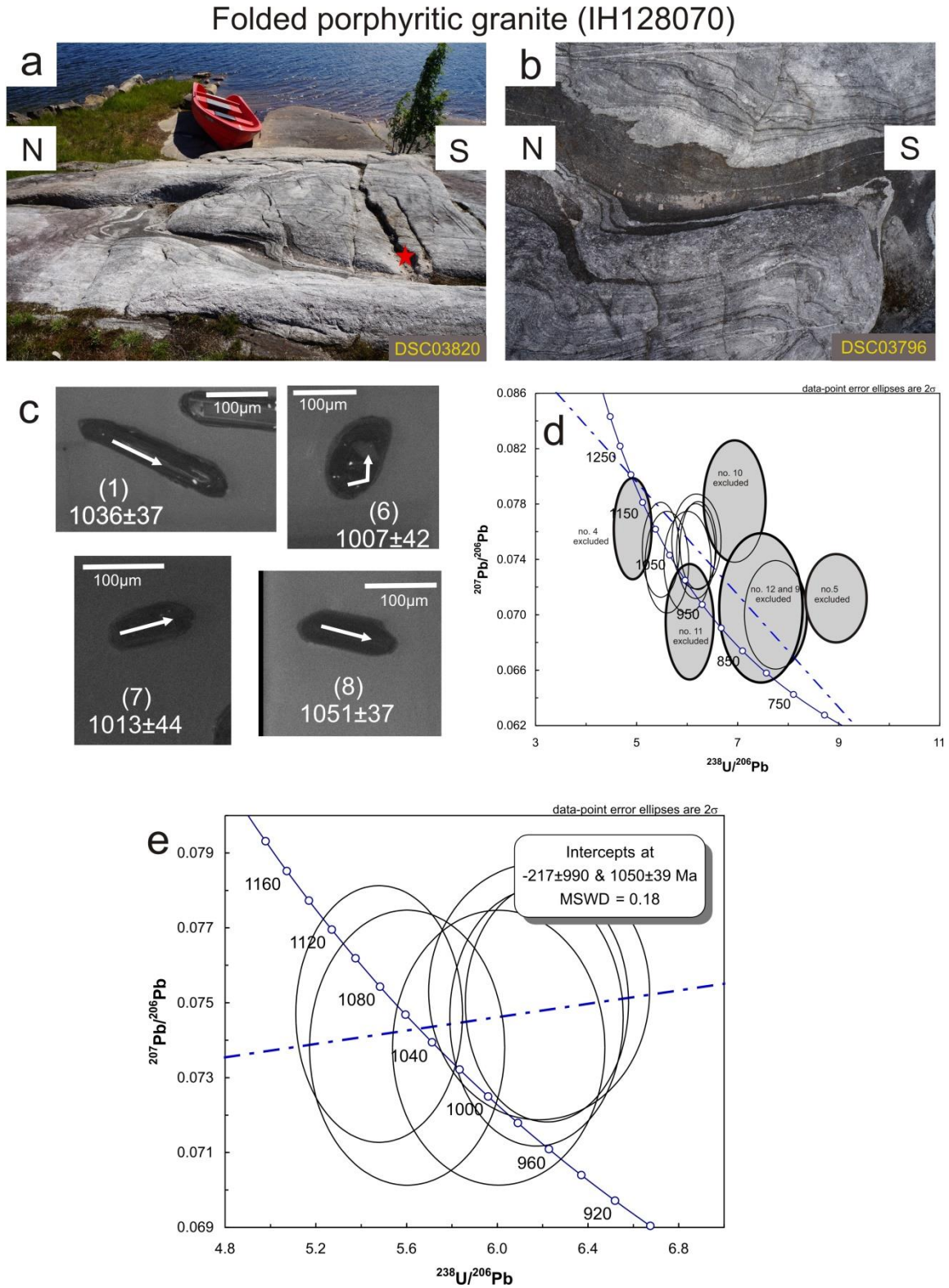


Figure 5.14: Sample IH128070, folded porphyritic granite. **(a)** Overview over the outcrop. Red star indicate where the sample was taken. **(b)** Field photograph showing folded granite, gneiss and amphibolite. **(c)** Four selected CL-images of dated zircons with arrows showing where the crystals were analysed. **(d)**, **(e)** Tera-Wasserburg plot of the U-Pb data. Six analyses were excluded to be able to calculate an age (no. 4, 5, 9, 10, 11 and 12).

Foliated porphyritic granite (IH128074)

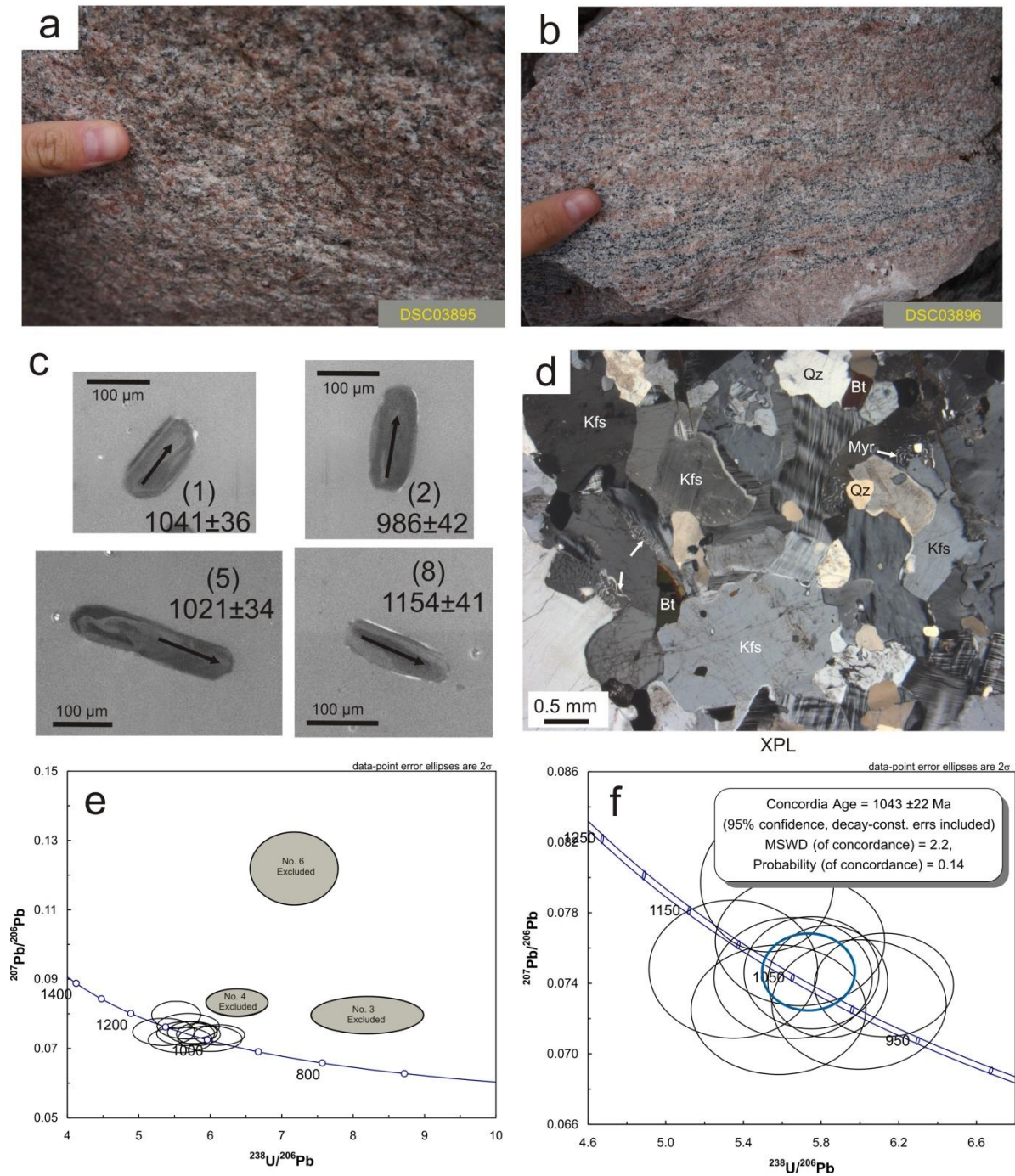


Figure 5.15: Sample IH128074, foliated porphyritic granite. (a), (b) Field photograph. (c) Four selected CL-images of dated zircons with arrows showing where the crystals were analysed. (d) The granite displays allotropic texture. K-feldspar, biotite and quartz are the main rock forming minerals. (e) Tera-Wasserburg plot of the U-Pb data. Three analyses were excluded (no. 3, 4 and 6). (f) Tera-Wasserburg plot of the U-Pb data.

Sample VAG084396 (granitic gneiss)

This sample was taken from the Gyadalen transect from a granitic gneiss (**Figure 5.16**) (32 V 356101, 6502651). The texture is medium-grained to locally granoblastic. Quartz and K-feldspar are the main rock forming minerals. Biotite is sparse and where found it is chloritized. The foliation is defined by large, elongated quartz crystals. The quartz also displays undulatory extinction. Apatite, zircons and opaque minerals are present as accessory phases. Myrmekite, perthite and alteration of feldspar are also present.

The zircons are rounded, c. 300 μm , stubby to prismatic and relative dark in the CL-images. Most of the zircons have rims which seem to cut into an older zonation.

Twelve analyses were taken from this sample, but only 10 were used to calculate an age. A regression line through the geochronological data of the cores intercept the concordia curve at 1048 ± 22 Ma (2σ , MSWD = 1.7). This age is interpreted to represent the crystallization age of the granite. The rims (red ellipses) are younger and are probably representing recrystallization of the zircons at c. 1017 Ma, but more analyses from the rims are needed to determine this.

Sample VAG084397 (quartz dioritic migmatitic gneiss)

This sample was taken from the Gyadalen transect from a quartz dioritic migmatitic gneiss (**Figure 5.17**) (32 V 357625, 6503462). The texture is medium-grained to granoblastic. The main rock forming minerals are quartz, hornblende, plagioclase, clinopyroxene, biotite and apatite. This sample contains a lot of apatite which are common for the migmatitic quartz dioritic gneisses in the surrounding area (**Coint, personal communication**). Zircons and opaque minerals are accessory phases. Hornblende displays yellow to brown pleochroism, indicating high temperature and Ti-rich conditions. Clinopyroxene is pale green and have two main directions of exsolution. The quartz have lobate grain boundaries and show undulatory extinction.

The zircons are rounded, c. 200 μm with rims that cut the cores, some of the rims are thick enough to be called mantles. Most of the cores have an oscillatory zonation, but some also have sector zonation.

Twelve analyses were taken from cores and rims in this sample. They were plotted using different colours (orange = core, black = rim). The cores yield a concordia age of 1029 ± 7 Ma (MSWD = 0.037). A regression line through the geochronological data for the rims

intercept the concordia curve at 1038 ± 34 Ma (2σ , MSWD = 0.18). The rims and the cores yield approximately the same age; one age were therefore calculated and yield an upper intercept at 1033 ± 17 Ma (2σ , MSWD = 0.37). The rims cut the zonation in the cores indicating that they are younger; the texture of the rock also indicates deformation. The best explanation of the age data is therefore that crystallization and metamorphism of the rock happened within the uncertainty of the data.

Sample VAG084399 (foliated porphyritic hbl bt granite)

This sample was taken from a foliated porphyritic hornblende biotite granite from the Gyadalen transect (**Figure 5.18**) (32 V 359379, 6504170). This granite has a porphyritic to local granoblastic texture. The main rock forming minerals are quartz, K-feldspar, plagioclase, hornblende and biotite. Apatite, zircon and opaque minerals are accessory phases. The foliation is defined by biotite, hornblende and large, elongated quartz grains. The quartz also displays undulatory extinction and lobate grain boundaries. Myrmekite is also present.

The zircons are c. 200 μm , rounded to euhedral and relative dark in the CL-image. Most of the grains have a patchy zonation, some have an oscillatory zonation and some do not show any internal structures. Some of the grains have rims which seem to cut the older zonation.

Twelve zircons were analysed from this sample. The geochronological data yield a concordia age of 1037 ± 7 Ma (2σ , MSWD = 0.01). The age is interpreted to represent the crystallization age of the granite.

Granitic gneiss (VAG084396)

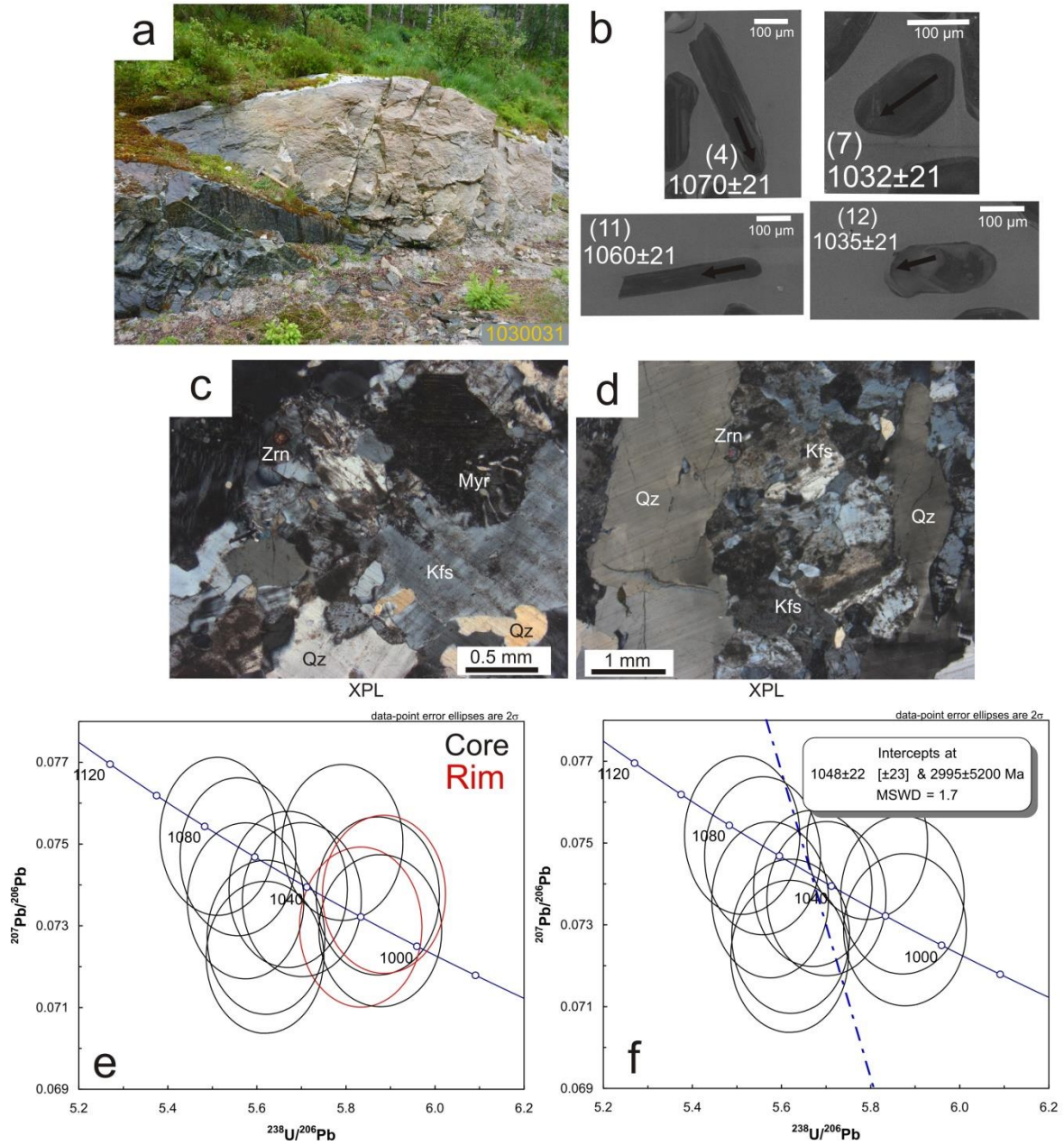


Figure 5.16: Sample VAG084396, granitic gneiss. *(a)* Field photograph: Nolwenn Coint. *(b)* Four selected CL-images of dated zircons with arrows showing where the crystals were analysed. *(c)*, *(d)* Photomicrographs. The granitic gneiss is medium-grained to locally granoblastic. K-feldspar and quartz are the main rock forming minerals. The foliation is defined by large, elongated quartz crystals. *(e)* Tera-Wasserburg plot of the U-Pb data. Red ellipses indicate analysed rims, black indicate analysed cores. *(f)* Tera-Wasserburg plot of the U-Pb data, only cores are plotted.

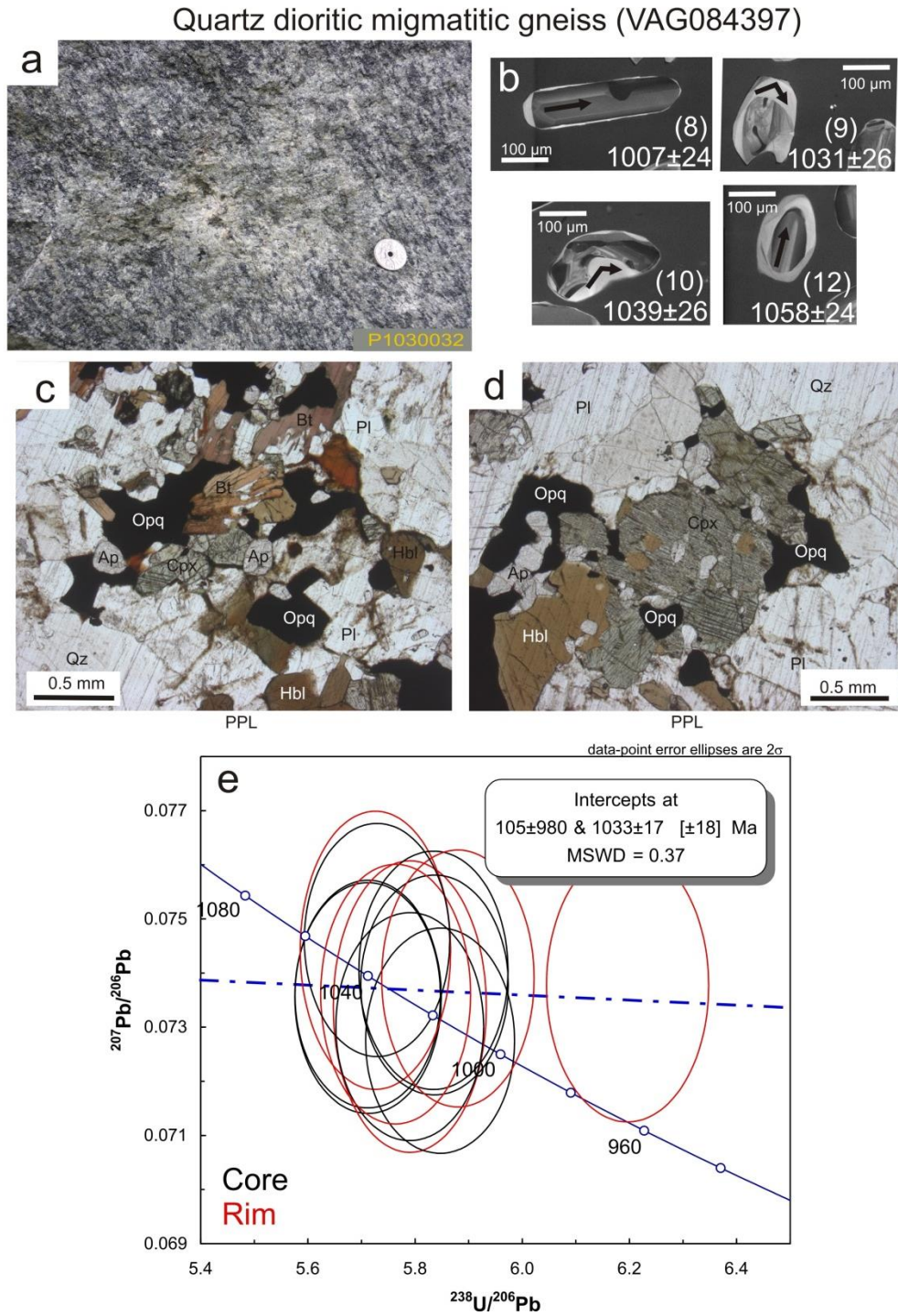


Figure 5.17: Sample VAG084397, quartz dioritic migmatitic gneiss. **(a)** Field photograph showing a leucosome. Photo: Nolwenn Coint. **(b)** Four selected CL-images of dated zircons with arrows showing where the crystals were analysed. **(c)**, **(d)** The quartz dioritic migmatitic gneiss is medium-grained to granoblastic. Quartz, hornblende, plagioclase, clinopyroxene, biotite and apatite are the main rock forming minerals. **(e)** Tera-Wasserburg plot of the U-Pb data.

Foliated porphyritic hbl bt granite (VAG084399)

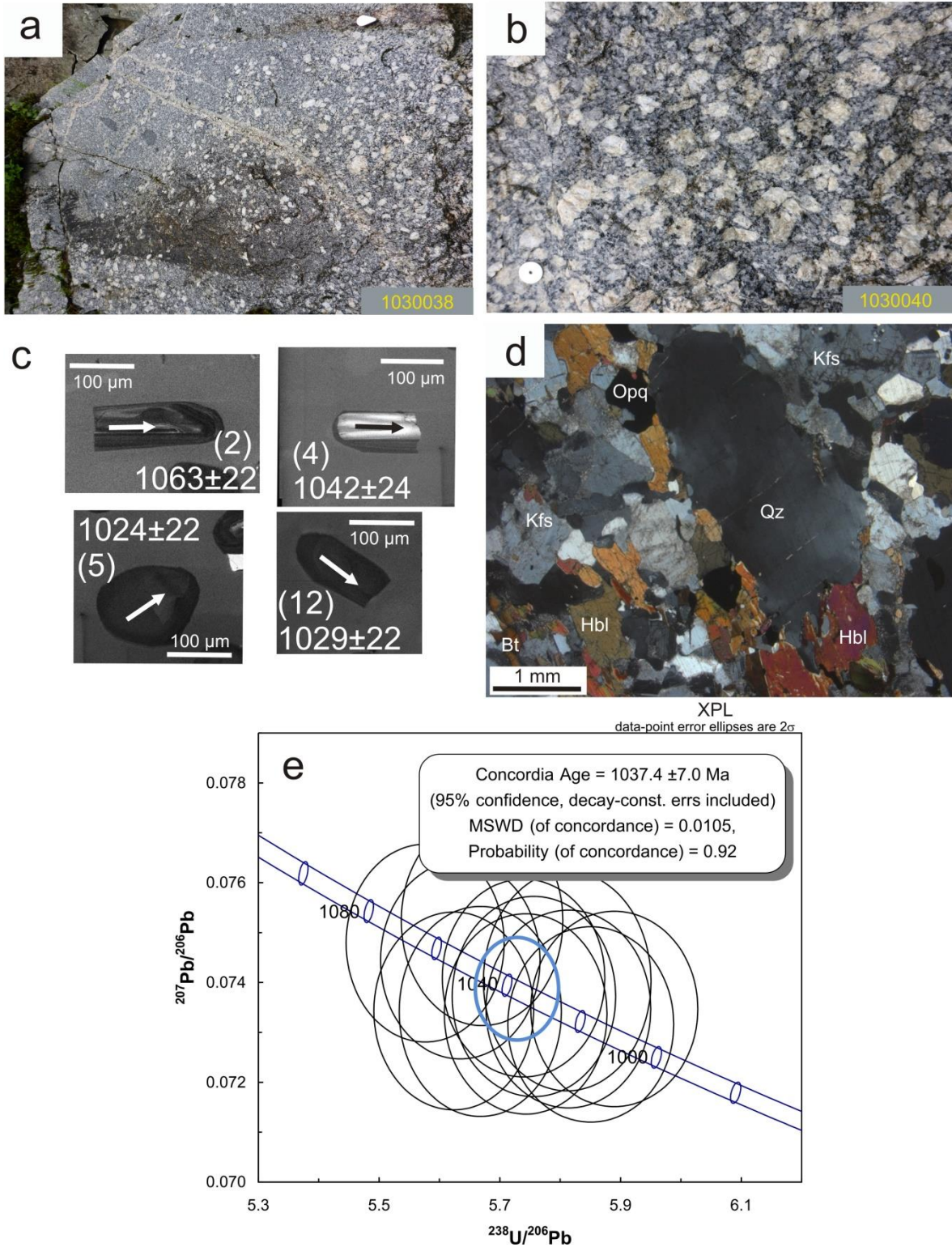


Figure 5.18: Sample VAG084399, foliated porphyritic hornblende biotite granite. (a), (b) Field photograph: Nolwenn Coint. (c) Four selected CL-images of dated zircons with arrows showing where the crystals were analysed. (d) The granite display porphyritic to local granoblastic texture. Quartz, K-feldspar, plagioclase, hornblende and biotite are the main rock forming minerals. (e) Tera-Wasserburg plot of the U-Pb data.

5.2.2 Migmatites

Zircon was separated from migmatites in order to obtain a protolith age, and more importantly, determine the age of the migmatization.

Sample IH128065A (mesosome) and IH128065B (leucosome)

Sample IH128065 was taken from a migmatite near Konsmo (32 V 403000, 6461183). It was divided into two samples to see if there was any difference in age between the mesosome and the leucosome (**Figure 5.19**). Sample A was taken from the mesosome and sample B from the leucosome. The migmatite is a stromatic migmatite which is characterized by a layered structure. The leucosomes and the melanosomes are more or less continuous. The foliation in the mesosome is defined by alignment of c. 2 mm- thick biotite layers in between c. 5mm-thick quartz, plagioclase and K-feldspar layers. The leucosome consist of larger K-feldspar and quartz grains. The thin sections show some seritization of the K-feldspar. Biotite is sparse in the leucosome, but when found it is chloritized. Opaque minerals, zircon, muscovite and chlorite are accessory phases in the leucosome while opaque minerals, zircon, chlorite, epidote and apatite are accessory phases in the mesosome.

IH128065A (mesosome)

The zircons are stubby to prismatic, up to 200 μm , brown with some inclusions. The internal structures are varied; some show an oscillatory zonation, some are CL-dark and others show a patchy zonation.

Twelve zircons were analysed from this sample. The geochronological data show an upper intercept at 1464 ± 21 Ma (2σ , MSWD = 0.28). This age is interpreted to be the age of the migmatitic protolith.

IH128065B (leucosome)

Half of the mounted zircons were colourless, up to 300 μm , prismatic with almost no inclusions. The other half of the mounted zircons were brown, up to 500 μm , prismatic with several inclusions. The CL-images show zircons with an oscillatory zonation and zircons with a patchy zonation. The colourless zircons are brighter than the brown zircons in the CL-images, indicating higher uranium content in the darker zircons.

Twelve zircons were analysed from this sample. Three of the colourless zircons (no.10, 11 and 12) and 9 brown zircons were dated. The geochronological data do not show any

difference between the colourless zircons and the brown zircons. A regression line through the geochronological data for the rims intercept the concordia curve at 1039 ± 17 Ma (2σ , MSWD = 1.7). Two outliers were excluded from the calculations (no. 4 and 8). This age is interpreted to be the age of the partial melting of the rock.

Sample IH128072 (migmatite)

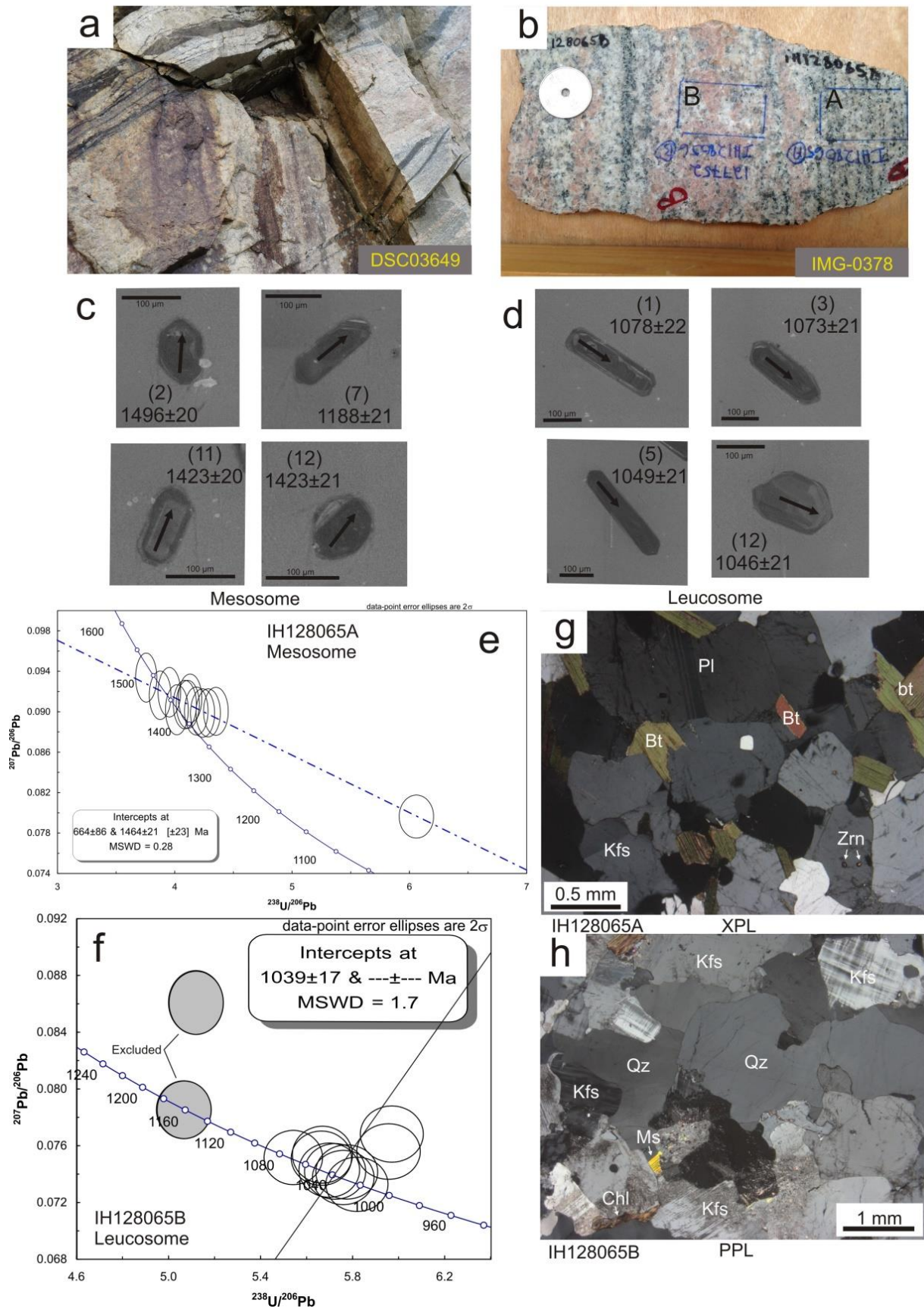
This sample was taken from a migmatite near Konsmo (**Figure 5.20**) (32 V 402995, 6461179). The migmatite has a nematoblastic texture where the foliation is defined by biotite and amphibolite rich layers and more leucocratic, quartzo-feldspathic layers which varies in thickness from c. 1 mm-5mm. The main rock forming minerals are hornblende, biotite, plagioclase and quartz. The hornblende and biotite constitute approximately 35% of the rock, while quartz and plagioclase constitute approximately 60% of the rock. The quartz show undulatory extinction and lobate boundaries, the hornblende has a yellow to dark green pleochrosim. Zircon, apatite and opaque minerals are present as accessory phases.

The zircons are colourless to brown, c. 150 μ m, rounded with some inclusions. Most of the zircons display very irregular zonation with zones of recrystallization and new growth. Some of the grains have a core with oscillatory zonation, but most of them have a patchy zonation.

Twelve analyses were taken from this sample. The zircons were divided into two populations; orange for rims and black for cores. A concordia age was calculated for the rims which yield an age of 1065 ± 23 Ma (2σ , MSWD = 0.38). This age is interpreted to represent the age of migmatization. The cores show ages around 1450 Ma, which probably represents the age of the protolith.

Figure 5.19 (facing page): Sample IH128065, migmatite. (a) Field photograph from where the sample was taken. (b) Hand sample showing where the two thin sections were taken. (c), (d) Four selected CL-images of dated zircons with arrows showing where the crystals were analysed. (e) Tera-Wasserburg plot of the U-Pb data from sample IH128065A. (f) Tera-Wasserburg plot of the U-Pb data from sample IH128065B. Two analyses were excluded (no.4 and 8). (g) IH128065A: Biotite, K-feldspar and quartz are the main rock forming minerals. (h) IH128065B: K-feldspar and quartz are the main rock forming minerals.

Migmatitic mesosome and leucosome (IH128065A and IH128065B)



Migmatite (IH128072)

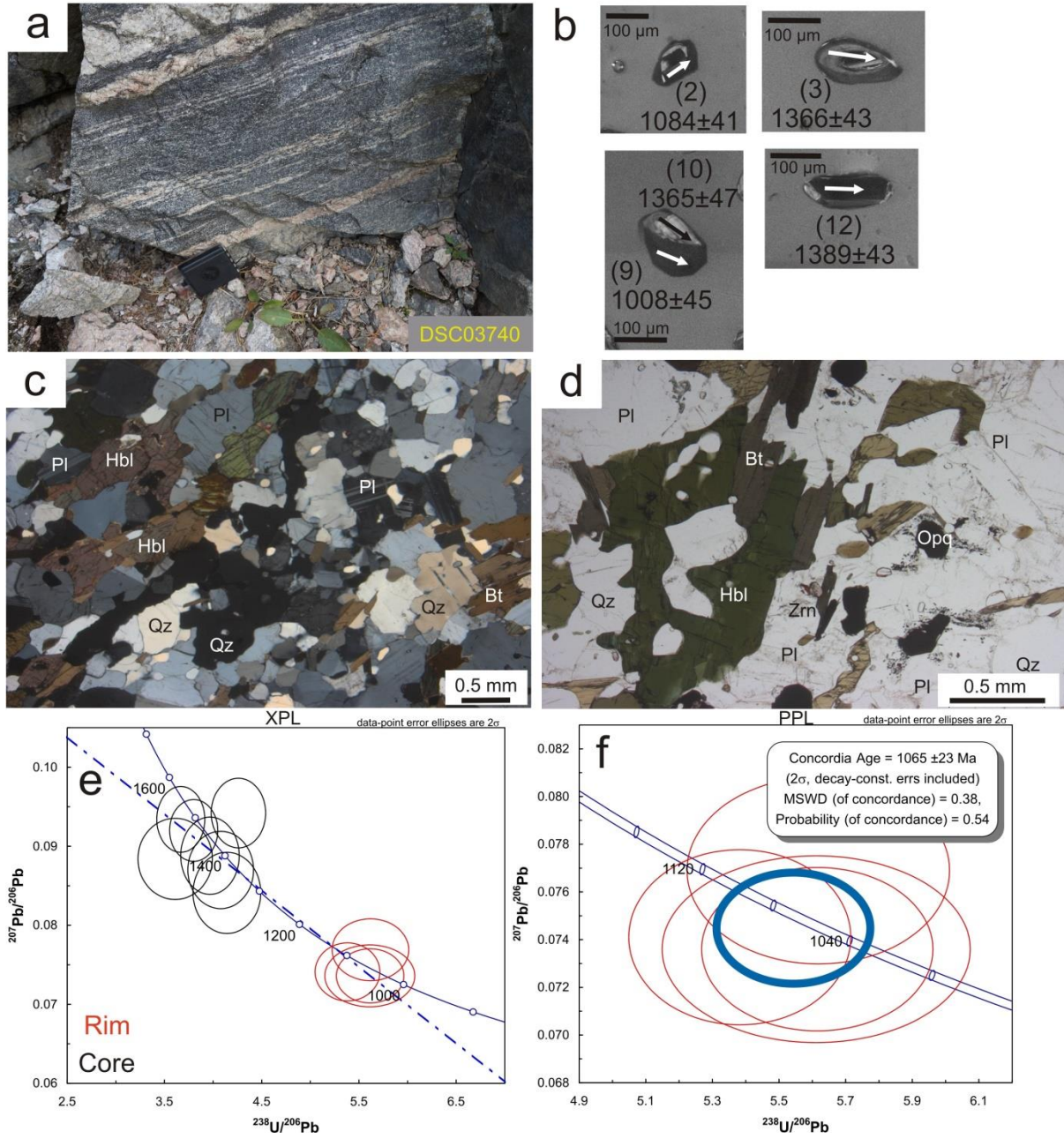


Figure 5.20: Sample IH128072, migmatite. (a) Field photograph. (b) Four selected CL-images of dated zircons with arrows showing where the crystals were analysed. (c) Thin section showing a leucosome and a part of a melanosome. (d) The migmatite displays nematoblastic texture with hornblende, biotite, plagioclase and quartz as the main rock forming minerals. (e) Tera-Wasserburg plot of the U-Pb data. Two distinct groups were identified, one group for the cores and one for the rims. (f) Tera-Wasserburg plot of the U-Pb data.

5.2.3 Metapelites

From the metapelites, zircon and monazite were separated (monazite data in **section 5.3**). Metapelites are metamorphic, fine grained rocks with a sedimentary protolith. These rocks have detrital zircons usually from different sources yielding different ages. The metapelites were dated to determine the age of deformation and metamorphism.

Sample IH128061 (metapelite)

This sample was taken from a metapelite from the xenolith-rich zone near Kvås (**Figure 5.21**) (32 V 395379, 6459660). Several closed- to isoclinal folds were observed in the metapelite, indicating high strain deformation. The metapelite has a patch migmatitic texture with leucosomes with irregular shapes and sizes. The melanosomes mainly consist of aligned biotite with smaller grains of quartz and plagioclase. The biotite shows micro-folding in the thin-sections. The leucosomes mainly consist of anhedral to subhedral quartz and plagioclase. The garnet is up to 2-3 cm and mainly found in the leucosomes. The garnet has inclusions of quartz, biotite and apatite. Zircon, monazite, apatite and opaque minerals are present as accessory phases. The biotite is chloritized several places. The edges of the plagioclase show some seritization. The monazite and the zircon are found in the leucosomes and the melanosomes as inclusions in garnet, plagioclase, quartz and biotite. The monazites are relative large, up to 0.5 mm.

The zircons are c. 100 μm . Most of the zircons have cores with younger rims. Some of the grains have cores that are bright in the CL-images, others are dark.

35 zircons were analysed from this sample. They plot along the concordia curve, as expected for a metapelite. The zircons were grouped using different colours; red for metamorphic rims, green for dark grains, blue for zircons with low Th/U and black for other zircons. One group of zircons that include rims and most of the dark grains were chosen for further calculations (**Figure 5.21g**). They had a vertical trend in the Tera-Wasserburg diagram, indicating common lead; the data were therefore anchored in common lead using the Two-stage model by **Stacey and Kramers (1975)** (at 1 Ga, $^{207}\text{Pb}/^{206}\text{Pb} = 0.9$). The zircons yielded an age of 1024 ± 9 Ma (2σ , MSWD = 2.0). This age is interpreted to represent the timing of metamorphism.

Two blue ellipses indicating low Th/U zircons yielded an age of c. 930 Ma. The metapelite is situated only 500 meters from a 951 Ma HBG-suite (**Slagstad, personal communication**); this age is therefore interpreted to represent recrystallization/resetting of the zircons.

A metapelite mostly consists of detrital zircons. The zircons that showed less than 10% central discordance and were older than 1100 Ma ($^{207}\text{Pb}/^{206}\text{Pb}$) were plotted in a probability plot. A total of 16 zircons were plotted. The probability plot shows ages ranging between 1100 and 3000 Ma with one distinct peak at 1550 Ma.

Sample ROG092326 (metapelite from Lysefjorden)

This sample was taken from a metapelite located near Lysefjorden (**Figure 5.22**) (32 V 3334213, 6532806). The metapelite has up to 3 cm big garnets located in the leucosomes. A 10 cm-thick granitic vein cuts into the metapelite. The metapelite is folded and show several closed- to isoclinal folds indicating high strain deformation. The metapelite has a patch migmatitic texture with irregular shapes and sizes leucosomes. Cordierite, plagioclase, biotite, quartz, garnet and sillimanite are the main rock forming minerals. Zircon, monazite, apatite, green spinel and opaque minerals are present as accessory phases. The sillimanite is present as prismatic inclusions in the garnets. This has been recorded in several other metapelites in the southwestern region (**Coint, personal communication**). Folding of garnet can be seen in the thin section (**Figure 5.22b**). The garnet has inclusions of cordierite, green spinel, sillimanite, opaque minerals and biotite. The sillimanite in the fold are aligned and follows the fold. The sillimanite in the other garnets are more chaotic and do not show any specific orientation. A lot of the cordierite has been altered to pinnite (muscovite). Zircon is found in cordierite, garnet and quartz. Zircons found in the cordierite display yellow haloes. Symplectite texture with reaction between green spinel, opaque minerals and sillimanite are observed (**Figure 5.22d**).

The zircons are c. 100 μm . Some of the grains show oscillatory zonation, some are dark with no internal structures and some of the zircons display very irregular concentric zonation that is overprinted by zones of recrystallization or new growth. Several of the grains have core zonation cut by rims.

42 analyses were taken from this sample. The zircons were grouped using different colours; red for dark grains and rims, the rest were coloured black. One group of rims and dark grains plotted around 1000 Ma and were chosen for further calculations. A regression line through

5 Results

the geochronological data intercept the concordia curve at 1035 ± 17 Ma (2σ , MSWD = 1.6). This age is interpreted to represent deformation of the metapelite.

Zircons which showed less than 10% central discordance and were older than 1400 Ma ($^{207}\text{Pb}/^{206}\text{Pb}$) were plotted in a probability plot. A total of 26 zircons were plotted. The probability plot shows ages ranging between 1300 Ma and 2100 Ma with one distinct peak at 1550 Ma.

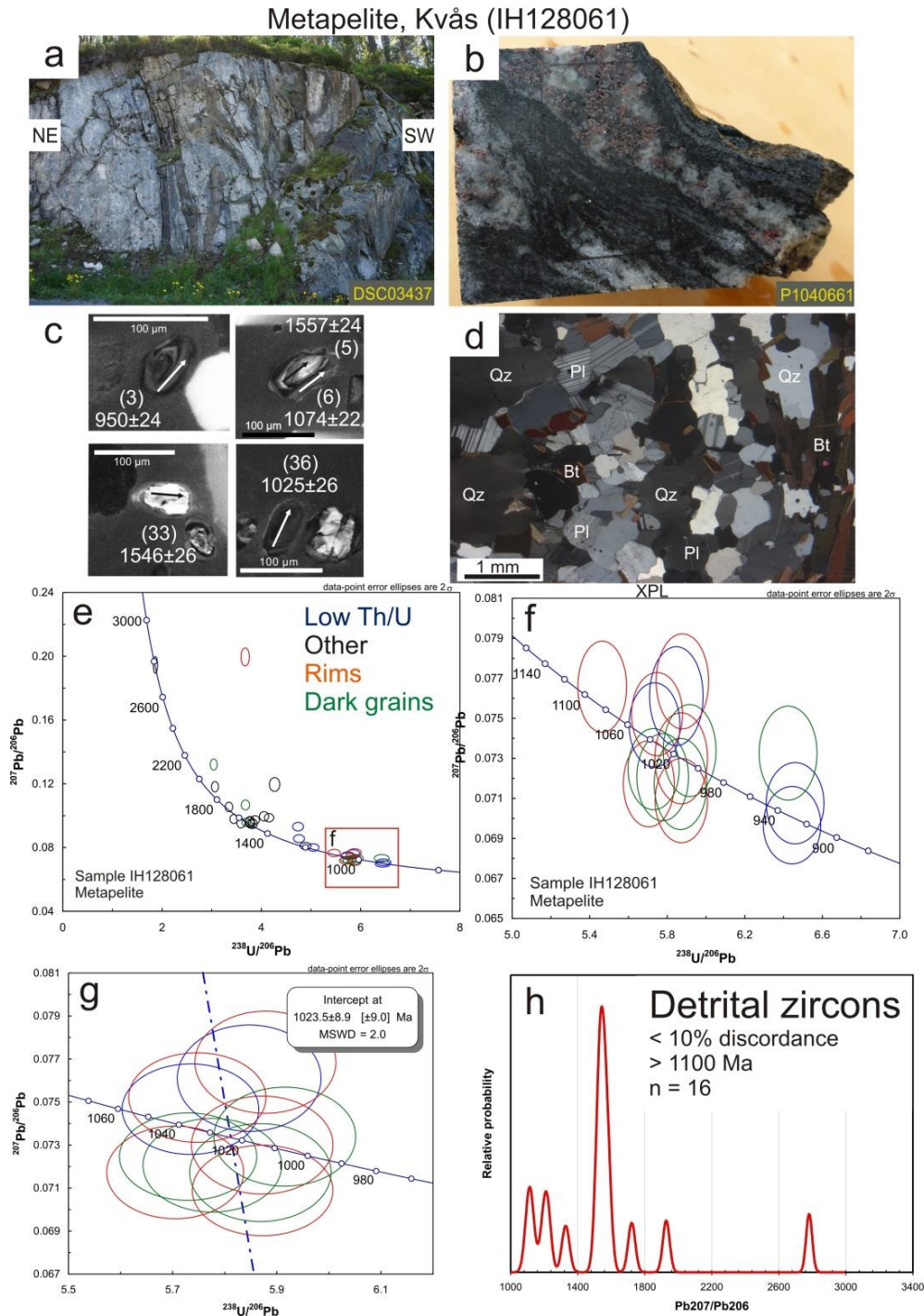


Figure 5.21 (previous page): Sample IH128061, metapelite. (a) Field photograph. (b) Hand sample showing where the thin section was taken. (c) Four selected CL-images of dated zircons with arrows showing where the crystals were analysed. (d) Quartz, biotite and plagioclase are the main rock forming minerals. (e) Tera-Wasserburg plot of the U-Pb data. (f) Tera-Wasserburg plot of the U-Pb data. (g) Tera-Wasserburg plot of the U-Pb data. (h) Probability plot of detrital zircons displaying a distinct peak at c. 1550 Ma.

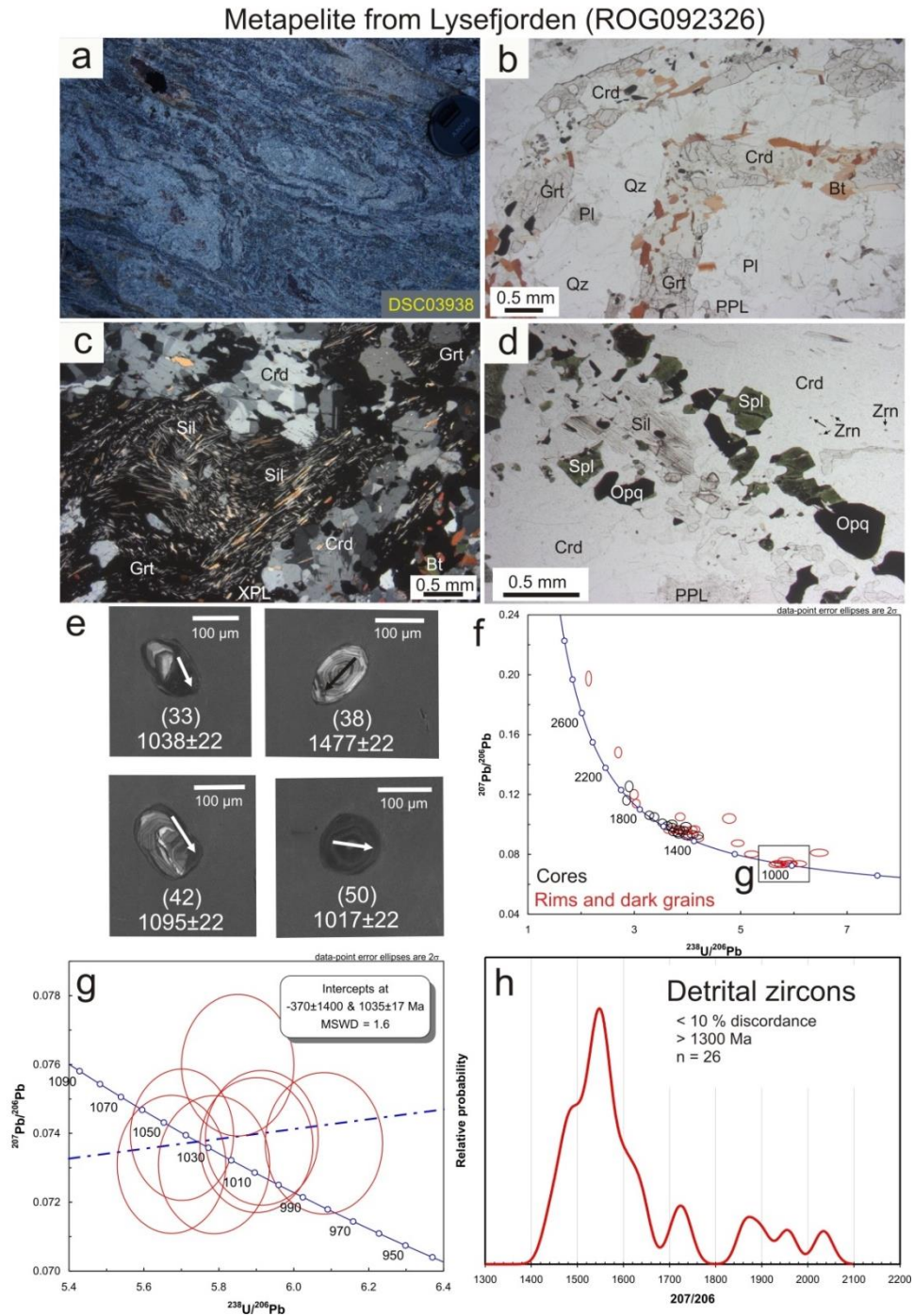


Figure 5.22 (previous page): Sample ROG092326, metapelite. (a) Field photograph showing folded migmatitic metapelite. (b) Photomicrograph displaying folding of garnet and cordierite. (c) Quartz, biotite, plagioclase, cordierite, garnet and sillimanite are the main rock forming minerals. (d) Symplectic texture with cordierite, green spinel, sillimanite and opaque minerals (e) Four selected CL-images of dated zircons with arrows showing where the crystals were analysed. (f) Tera-Wasserburg plot of the U-Pb data. (g) Tera-Wasserburg plot of the U-Pb data. (h) Probability plot of detrital zircons displaying a distinct peak at c. 1550 Ma.

5.3 Monazite geochronology

In this section geochronology data from monazite analysed from a metapelite from Kvås and a foliated granitic gneiss from Lysefjorden will be presented. Element maps from a Scanning Electron Microscope (SEM) were taken to be able to decide where the analyses should be taken. All the element maps are found in **Figure 5.23**.

Complete data from the monazite analyses are found in Appendix C.

5.3.1 IH128061 (metapelite, Kvås)

This sample was taken from a metapelite near Kvås (32 V 395379, 6459660) and was dated with both monazite and zircon as geochronometers to be able to compare the results (for zircon geochronology and field description see **5.2.3**). The monazites are c. 150 μm , sub-rounded to rounded and yellowish. The monazites were situated in garnets and in the matrix of the metapelite. Domains from four different monazite grains were analysed.

Grain 1

This monazite grain has a patchy zonation; lighter colour indicates higher Th content. The two different domains have lobate boundaries. In the middle of the grain there is a darker area which most likely is an inclusion of another mineral. The grain shows some small differences in Y content (**Figure 5.23**). Twenty analyses were taken from this grain (**Figure 5.24**) and divided into two populations based on the different domains in the thorium element map (orange and yellow). The two domains yield approximately the same age; one age for all the analyses was therefore calculated. The data yield an upper intercept at $930 \pm 14 \text{ Ma}$ (2σ , MSWD = 1.19).

Grain 2

This monazite grain has a core with lower Th and U content, but a higher Nd content than the rim (**5.23**). Twenty analyses were taken from this grain (**Figure 5.24**) and divided into two populations based on the different domains in the thorium element map. The two domains yield approximately the same age; one age for all the analyses was therefore calculated. The data yield an upper intercept at 914 ± 13 Ma (2σ , MSWD = 0.60).

Grain 13

This monazite grain display a core, an inner rim and an outer rim. The core has lower Th content than the inner and outer rim. The outer rim has the highest Th content. The element map shows some small differences in Y content (**5.23**). Twenty analyses were taken from this grain and divided into three populations based on the different domains in the thorium element map; green for outer rim, orange for inner core and black for the rest (**Figure 5.25**). The data plotted in two groups, two ages were therefor calculated. Five of the data points representing the outer rim (green) plots in one group yielding a upper intercept at 898 ± 17 Ma (2σ , MSWD = 1.13). The other data points plot in an older group yielding a lower intercept at 960 ± 16 Ma (2σ , MSWD = 1.5).

Grain 19

This monazite grain shows two different domains. The core has lower Ce content than the rim. The core has a slightly higher Y content than the rim (**Figure 5.23**). Twenty analyses were taken from this grain and divided into two populations; green for analyses from yellow domain (lower Ce), blue for analysis from orange domain (higher Ce) (**Figure 5.25**). The orange domain yield an upper intercept of 977 ± 12 Ma (2σ , MSWD = 0.63). The yellow domain yield an upper intercept at 928 ± 13 Ma (2σ , MSWD = 2.4).

Summary – IH128061

All the monazite geochronology data from this sample are plotted in **Figure 5.26**. The data shows a spreading along the concordia diagram from c. 980 Ma to 900 Ma. This is interpreted to represent metamorphic ages.

5.3.2 ROG092322 (foliated granitic gneiss, Lysefjorden)

This sample was taken from a strongly foliated granitic gneiss near Lysefjorden (**Figure 5.28**) (32 V 335928, 6538186). The rock was taken approximately 100 m south of the contact between the SMB granite and the host rock. This sample is a part of the host rock of the SMB

and is found associated with sheets of migmatitic granitic gneisses containing rafts of amphibolite and leucogranites. The foliation is defined by 0.5-2 cm long smoky quartz. The main rock forming minerals are K-feldspar and quartz which constitutes approximately 85% of the rock. Biotite and altered orthopyroxene are also present. Zircon, monazite, apatite and opaque minerals are present as accessory phases. K-feldspar phenocrysts, perthite and myrmekite are also present. The quartz displays undulatory extinction and lobate grain boundaries.

The monazites are c. 100 μm , sub-rounded to rounded and yellowish. Domains from two different monazite grains were analysed.

No zircon age were obtained from this sample due to very high common lead values and discordance.

Grain 1

The thorium element map shows several distinct domains with different thorium concentration. The core has the lowest Th content, but has a slightly higher Ce, Nd and Y content (**Figure 5.23**). Ten analyses were taken from the grain; three from the core and seven from the rim. The data were divided into two different domains; green for core and red for rim. The core and the rim gave approximately the same age, one age was therefore calculated. Two outliers were excluded (no. 10 and 4). The data yield an upper intercept at 1028 ± 35 Ma (2σ , MSWD = 0.78).

Grain 2

The thorium element map shows two domains, the core has a slightly lower Th content than the rim. Ten analyses were taken from this grain; four from the rims (no. 3, 8, 9 and 10) and six from the cores (no. 1, 2, 4, 5, 6, 7). The core and the rim gave approximately the same age, one age were therefore calculated. The data yield an intercept at 1031 ± 16 Ma (2σ , MSWD = 2.6).

Summary – ROG092322

All the monazite geochronology data from this sample are plotted in **Figure 5.27**. Due to a horizontal array in the concordia diagram, a weighted $^{207}\text{Pb}/^{206}\text{Pb}$ age was calculated. The data yield an age of 1025 ± 16 Ma which most likely indicate an age of recrystallization/resetting.

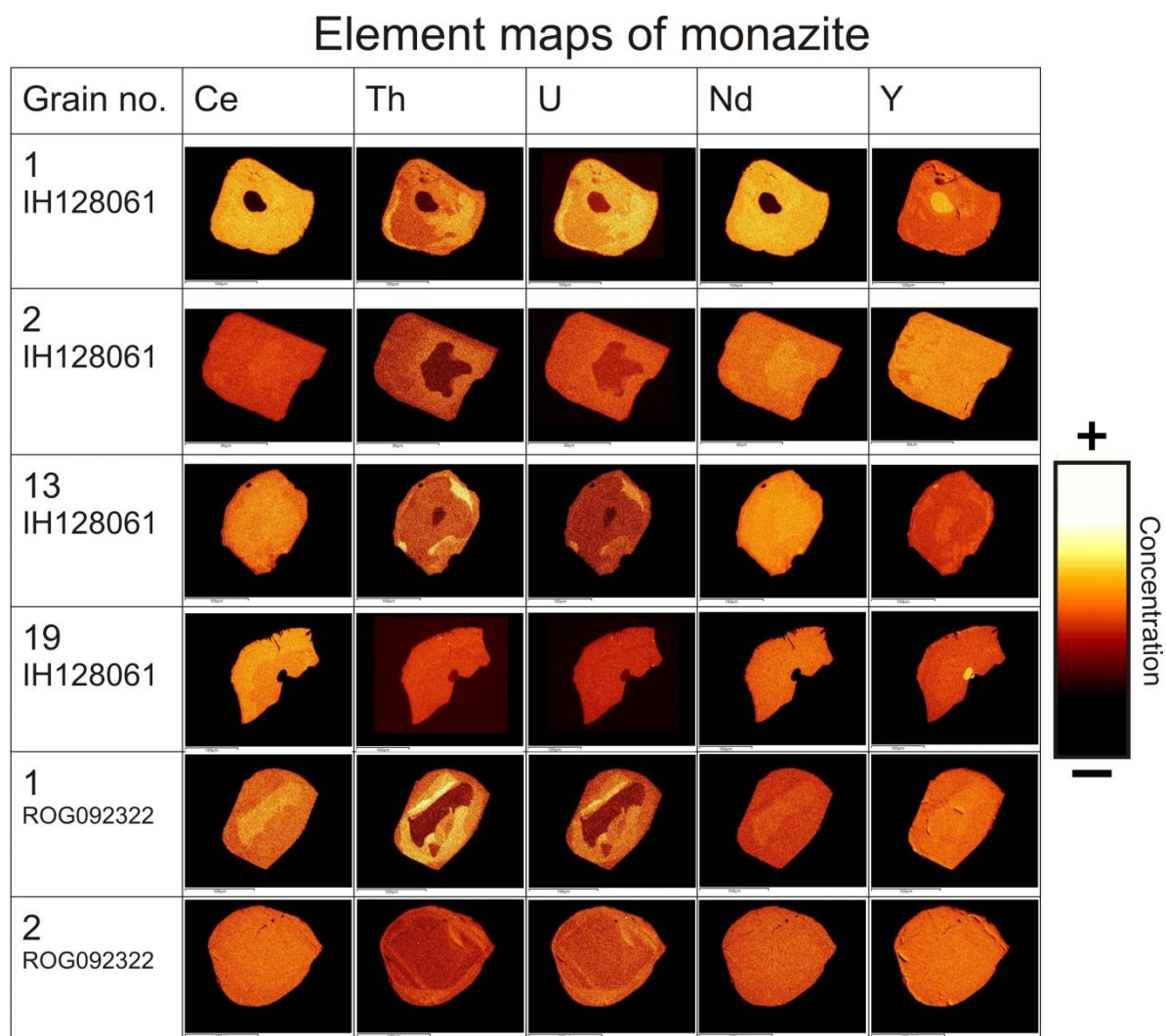
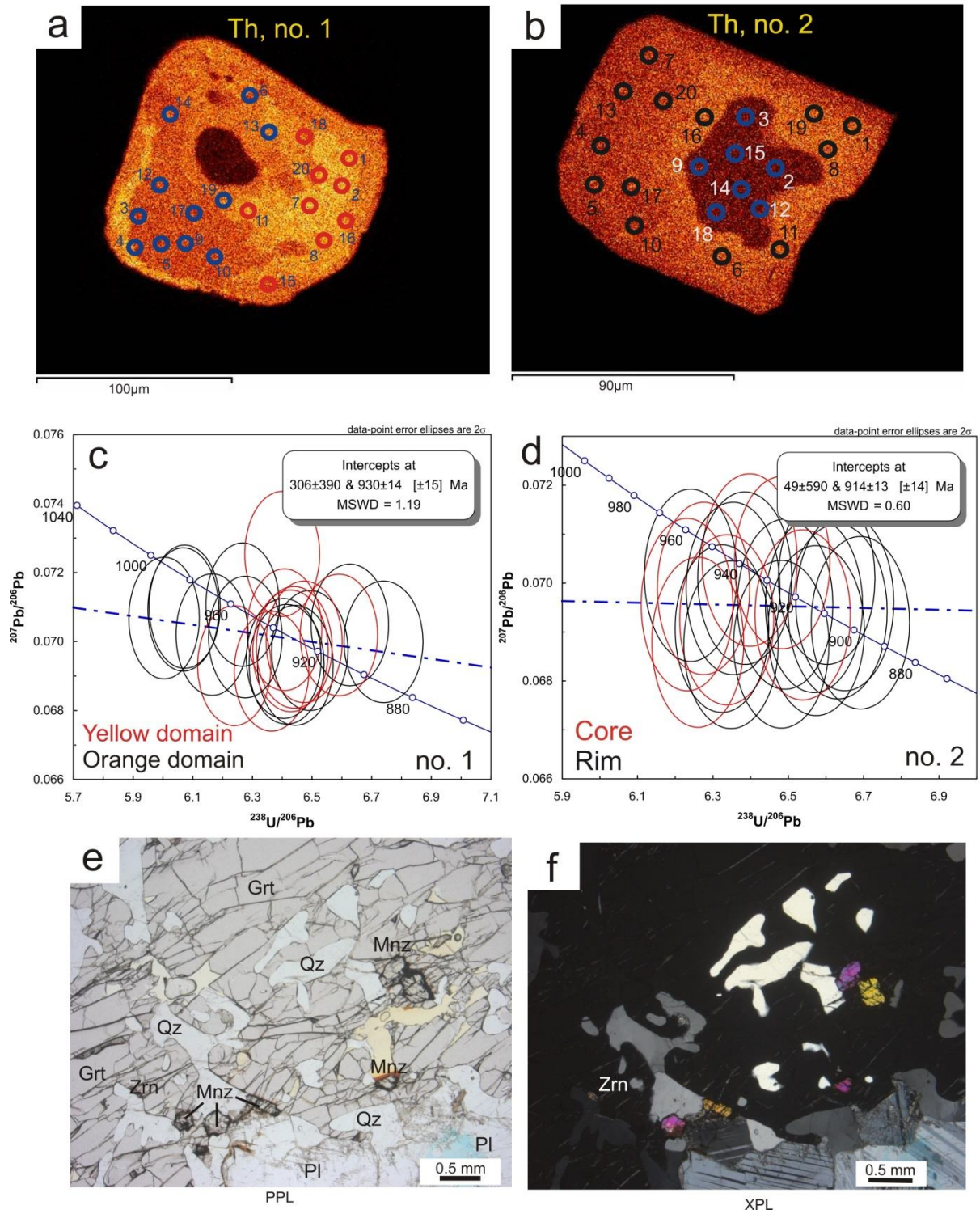


Figure 5.23: Each grain was scaled separately to highlight zoning. White indicate high counts, black low.

Figure 5.24 (facing page): Sample IH128061, metapelite. (a) Th element map of grain no. 1. Two domains were identified. Lighter domains indicate higher Th concentrations. (b) Th element map of grain no. 2. A core and a rim were identified. (c) Tera-Wasserburg plot of the U-Pb data of grain no. 1. (d) Tera-Wasserburg plot of the U-Pb data of grain no. 2. (e), (f) Thin sections showing monazites as inclusions in garnet.

Metapelite (IH128061-grain 1 and 2)



Metapelite (IH128061-grain 13 and 19)

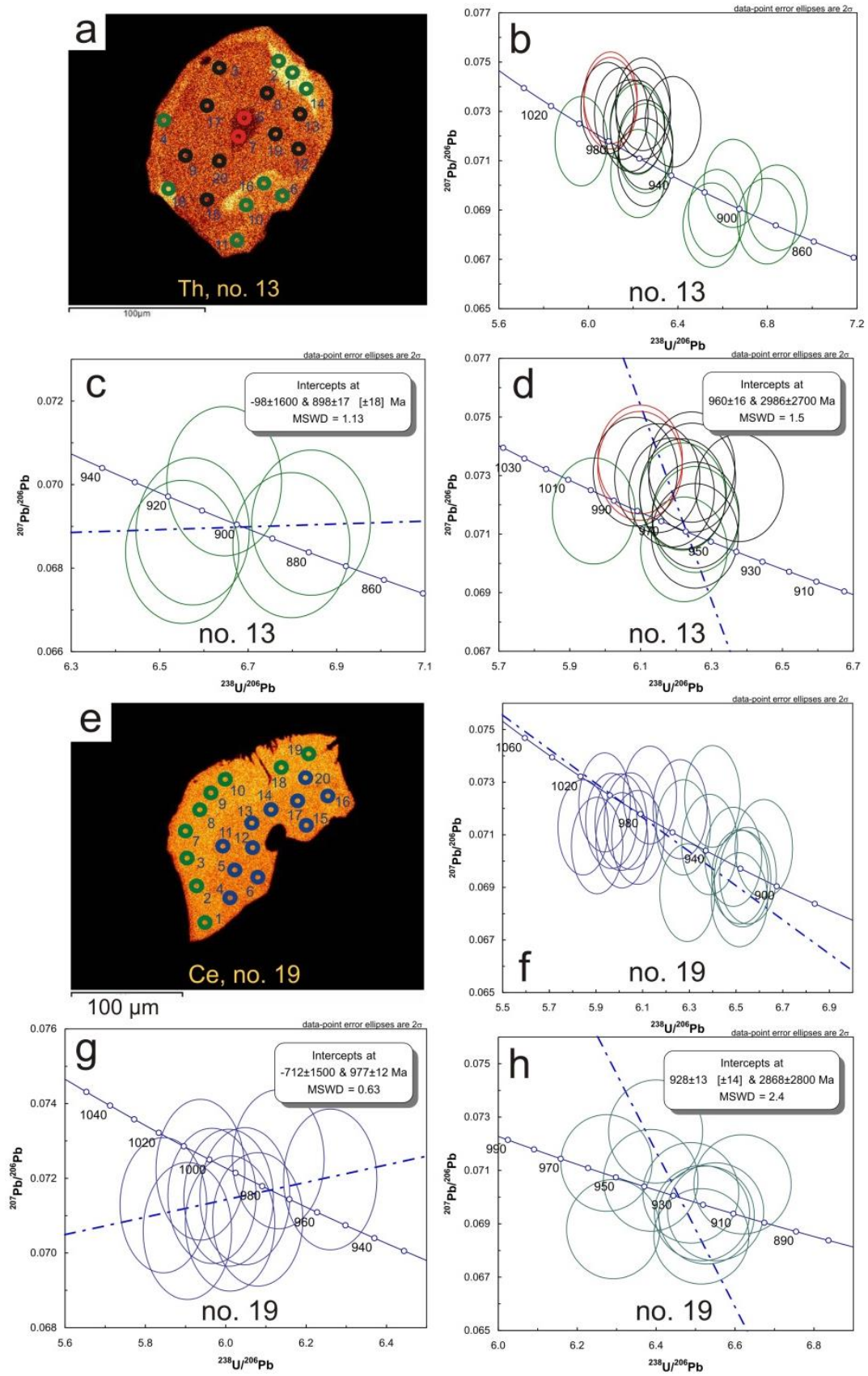


Figure 5.25 (Previous page): Sample IH128061, metapelite. (a) Th element map of grain no. 13. Three domains were identified. Lighter domains indicate higher Th concentrations. (b) Tera-Wasserburg plot of the U-Pb data of grain no. 1. Two age groups were identified. (c) An age was calculated from the outer rim. (d) An age was calculated from the inner and outer core. (e) Ce element map of grain no. 19. Two domains were identified. Lighter domains indicate higher Ce concentrations. (f) Tera-Wasserburg plot of the U-Pb data of grain no. 19. Two age groups were identified. (g) An age was calculated from the core. (h) An age was calculated from the rim.

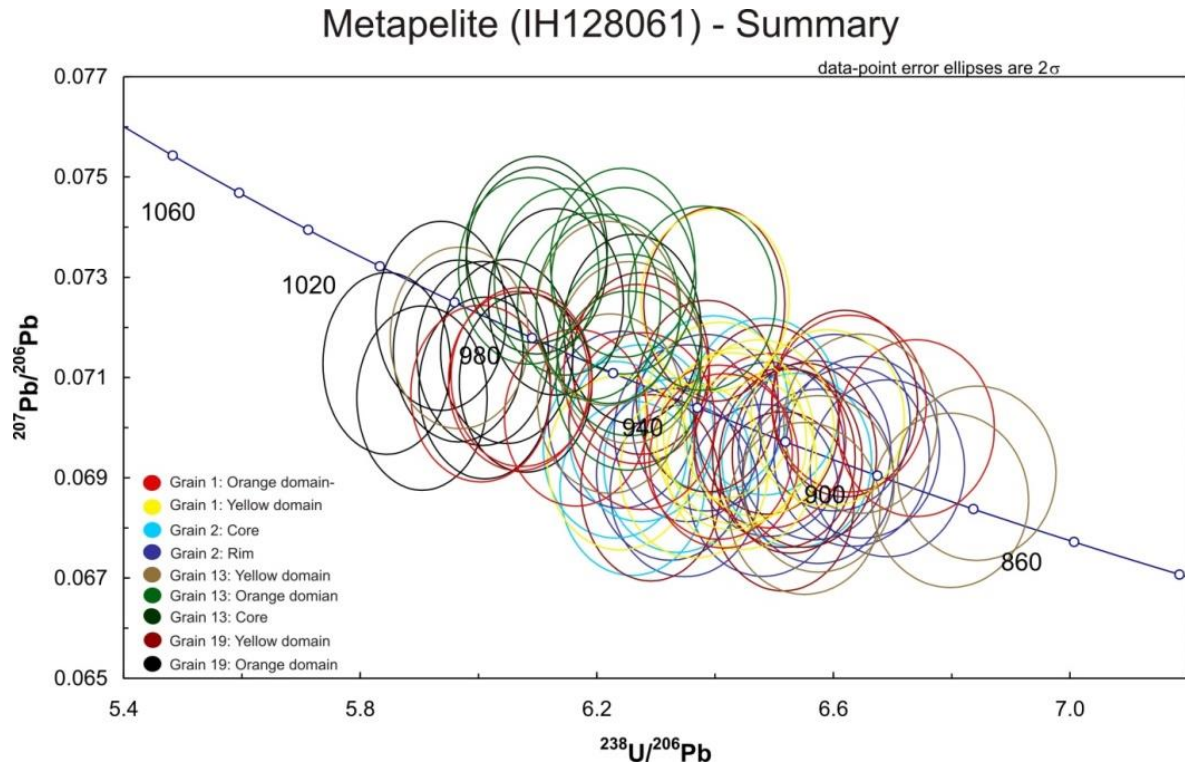


Figure 5.26: Summary of the monazite geochronology data from IH128061. The data shows a spreading along the concordia from c. 980 to 900 Ma.

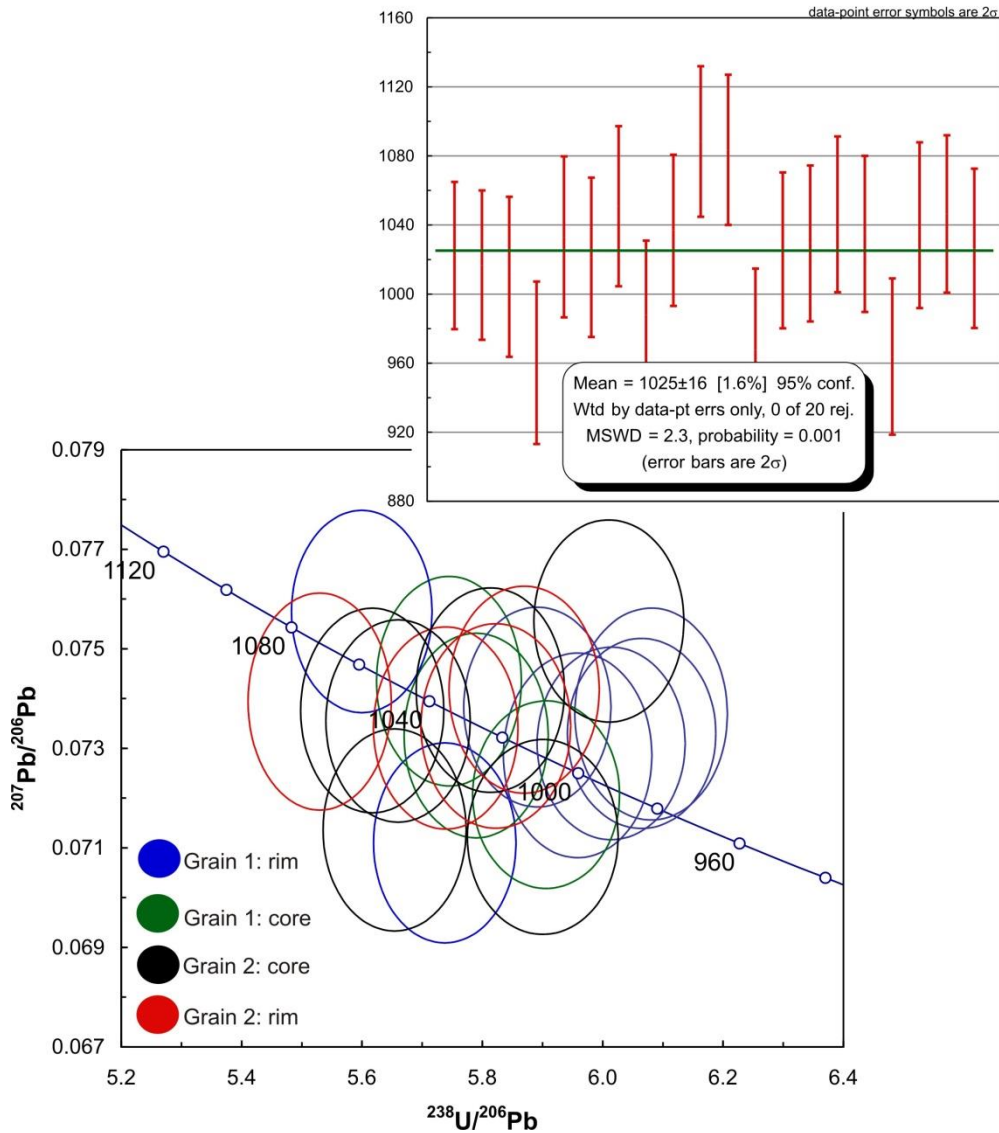
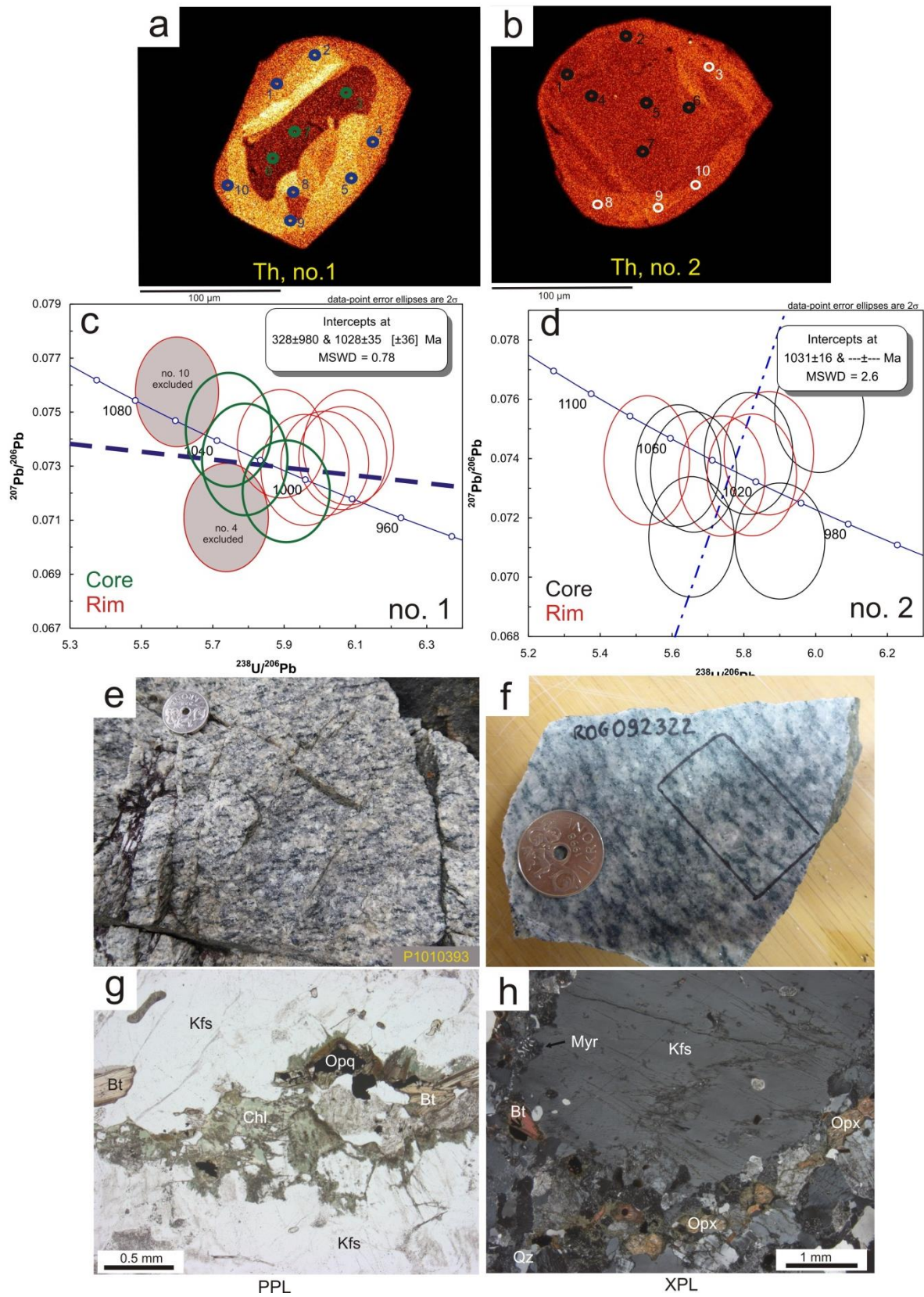


Figure 5.27: Summary of the monazite geochronology data from ROG092322. The data shows an age of 1025 ± 16 Ma.

Figure 5.28 (facing page): Sample ROG092322, foliated granitic gneiss. (a) Th element map of grain no. 1. Lighter domains indicate higher concentrations of Th. (b) Th element map of grain n. 2. (c) Tera-Wasserburg plot of the U-Pb data of grain no. 1. Cores are marked in green, rims in red. (d) Tera Wasserburg plot of the U-Pb data of grain no. 2. Cores are marked in black, rims in red. (e) Field photograph by Nolwenn Coint. A strongly foliated granitic gneiss where the foliation is defined by smoky quartz rich patches. (f) Hand specimen. The thin section is marked with black. Photo by Nolwenn Coint. (g), (h) Photomicrographs. K-Feldspar and quartz are the main rock forming minerals. Altered orthopyroxene and biotite are also present.

Foliated granitic gneiss, Lysefjorden (ROG092322-grain 1 and 2)



5.4 Structures

Structural geology has been given limited attention in this project. Detailed and systematic work need to be done in the future to be able to understand the structural geology and the tectonic evolution of the Kvås-Konsmo area. However, in this section some of the structures observed in the Kvås-Konsmo area are presented. One outcrop, at Hellevatn was studied in some detail (**5.4.2**).

5.4.1 Foliation, lineation and folding

Most of the Sirdal Magmatic Belt is undeformed, the deformation that is observed is mostly local and concentrated in xenolith-rich zones where complex deformation relationships are observed (**Stormoen, 2015; Henderson & Slagstad, personal communication**). This also applies for the Kvås-Konsmo area where ductile deformation is limited to the xenolith-rich zones.

Lineation

Some of the porphyritic granites in the Kvås-Konsmo area display a lineation with alignment of K-feldspar without any significant recrystallization.

Foliation

Tectonic foliation can be seen in the xenolith-rich zones in gneisses, migmatites and granitic gneisses. The strike direction of the foliation varies from each outcrop, but on a large scale it shows a N-S trending direction, with a vertical dip direction.

Folding

Folding is observed in the Kvås-Konsmo area (**Figure 5.29**) and is mostly constrained to the xenolith-rich zones. Several localities show amphibolite fragments that are folded inside porphyritic granite, probably as a result of granite intrusion and magmatic flow (**Figure 5.29a**). Folding is also seen in several gneiss-xenoliths (**Figure 5.29c**). In the metapelites isoclinal, upright folds are typical in both large scale and small scale (**Figure 5.29d and e**). Folded amphibolite, gneiss and granite are found at Hellevatn.

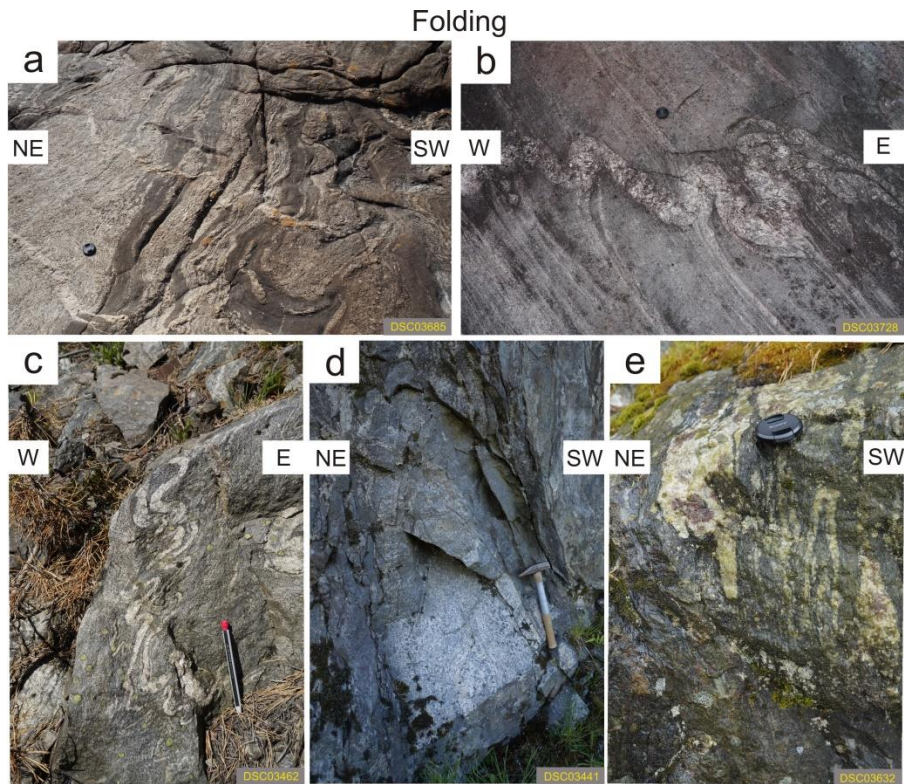


Figure 5.29: Field photographs from folding in the Kvås-Konsmo area. (a) Folded amphibolite in porphyritic granite. (b) Gneiss cut by asymmetrical pegmatitic fold. (c) Folding of quartz in gneiss. (d) Isoclinal, upright fold in metapelite. (e) Folded leucosome with garnets in metapelite.

5.4.2 Hellevatn outcrop

The outcrop by the Hellevatn waterfront is well exposed. It occurs in a N-S oriented xenolith-rich zone. The outcrop consists of asymmetrical folded gneiss, granite, amphibolite and pegmatite (**Figure 5.30, 5.32**). The foliation in the gneiss is well developed, clearly as a secondary, tectonic foliation. The gneiss is steeply dipping, almost vertical towards SE (**Figure 5.31**). The granitic fold is much thicker in the hinge than in the limbs. There is no sign of deformation in the limbs of the fold. A sample from this granite was dated and described in **section 5.2.1**. The granite yields an age of 1050 ± 39 Ma. The pegmatitic veins in the gneiss are steeply dipping, almost vertical towards NW and cut the foliation (**Figure 5.31**). The pegmatites display different amount of folding which can indicate several generations of pegmatite intrusion. The pegmatitic folds and the folding in the gneiss have gently dipping fold-axis towards S (**Figure 5.31**).

Despite a limited amount of data from the outcrop a summary of the interpreted structural evolution of the outcrop can be made (**Figure 5.33**), based on field observations and age data. Several kinematic indicators from the outcrop indicate several directions of movement. The

asymmetrical amphibolite, gneiss and granite fold indicates dextral movement. Due to no deformation in the limbs of the granitic fold and a thickening of the hinge it is speculated whether the granite was emplaced during dextral shearing in a rhomb-shaped cavity. The pegmatitic veins cut the gneiss with a geometrical relationship to the foliation which suggests that they originally formed as en échelon tension gash structures. The asymmetrical folding in the pegmatites indicates a sinistral movement.

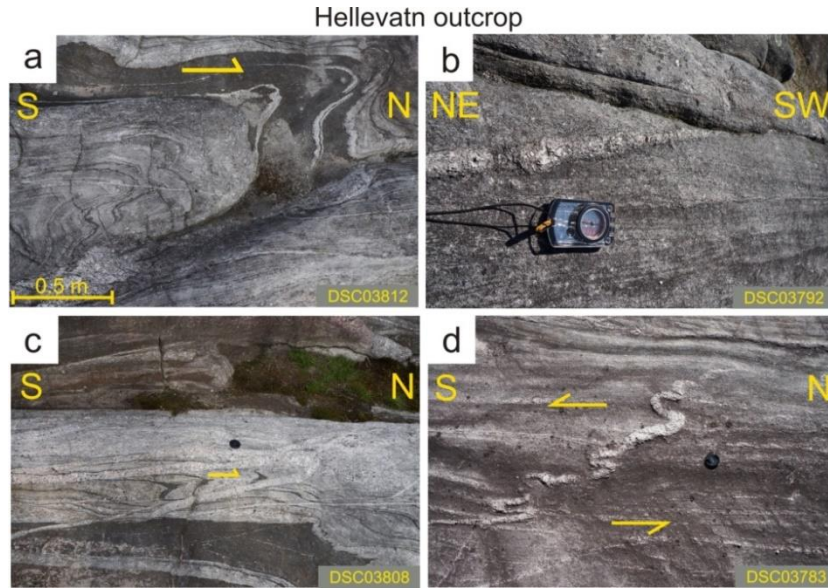


Figure 2.30: (a) Folded granite, gneiss and amphibolite. Dextral folding. (b) Pegmatite cuts the foliation in gneiss. (c) Folded pegmatitic vein with smaller folds of amphibolite and gneiss. (d) Folded pegmatite cuts the foliation in gneiss.

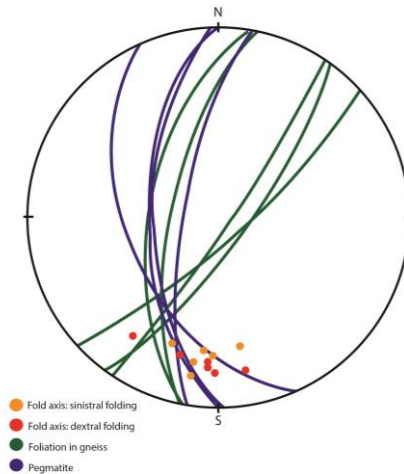


Figure 5.31: Stereonet showing foliation in gneiss and pegmatite and fold axis from sinistral- and dextral folds at Hellevatn. The plot display gentle dipping fold axis towards south. The orientation of the pegmatitic en-échelon tension gash veins cut the foliation in the gneiss indicating sinistral movement.

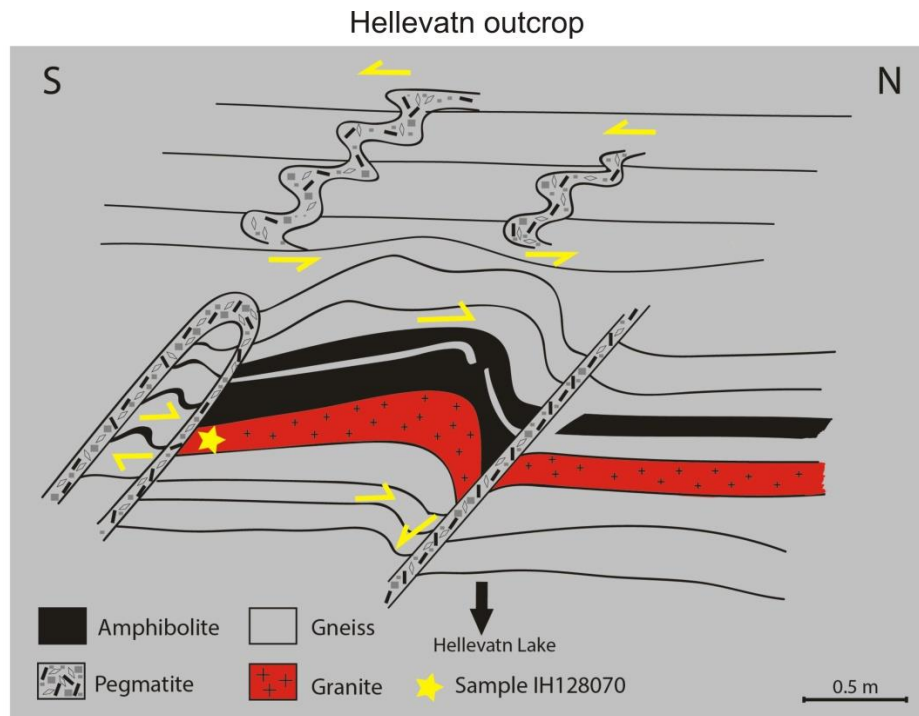


Figure 5.32: Sketch of the most important observations at Hellevatn. Yellow arrows indicate direction of movement. Folded gneiss, granite and amphibolite show asymmetrical movement. Pegmatitic veins with different amount of folding cut the foliation in the gneiss. Yellow star marks where the sample was taken.

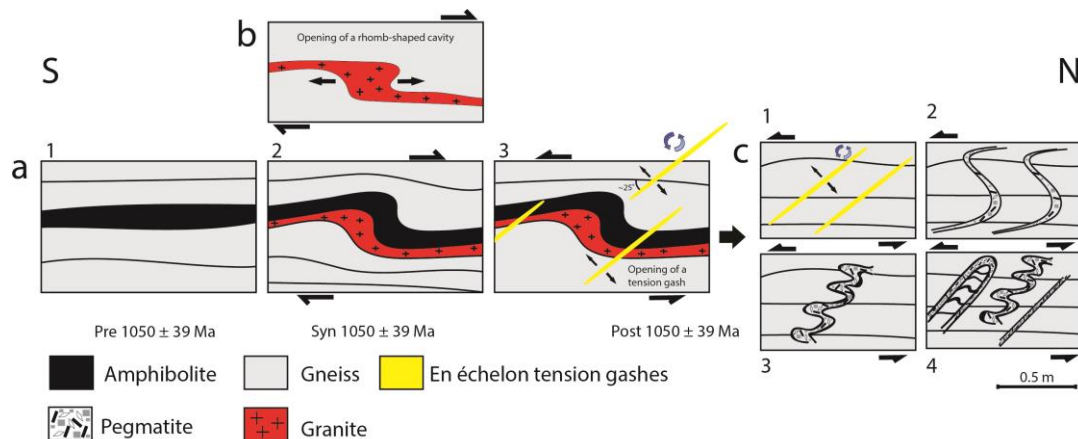


Figure 5.33: Tectonic evolution at Hellevatn. (a) (1) Pre 1050 ± 39 Ma: Gneiss and amphibolite before shearing and dextral folding. (b) Granite intruding into a rhomb-shaped cavity. (2) Syn 1050 ± 39 Ma: Dextral folding. (3) Post 1050 ± 39 Ma: several generations of asymmetrical folding of pegmatite. (c) Evolution of pegmatite folds. (1) Opening of tension gashes during subsequent sinistral shearing. (2) Pegmatite has filled the cavities. The en échelon asymmetrical sigmoidal (s-shaped) is formed when the central part of the vein rotates while the vein is lengthening during deformation. (3) Asymmetrical pegmatite folds. (4) Three generations of pegmatite veins. Oldest to the left and youngest to the right.

6 Discussion

6.1 Magmatic evolution of southwestern Norway

Southwestern Norway is characterized by long lasting plutonic activity (c. 150 Myr), where three main plutonic associations have been documented. The Sirdal Magmatic Belt (SMB) formed between c. 1060 and 1020 Ma (**Coint et al., 2015; Slagstad et al., 2013a**), the hornblende-biotite-granitic (HBG) suite formed between c. 990 and 920 Ma (**Vander Auwera et al., 2011**) and the Rogaland Igneous Complex (RIC) formed between c. 950 and 920 Ma (**Bybee et al., 2014; Vander Auwera et al., 2011**). Geochemically the SMB is calc-alkaline, magnesian with enrichment of large ion lithophile elements (LILE). The HBG is a more alkaline, ferroan type of granite (“A-type”) (**Slagstad et al., 2013a**). Based on geochemical and isotopic data **Vander Auwera et al. (2011)** suggested that the RIC and the HBG were produced by partial melting of lower crustal sources which were previously underplated. **Vander Auwera et al. (2011)** also suggested that regional metamorphism reaching granulite facies conditions was necessary to form the anhydrous lower crustal source that were needed to produce the RIC. According to **Bybee et al. (2014)** voluminous basaltic underplating started at c. 1040 Ma. The age of the basaltic underplate corresponds to the age of the SMB formation (**Coint et al., 2015**). Mafic upwelling forming mafic underplating was suggested by **Slagstad et al. (2013a)** to be a potential heat source for generating such large volumes of granite as the SMB. **Coint et al. (2015)** estimated the crystallization pressures for the SMB yielding pressures between 4 and 5 kbar, which correspond to mid-crustal depth of 12-15 km. A long-lived Andean-type margin appears to be the most likely setting for such a long-lived magmatic system.

The porphyritic granites surrounding the xenolith-rich zones in the Kvås-Konsmo area are undeformed to weakly deformed and do not show any evidence of regional metamorphic overprinting. The porphyritic granites display zircon ages ranging from c. 1050 Ma to 1030 Ma (**Figure 6.2**). These ages are interpreted to represent crystallization of the granites. This is compatible with the previously recorded magmatic activity in the SMB. The HBG-suite in the Kvås-Konsmo area is dated to c. 951 Ma (**Slagstad, personal communication**).

In addition to the main granitic magmatism in southwestern Norway, mafic magmatism has been recorded. In this study a diorite from the Kvås-Konsmo area was analysed and yield a crystallization age of 991 ± 11 Ma (IH128058) (**Figure 6.2**). Mafic intrusions have also been

recorded further north in the Finse area (**Figure 1.1**). Here zircon ages from granite, gabbro and granodiorite yield crystallization ages of c. 986 Ma (**Jensen and Corfu, 2016**). The Finse batholith was interpreted to represent one of the earliest members of the hornblende-biotite-granite in the western part of the Sveconorwegian orogen (**Jensen and Corfu, 2016**). This study also documents older, mafic intrusions in Gyadalen (c. 1030 Ma) (see section **6.2.2**).

The documentation of mafic intrusions suggests that underplating associated with an accretionary margin is more likely as a tectonic setting for the formation of southwestern Norway than a continent-continent collision.

6.2 Metamorphic evolution of southwestern Norway

6.2.1 Regional high grade metamorphism?

Previous interpretations of the metamorphic evolution of southwestern Norway are mainly based on geochronological data. **Bingen and van Breemen (1998b)** dated two different units, the Feda augen gneiss and charnockite gneiss. These units are located near the RIC and were analysed using monazite, titanite and allanite as geochronometers. Their data showed a spread along concordia from c. 1024 to 860 Ma. **Bingen and van Breemen (1998b)** divided these ages into three groups: 1024-997 Ma, 930-925 Ma and 912-904 Ma and interpreted these data to point to two distinct metamorphic events, M1 and M2. M1 is described as a high-grade regional event between 1035 and 970 Ma caused by crustal thickening during continent-continent collision. M2 is interpreted to be a younger contact-metamorphic event related to the emplacement of the RIC at c. 930 Ma (**Bingen et al., 2008a**). The third group (912-904 Ma) was from U-poor monazites from hornblende-rich samples which they interpreted to be related to fluid mobilization associated with a regional hydrothermal event (**Bingen and van Breemen, 1998b**). During the M1 event **Bingen et al. (2008a)** suggested that southwestern Norway had undergone a regional high-grade metamorphism, peaking at granulite-facies conditions. The exposed crust in southwestern Norway is said to have been ductile after 970 Ma during gravitational collapse of the orogen (**Bingen et al., 2006**). Most of the SMB is, however, undeformed and ductile deformation has only been documented in xenolith-rich zones in the SMB (**Coint et al., 2015; this study; Stormoen, 2015**).

Coint et al. (2015) discuss if the high-grade regional metamorphism at 1030-970 Ma took place at all. **Bingen et al. (2008b)** assume that the SMB is “orogenic” and a result of melting of the crust due to orogenic thickening. If the regional metamorphism was a result of

continent-continent collision and crustal thickening it would be expected to find evidence that crustal thickening and metamorphism occurred prior to the earliest SMB magmatism (c. 1070-1060 Ma). According to **Coint et al. (2015)** there are no available data to support this theory at the current stage. **Coint et al. (2015)** have, however, documented several localities where metamorphism took place just before or during the SMB emplacement. One example is from a grt-bearing paragneiss from Oltedal (**Figure 1.1**) which yield a metamorphic age of 1039 ± 27 Ma, this age overlaps with the nearby cross-cutting garnet granite dated to be between 1035 ± 6 and 1027 ± 4 Ma (**Coint et al., 2015**).

UHT metamorphism has been described southwest of the SMB by several authors (e.g., **Drüppel et al., 2013**; **Hermans et al., 1975**; **Möller et al., 2003**; **Westphal et al., 2003**). **Möller et al. (2003)** dated overgrowth in zircon from rocks sampled between Osen and Egersund in the Rogaland Vest-Agder Sector (**Figure 1.1**). Zircon overgrowth yield ages around 930 Ma, which are consistent with the emplacement age of the RIC. They therefore interpreted the result to be evidence for UHT metamorphism caused by the intrusions of the RIC. **Drüppel et al. (2013)** dated UHT rocks in the Ivesdalen area (**Figure 1.1**). The rocks yield ages of c. 1010 Ma which is much older than the crystallization age of the RIC. They therefore suggested that the rocks recorded a clockwise P-T path under UHT conditions (c. 1000 °C at c. 7.5 kbar) caused by crustal thickening during continent-continent collision. **Slagstad et al. (2013a, b)** argued that UHT metamorphism was unlikely to result only from continent-continent collision. **Blereau et al. (in review)** interpreted that the regional metamorphism in the Rogaland Vest-Agder Sector during the Sveconorwegian Orogeny followed a clockwise P-T path which reached peak conditions at c. 1035 Ma (c. 900-950 °C, c. 7 kbar) and remained hot for a long time. They suggested that these conditions favour a long-lived accretionary orogen relative to a continent-continent collision. **Coint et al. (2015)** acknowledge that the UHT metamorphism in southwestern Norway is complex and not fully understood, but that the UHT metamorphism close to the RIC is probably related to the thermal effects of the emplacement of the RIC.

6.2.2 1065-1030 Ma (underplating, mafic magmatism, SMB and metamorphism)

The xenoliths observed in the Kvås-Konsmo area are amphibolite, migmatite, metapelite and flaser gneiss. The amphibolite was not dated because no zircons were found. Amphibolite is, however, found as xenoliths in porphyritic granite, flaser gneiss, metapelite and also in migmatite, suggesting that the amphibolite is one of the oldest lithologies in the area. Flaser gneiss at Knaben was dated by **Stormoen (2015)** yielding an age of c. 1260 Ma, indicating

pre Sveconorwegian magmatism. Zircon cores and zircons from mesosomes from the Kongsmo migmatites yield ages of c. 1450 Ma, suggesting that the protoliths are pre Sveconorwegian.

Zircons from leucosomes in the Kvås metapelite and the Kongsmo migmatites yield ages of 1024 ± 9 Ma (IH128061), 1039 ± 17 Ma (IH128065) and 1065 ± 23 Ma (IH128072), respectively (**Figure 6.2**). These ages are interpreted to represent partial melting and recrystallization of the zircons during the Sveconorwegian orogeny. The metamorphic ages indicate that the partial melting is spatially and temporally correlated to the emplacement of the granites. Another example that can support this theory is found in Gyadalen.

Figure 6.1 shows a schematic cross section of the Gyadalen transect (Coint et al., 2015) where the VAG-samples were sampled. Quartz dioritic migmatitic gneiss (VAG084397) from the Gyadalen transect was analysed and yield an age of 1033 ± 17 Ma (**Figure 6.2**). This rock is clearly migmatized and contains leucosomes indicating partial melting. The zircons also clearly show that younger rims cut older cores. However, the cores and the rims yield the same age. It is therefore suggested that the crystallization and the partial melting of the quartz diorite happened within the uncertainty of the data. The age of the metamorphism of the quartz diorite overlaps with the age of a nearby cross-cutting porphyritic granite (VAG084399). This granite was dated and yields an age of 1037 ± 7 Ma (**Figure 6.2**). This supports the theory that high-grade metamorphism and magmatic intrusions in the SMB happened within a short period of time. A granitic gneiss from the same area yields an age of 1048 ± 22 Ma (**Figure 6.2**). Analyses of two younger rims probably represent recrystallization of the zircons at c. 1017 Ma, but more analyses from the rims are needed to determine this.

Geochronology data from Lysefjorden also indicate that partial melting can be correlated with emplacement of the SMB. Zircon rims and dark grains from the Lysefjorden metapelite yield an age of 1035 ± 17 Ma (**Figure 6.2**). This age is interpreted to represent the timing of partial melting of the metapelite. The mineral assemblage in the metapelite is associated with granulite facies (see section 6.3) indicating that partial melting of the rock occurred during high-grade metamorphism.

Analysed monazite grains from the Lysefjorden granitic gneiss clearly display different domains where the rims generally display higher thorium content than the cores. The cores and the rims yield approximately the same age, 1025 ± 16 Ma (**Figure 6.2**). This gneiss is a part of the host rock of the SMB and it is proposed that the monazite age is a metamorphic age.

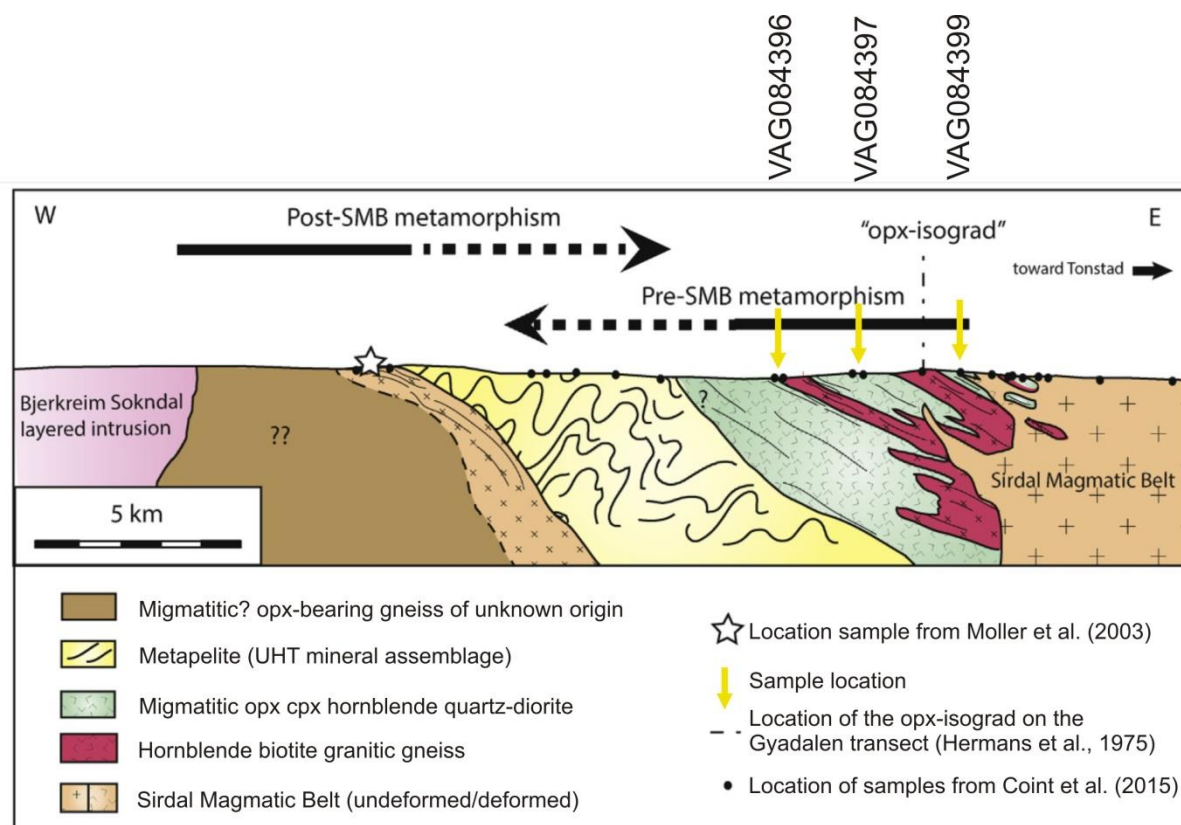


Figure 6.1: Schematic cross section for the Gyadalen transect, illustrating the rock relationships. Yellow arrows indicating where sample VAG084396, 97 and 99 were taken. Figure modified after Coint et al. (2015).

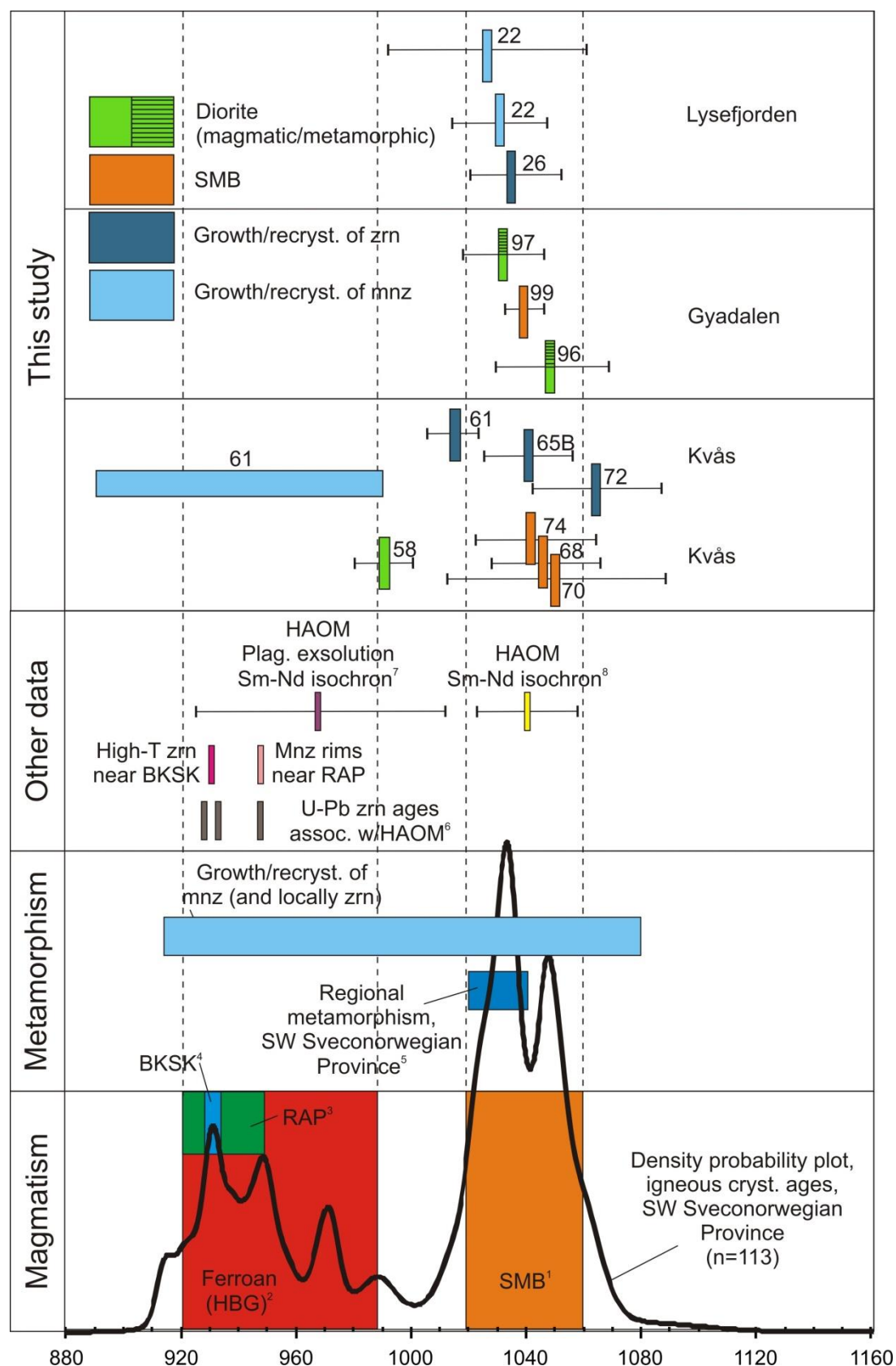


Figure 6.2: Summary of magmatic and metamorphic geochronology data in southwestern Norway. The U-Pb data from this study are shown at the top of the figure. The sample numbers are marked with the two last numbers (e.g. IH128061 = 61). Figure modified after Slagstad, unpublished.

6.2.3 1000 Ma – 900 Ma (metamorphism and magmatism)

Two zircons from the Kvås metapelite yield an age of c. 930 Ma, indicating a younger metamorphic event. The metapelite is situated only 500 meters from a c. 951 Ma HBG-granite (**Slagstad, personal communication**). Intrusion of the HBG between 990 and 920, mafic intrusion at c. 990 Ma and emplacement of the RIC between 950 and 920 Ma indicate that the system was magmatically active for several 10s of million years. This can have caused recrystallizing of the zircons in the Kvås metapelite. The dataset is, however, too small to make any conclusions.

The analysed monazite grains from the Kvås metapelite clearly display different domains where the rims generally yield younger ages and higher thorium content than the cores. The monazite ages range from c. 980 Ma to 900 Ma (**Figure 6.2**) which is approximately the same spread as documented by **Bingen and van Breemen (1998b)**. However, there are no field observations in the Kvås-Konsmo area which can support **Bingen and van Breemen (1998b)** age grouping. **Bingen and van Breemen (1998b)** interpreted the oldest ages (1024-997 Ma) to date crustal thickening during continent-continent collision. The oldest ages are not recorded in the monazites from the Kvås metapelite, only in the zircons. The monazites may have been recrystallized/reset so that the oldest ages may have been erased. If the monazite ages record crustal thickening it would be expected to see deformation in the granites surrounding the xenoliths, but the granites in the Kvås-Konsmo area and most of the SMB are undeformed. It therefore seems unlikely that the monazite ages represent regional metamorphism due to crustal thickening. The second group, 930-925 Ma may represent a younger contact-metamorphic event related to the emplacement of the Rogaland Igneous Complex at c. 930 Ma (**Bingen et al., 2008a**). Kvås is, however, situated approximately 30 km away from the RIC contact. It therefore seems unlikely that the monazite ages recorded in Kvås are a result of a contact-metamorphic event related to the emplacement of the RIC. The intrusion of the HBG-suite and the diorite are, however, closer and may have affected the monazites and resulted in recrystallization. However, it is questionable if the intrusion of the HBG and the diorite alone has caused the scatter along the concordia. It is suggested that a generally high heat flow in the southwestern Norway can have caused the scatter along the concordia. The last age group (912-904 Ma) was interpreted to be related to fluid mobilization associated with a regional hydrothermal event (**Bingen and van Breemen, 1998b**). It is suggested that the monazite ages represent a geological event which was recorded in monazites and not in zircons. At the time of monazite recrystallizing there was probably still a

lot of heat in the system which can have caused recrystallization of the monazite. Several pegmatites in the Evje-Iveland area are dated to 910 ± 14 Ma (**Scherer et al., 2001**) and jotunite dykes from the Egersund area are dated to 916 ± 9 Ma (**Vander Auwera et al., 2011**). Intrusion of pegmatites and jotunitites may also have affected the monazites.

6.2.4 Interpretation of the U-Pb geochronology of monazite

The most important question when acquiring age data is: what are we actually dating? In order to understand the significance of monazite ages, it is important to establish a link between the monazite ages, monazite-forming reactions, and metamorphic conditions (**Smith and Barreiro, 1990**). But first and foremost it is important to have a good understanding of the field relationships when interpreting the geochronology data.

Several experimental and empirical studies have shown that monazite is robust to volume diffusion under dry conditions and that diffusional loss of Pb might be negligible for most natural monazite (e.g., **Bingen and van Breemen, 1998b; Cherniak et al., 2004; McFarlane and Harrison, 2006**). However, several recent studies (e.g., **Budzyn et al., 2011; Harlov et al., 2011; Kelly et al., 2012; Williams et al., 2011**) show that a variety of primary and secondary processes can influence monazite U-Pb dates. Diagenesis, hydrothermal alteration, pegmatite intrusion, deformation and weathering are examples of processes that can cause remobilization of U, Th, Pb and REE in monazite. It has been documented that the potential for monazite recrystallization dramatically increases when fluids are present, especially with alkali-bearing fluids. Fluid infiltration can result in chemical and isotopic changes in monazite. These mechanisms usually lead to compositional zoning and specific microstructures that can be identified by EMP/BSE analyses. It has been suggested that monazite grains of 50-200 μm in size can lose significant amounts of Pb if they remain at temperatures above $\sim 600\text{-}700$ °C for more than 10 Ma (e.g., **Smith and Giletti, 1997**). It has also been shown that monazite can grow during prograde and retrograde metamorphism (**Högdahl et al., 2012**), which implies that the obtained monazite ages does not necessarily reflect the timing of peak metamorphism.

These studies show that monazite can be affected by several primary and secondary processes. This means that caution needs to be taken when interpreting monazite data.

Most of the analysed monazite grains from the Kvås metapelite and the Lysefjorden granitic gneiss clearly display different domains where the rims generally yield younger ages and higher thorium content than the cores. Some of the monazite grains are clearly zoned, but do

not show any difference in age. It is possible that the core and the rim yield different ages but that the difference is too small to be seen in the concordia diagram.

Another possibility is that the zonation and the ages are real suggesting that a process has changed the monazite without changing the age. It has been documented that monazite grains can be overgrown by a Th-enriched or Th-poor monazite rim during later periods of growth (**Harlov et al., 2011**).

Monazite dates from the analysed granitic gneiss from Lysefjorden yield only one age of 1025 ± 16 Ma and not the younger ages which are recorded in the metapelite in Kvås. A higher heat flow in the Kvås-Konsmo area compared to Lysefjorden could have been an explanation. This is, however, unlikely, because the Lysefjorden metapelite not far from the granitic gneiss show a mineral assemblage indicating granulite facies conditions during metamorphism. The deformed rocks in the Kvås-Konsmo area have most likely only been through amphibolite facies conditions (see section 6.3).

The fluid content in the analysed rocks may have been an important factor resulting in the scatter along the concordia. Metapelites are usually more hydrous than granites. Southwestern Norway was magmatically active for approximately 150 Ma, producing a lot of heat. As suggested by **Blereau et al. (in review)** small amounts of melt may have remained at temperatures above the solidus in the metapelite for a long period of time causing recrystallization of monazite. This could also explain the large spread in the concordia diagram.

The documented scatter of the metamorphic monazite dates seem to be recorded throughout southwestern Norway (**Bingen and van Breemen, 1998b**). This suggests that the geological event causing the monazite scatter is most likely a regional event and not a local event.

It is common in high-grade metamorphic rocks that zircon yield older ages than monazite. It is also common that zircon survives heating up to peak temperatures and a following isothermal decompression, whereas monazite may be completely consumed (**Kelsey et al., 2008**). This could be a possible explanation for why only the younger ages are recorded in the monazites in the Kvås metapelite.

Based on the monazite data presented in this study it appears that the monazite ages may be linked to long-lived magmatism. But it is suggested that further studies combine U-Pb geochronology with trace element analyses of monazite to better understand the metamorphic response of monazite and its host rocks during the Sveconorwegian orogeny. It is also suggested that in situ monazite analyses are applied to be able to control what is actually being dated.

6.3 Regional variation in metamorphic grade

The metapelite sampled near Lysefjorden contains minerals including garnet, sillimanite, green spinel and cordierite. These minerals are associated with granulite facies which suggest up to UHT conditions. Sillimanite occurs as inclusions in garnet, but also in symplectitic texture with green spinel, cordierite and opaque minerals (**Figure 5.**). This can indicate that there are two generations of sillimanite growth. The metapelite has a similar mineral association as documented in **Drüppel et al. (2013)**. They suggest metamorphic conditions with temperatures higher than 800 °C and pressures around 6.5 kbar. Lysefjorden is located approximately 30 km north of the RIC. It is therefore unlikely that heat from the RIC was enough to cause UHT conditions in the metapelite. The question is therefore what caused the UHT metamorphic conditions in Lysefjorden?

The Gyadalen quartz dioritic migmatitic gneiss also indicates high-temperature. Only clinopyroxene and no orthopyroxene were found in this sample, but other quartz dioritic gneisses from the Gyadalen transect (**Coint et al., 2015**) contain both clinopyroxene and orthopyroxene, indicating granulite-facies conditions.

The Kvås metapelite is migmatitic which indicates high-temperature metamorphic conditions (**Winter, 2001**). No sillimanite was observed in this sample suggesting that the temperature did not reach as high as the sillimanite zone. Sillimanite may have been present, but reacted during retrograde metamorphism. The mineral assemblage in the migmatites nearby suggests amphibolite-facies conditions which can indicate that the Kvås-Konsmo area did not reach as high temperatures as the Lysefjorden metapelite. Estimates of the crystallization pressures for the SMB yield pressures between 4 and 5 kbar, which correspond to mid-crustal depth of 12-15 km (**Coint et al., 2015**). Estimated pressures for the UHT metamorphism in southwestern Norway are much higher, up to 7-8 kbar (**Blereau et al., in review**).

To be able to explain the different metamorphic conditions in southwestern Norway two different theories are suggested. An irregular body of underplating is suggested (**Figure 6.5**) to explain why the Lysefjorden show UHT metamorphism while the metapelite in Kvås show lower degree of metamorphism. This theory can, however, not explain the different pressure conditions found throughout the orogen.

A dome structure formed in the Rogaland-Vest Agder Sector during the Sveconorwegian orogeny may explain different pressure estimates in the region. This can explain why some parts of the region show metamorphism with pressures up to 7-8 kbar and why other parts, e.g. the SMB only show pressures up to 4-5 kbar. A dome structure may cause a high heat flow, which can result in a high temperature gradient. A relative small difference in depth (p) will then result in a high temperature difference. Hypothetically, if the temperature gradient was 50 °C/km, then a 10 km difference would result in a 500 °C difference in temperature. The RIC may have formed the core of this dome structure.

6.4 Structures

Few structural and kinematic studies across the Sveconorwegian orogen have been undertaken. The structural evolution of the orogen is therefore not well understood. Most of the Sirdal Magmatic Belt (SMB) is undeformed; the deformation that is observed is mostly local and concentrated in xenolith-rich zones where complex deformation relationships are observed (**Coint et al., 2015; Stormoen, 2015; Henderson & Slagstad, personal communication**). This is also consistent with the observations from the Kvås-Konsmo area, where deformation only is observed in the xenolith-rich zones.

A detailed study of structural evolution of a xenolith-rich zone at Knaben is done by **Stormoen (2015)**. The Knaben Zone is situated in the SMB in the Kvinesdal County and show both similarities and differences with the Kvås-Konsmo area.

Stormoen (2015) describes the Knaben Zone as a N-S oriented zone with a large amount of xenoliths, deformation, and also molybdenite deposits. Both ductile and brittle structures are observed in the zone, but the ductile structures are the most dominant. The structures are interpreted to be related to the emplacement of the granites. In the Knaben Zone (**Stormoen, 2015**) mineral lineation was observed without any significant recrystallization, here the mineral lineation was interpreted to be formed by magmatic to submagmatic flow. The

mineral lineation in the undeformed granites in the Kvås-Konsmo area has therefore also been interpreted to be formed by magmatic to submagmatic flow.

The pre Sveconorwegian host rock in Knaben is deformed, resulting in moderate east-dipping structures that were exploited by Sveconorwegian west-verging thrusting and emplacement of the SMB (**Stormoen, 2015**). A regional-scale east-west compressive, top-to-the-west kinematic shear zone network with synkinematic magmatism is proposed by **Stormoen (2015)** for the SMB (**Figure 6.3 and 6.4**). **Coint et al. (2015)** suggested that the SMB intruded into the country rock as multiple sheets over a period of c. 50 Myr. West verging movement has also been documented other places in southwestern Norway (e.g., **Henderson and Ihlen, 2004; Scheiber et al., 2015**). The Knaben zone has been interpreted to represent a contact zone between different intrusive bodies. This speculation is also supported by TIMS analysis from each side of the Knaben Zone, resulting in an age of 1019 ± 2 Ma on the east side and 1029 ± 3 Ma on the west side (**Slagstad et al., unpublished TIMS data, 2015**).

The geometry of the xenolith-rich zone in the Kvås-Konsmo area seems to be a little different from the Knaben zone. The Knaben Zone seems to be more continuous than the xenolith-rich zones in the Kvås-Konsmo area. The Kvås-Konsmo area seems to be situated between two larger xenolith-rich zones, the Kvås zone and the Konsmo zone. The pre Sveconorwegian rocks in the Knaben zone are moderately dipping towards east, while in the Kvås-Konsmo they are almost vertical. In Knaben the xenolith-rich zone show the same thickness throughout the whole zone, while in the Kvås-Konsmo area one of the xenolith-rich zones are folded and do not show the same thickness. One possibility is that the intrusion of the HBG-suite may have contributed to the more complex geometries found in the Kvås-Konsmo area compared to the Knaben zone.

Stormoen (2015) divided the evolution of the Knaben zone into three stages (**Figure 6.3 and 6.4**); these are comparable with the evolution of the Kvås-Konsmo area. Stage 1 is suggested to be pre-Sveconorwegian when the formation of the xenoliths in the xenolith-rich zone was formed. This includes the formation of the amphibolites, the migmatite protholith, the flaser gneiss and the metapelites. Stage 2 is divided into four stages; 2a, b, c and d. Stage 2 is dominated by the intrusions of the SMB, the RIC, the HBG and also metamorphism. Stage 3 is post Sveconorwegian.

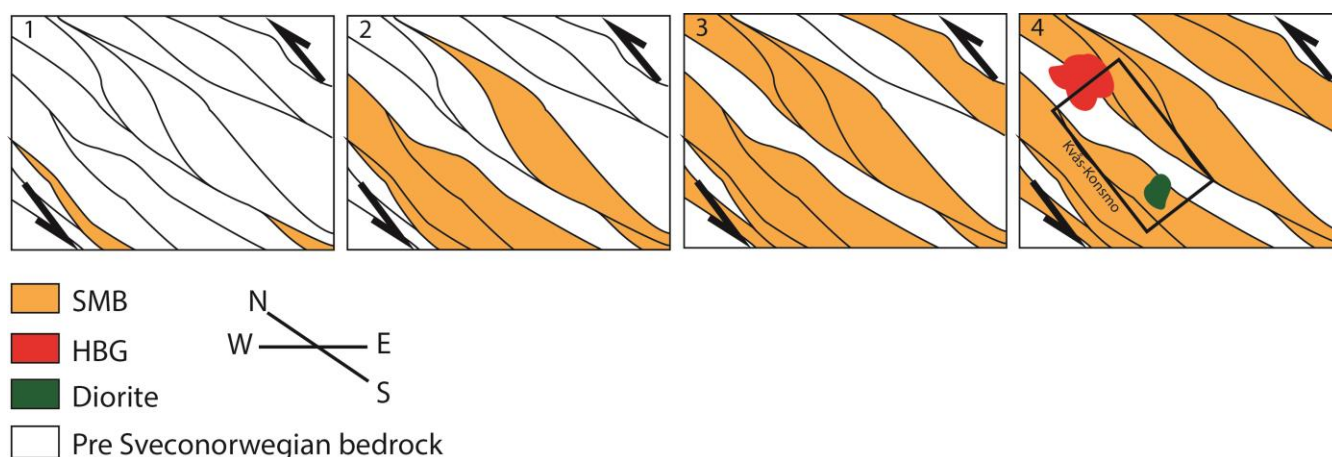


Figure 6.3: A schematic emplacement model of the Sirdal magmatic Belt in a continuous kinematic setting. The Kvås-Konsmo area is marked in a square. Figure modified after Stormoen (2015).

	Pre-Sveconorwegian	Schematic Sveconorwegian evolution in the Knaben zone				Post-Sveconorwegian
	Stage 1	Stage 2a	Stage 2b	Stage 2c	Stage 2d	Stage 3
The Knaben zone	<p>Map</p> <p>Profile</p> <p>W E</p>	<p>Map</p> <p>Profile</p> <p>W E</p>	<p>Map</p> <p>Profile</p> <p>W E</p>	<p>Map</p> <p>Profile</p> <p>N S</p>	<p>Map</p> <p>Profile</p> <p>NW SE</p>	<p>Map</p> <p>Profile</p> <p>N S</p>
Structural expression	Development of regional foliation	-Ductile top-to-the-W duplex-thrusting, kinematics and E-W compressive folding -N-S directed lateral extrusion and corresponding E-W-oriented pure shear component		-More heterogenous and s.-s. strain + open folds -E-W pegmatites along duplex transfer zones	-Sparse observations of down-to-SE extension, cutting general foliation, reactivating weaknesses	1) 850Ma dykes 2) Caledonian shear zones 3) Late brittle joints
Magmatic events	Flaser gneiss -1260Ma	-Porphyritic granite 1040-1020Ma -Synkinematic emplacement	-Grey granite (1030Ma) and Mo-pegmatites -Strain-assisted melt-fractionation	-Irregular leucogranitic intrusions -Subvertical E-W pegmatites	(possibly close in time and related to Stage 2c)	Hunndalen dykes -850Ma -Approximately E-W striking
Regional correlation	Lithological and geochronological regional correlation	-SMB - correlation -Similar kinematics as PKFZ and KTBZ			Extensional reactivation along all major shear zones in the orogen, related to gravitational collapse	

Lithology and map colour
Porphyritic granite (PG)
Grey granite
Minor granulitoid variations
Amphibolite
Flaser gneiss
Biotite gneiss
Migmatite
Mafic dyke

Lithology and map colour
Porphyritic granite (PG)
Grey granite
Minor granitoid variations
Amphibolite
Flaser gneiss
Biotite gneiss
Migmatite
Mafic dyke

Figure 6.4: The figure illustrates the geological evolution of the Knaben Zone. The evolution of the Kvås-Konsmo area is most likely similar to the Knaben zone. Illustration from Stormoen (2015).

6.5 Continent-continent collision or a long lived accretionary margin?

Based on extensive mapping, new field data and new geochronology data **Slagstad et al. (2013a)** questioned the traditional continent-continent collision model and suggested that a long-lived accretionary margin could better explain the metamorphic and magmatic evolution in southwestern Norway.

In light of new field and geochronological data from this study it appears that the metamorphism in southwestern Norway is caused by magmatic processes and not by crustal thickening and radioactive self-heating as previously suggested. It is, however, questioned if the heat from the emplacement of the granites, anorthosites and the diorites are enough to cause high-grade metamorphism. It is therefore suggested that voluminous basaltic underplating can have contributed to the heat that was necessary to cause high-grade metamorphism. According to **(Bybee et al., 2014)** voluminous basaltic underplating started at c. 1040 Ma. An irregular body of underplating can be an explanation for the different metamorphic condition throughout the orogen (**Figure 6.5**). A dome structure formed in the Rogaland-Vest Agder Sector during the Sveconorwegian orogeny may explain different pressure estimates in the region. This can explain why some parts of the region show metamorphism with pressures up to 7-8 kbar and why other parts, e.g. the SMB only show pressures up to 4-5 kbar. A dome structure may cause a high heat flow, which can result in a high temperature gradient; this can be an explanation for the different metamorphic condition throughout the orogen.

This study suggests that the timing of high-grade metamorphism and granitic intrusions in the SMB happened within a short period of time. This can explain the field relationships where undeformed granites cut high-grade metamorphic rocks with almost the same age.

The metamorphic and magmatic evolution of southwestern Norway cannot satisfactorily be explained by crustal thickening and radioactive self-heating. It is therefore suggested that the zircon and monazite ages are a result of magmatically driven UH/UHT metamorphism.

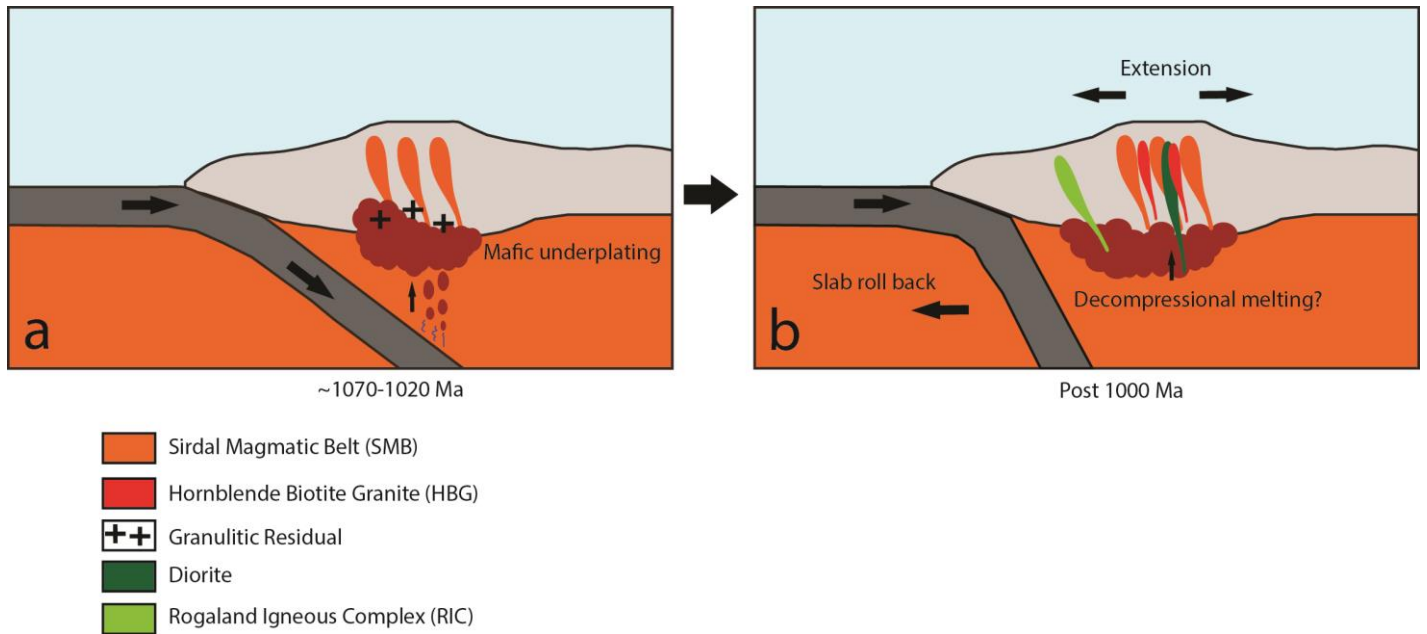


Figure 6.5: A schematic illustration of how the magmatic processes in southwestern Norway may have looked like. **(a)** Between c. 1070 and 1020 Ma. Mafic underplating causes the lower crust to melt. Magma rises and the SMB intrude into the pre Sveconorwegian bedrock. After melting the lower crust a granulitic residual are formed. **(b)** After c. 1000 Ma. Extension of the continent can cause decompressional melting which can cause more mafic underplating. Diorite, HBG and RIC are intruding into the pre Sveconorwegian bedrock. HBG can have formed from melting of the granulitic residual in the lower crust. Irregular underplating can have been one of the reasons for a varied degree of metamorphic conditions.

7 Conclusions

- Field relationship and geochronological data from Gyadalen indicate that magmatism and metamorphism happened within a short period of time, at c. 1040 Ma. Field relationships from Lysefjorden and Kvås suggest that this was a regional event.
- In light of the new field and geochronological data, it appears that the evolution of the regional metamorphism in the Rogaland- Vest Agder Sector during the Sveconorwegian Orogeny may be linked to the magmatic evolution. It is suggested that the spread in metamorphic zircon and monazite ages is a result of magmatically driven UH/UHT metamorphism.
- In this study long-lasting mafic magmatism is documented in southwestern Norway. In Gyadalen, a quartz dioritic migmatitic gneiss yields an age of 1033 ± 17 Ma and in the Kvås-Konsmo area a diorite yields an age of 991 ± 11 Ma. This supports previous suggestions of mafic underplating throughout large parts of the orogen. It is also suggested that voluminous basaltic underplating can have contributed to the heat that was necessary to cause high-grade metamorphism in southwestern Norway.
- The documentation of long-lasting mafic intrusions and granitic magmatism and no record of significant crustal thickening suggest that underplating associated with an accretionary/Andean-type margin is more likely as a tectonic setting for the magmatic and metamorphic evolution of southwestern Norway.
- A dome structure formed in the Rogaland-Vest Agder Sector during the Sveconorwegian orogeny is suggested to explain the large local variation in temperatures and pressures in southwestern Norway.

8 Further research

- It is suggested that several more monazite geochronological analyses are performed for southwestern Norway to better understand the significance of the monazite ages. High-precision dating (e.g. TIMS or SHRIMP) would be of interest to be able to distinguish between overlapping magmatic and metamorphic ages.
- It is also suggested that further studies combine U-Pb geochronology and in situ analyses with trace element analyses of monazite and zircon to better understand the timing of metamorphic reactions during the Sveconorwegian orogeny.
- Structural geology has been given limited attention in this project, and to be able to understand the structural geology and the tectonic evolution of the Kvås-Konsmo area, detailed and systematic work need to be done in the future. This would be of interest for better understand the emplacement of the SMB. Detailed structural research for southwestern Norway would be of interest to better understand the tectonic evolution of the Sveconorwegian Province.

9 References

- Andersen, T., 2002, Correction of common lead in U-Pb analysis that do not report ^{204}Pb : *Chemical Geology*, v. 192, p. 59-79.
- , 2005, Terrane analysis, regional nomenclature and crustal evolution in the Southwest Scandinavian Domain of the Fennoscandian Shield: *Geologiska Föreningen i Stockholm Förhandlingar*, v. 127, p. 159-168.
- Bingen, B., 1989, Geochemistry of Sveconorwegian augen gneisses from SW Norway at the amphibolite-granulite facies transition: *Norsk Geologisk Tidsskrift*, v. 69, p. 177-189.
- Bingen, B., Andersson, J., Söderlund, U., and Möller, C., 2008, The Mesoproterozoic in the Nordic countries: Episodes, v. 31, p. 1-6.
- Bingen, B., Davis, W. J., Hamilton, M. A., Engvik, A. K., Stein, H. J., Skår, Ø., and Nordgulen, Ø., 2008a, Geochronology of high-grade metamorphism in the Sveconorwegian belt, S. Norway: U-Pb, Th-Pb and Re-Os data: *Norwegian Journal of Geology*, v. 88, p. 13-42.
- Bingen, B., Nordgulen, Ø., Sigmond, E. M. O., Tucker, R. D., Mansfeld, J., and Högdahl, K., 2003, Relations between 1.19-1.13 Ga continental magmatism, sedimentation and metamorphism, Sveconorwegian province, S. Norway: *Precambrian Research*, v. 124, p. 215-241.
- Bingen, B., Nordgulen, Ø., and Viola, G., 2008b, A four phase model for the Sveconorwegian orogeny, SW Scandinavia: *Norwegian Journal of Geology*, v. 88, p. 43-72.
- Bingen, B., Skår, Ø., Marker, M., Sigmond, E. M. O., Nordgulen, Ø., Ragnhildstveit, J., Mansfeld, J., Tucker, R. D., and Liégeois, J.-P., 2005, Timing of continental building in the Sveconorwegian orogen, SW Norway: *Norwegian Journal of Geology*, v. 85, no. 1&2, p. 87-116.
- Bingen, B., Stein, H. J., Bogaerts, M., Bolle, O., and Mansfeld, J., 2006, Molybdenite Re-Os dating constrains gravitational collapse of the Sveconorwegian orogen, SW Scandinavia: *Lithos*, v. 87, p. 328-346.
- Bingen, B., and van Breemen, O., 1998a, Tectonic regimes and terrane boundaries in the high-grade Sveconorwegian belt of SW Norway, inferred from U-Pb zircon geochronology and geochemical signature of augen gneiss suites: *Journal of the Geological Society of London*, v. 155, p. 143-154.
- , 1998b, U-Pb monazite ages in amphibolite- to granulite-facies orthogneisses reflect hydrous mineral breakdown reactions: Sveconorwegian Province of SW Norway: *Contributions to Mineralogy and Petrology*, v. 132, p. 336-353.
- Blereau, E., Johnson, T. E., Clark, C., Taylor, R. J. M., Kinny, P. D., and Hand, M., in review, Reappraising the P-T evolution of the Rogaland-Vest Agder Sector, southwestern Norway.
- Bosse, V., Boulvais, P., Gautier, P., Tiepolo, M., Ruffet, G., Devidal, J. L., Cherneva, Z., Gerdjikov, I., and Paquette, J. L., 2009, Fluid-induced disturbance of the monazite Th-Pb chronometer: In situ dating and element mapping in pegmatites from the Rhodope (Greece, Bulgaria): *Chemical Geology*, v. 261, no. 3-4, p. 286-302.

- Brewer, T. S., Åhäll, K.-I., Menuge, J. F., Storey, C. D., and Parrish, R. R., 2004, Mesoproterozoic bimodal volcanism in SW Norway, evidence for recurring pre-Sveconorwegian continental margin tectonism: *Precambrian Research*, v. 134, p. 249-273.
- Budzyn, B., Harlov, D. E., Williams, M. L., and Jercinovic, M. J., 2011, Experimental determination of stability relations between monazite, fluorapatite, allanite, and REE-epidote as a function of pressure, temperature, and fluid composition: *American Mineralogist*, v. 96, no. 10, p. 1547-1567.
- Bybee, G. M., Ashwal, L. D., Shirey, S. B., Horan, M., Mock, T., and Andersen, T. B., 2014, Pyroxene megacrysts in Proterozoic anorthosites: Implications for tectonic setting, magma source and magmatic processes at the Moho: *Earth and Planetary Science Letters*, v. 389, no. 0, p. 74-85.
- Charlier, B., Duchesne, J.-C., Vander Auwera, J., Storme, J.-Y., Maquil, R., and Longhi, J., 2010, Polybaric fractional crystallization of high-alumina basalt parental magmas in the Egersund-Ogna massif-type anorthosite (Rogaland, SW Norway) constrained by plagioclase and high-alumina orthopyroxene megacrysts: *Journal of Petrology*, v. 51, p. 2515-2546.
- Cherniak, D. J., Watson, E. B., Grove, M., and Harrison, T. M., 2004, Pb diffusion in monazite: A combined RBS/SIMS study: *Geochimica et Cosmochimica Acta*, v. 68, p. 829-840.
- ChiuHuang, C.-K., Zhou, C., and Shadow Huang, H.-Y., 2014, In Situ Imaging of Lithium-Ion Batteries Via the Secondary Ion Mass Spectrometry: *Journal of Nanotechnology in Engineering and Medicine*, v. 5, no. 2, p. 021002-021002.
- Coint, N., Slagstad, T., Roberts, N. M. W., Marker, M., Røhr, T., and Sørensen, B. E., 2015, The Late Mesoproterozoic Sirdal Magmatic Belt, SW Norway: Relationships between magmatism and metamorphism and implications for Sveconorwegian orogenesis: *Precambrian Research*, v. 265, p. 57-77.
- Dodson, M. H., 1973, Closure temperature in cooling geochronological and petrological systems: *Contributions to Mineralogy and Petrology*, v. 40, p. 259-274.
- Drüppel, K., Elsäßer, L., Brandt, S., and Gerdes, A., 2013, Sveconorwegian Mid-crustal Ultrahigh-temperature Metamorphism in Rogaland, Norway: U–Pb LA-ICP-MS Geochronology and Pseudosections of Sapphirine Granulites and Associated Paragneisses: *Journal of Petrology*, v. 54, no. 2, p. 305-350.
- Falkum, T., 1982, Geologisk kart over Norge, berggrunnskart MANDAL, 1:250,000: Norges geologiske undersøkelse, scale 1:250,000.
- Faure, G., and Mensing, T. M., 2005, *Isotopes: Principles and Applications*, Hoboken, New Jersey, John Wiley & Sons Inc, 897 p.:
- Gasquet, D., Bertrand, J.-M., Paquett, J. L., Guedes, R. D. A., Tiepolo, M., Boullier, A.-M., Scaillet, S., and Nomade, S., 2010, Miocene to Messinian deformation and hydrothermal activity in a pre-Alpine basement massif of the French western Alps: new U-Th-Pb and aragon ages from the Lauzière massif: *Bulletin de la Societe Geologique de France*, v. 181, p. 227-241.
- Gorbatshev, R., and Bogdanova, S., 1993, Frontiers in the Baltic Shield: *Precambrian Research*, v. 64, p. 3-21.

- Gower, C. F., Kamo, S., and Krogh, T. E., 2008, Indentor tectonism in the eastern Grenville Province: *Precambrian Research*, v. 167, no. 1-2, p. 201-212.
- Gower, C. F., Ryan, A. B., and Rivers, T., 1990, Mid-Proterozoic Laurentia-Baltica: an overview of its geological evolution and a summary of the contributions made by this volume, *in* Gower, C. F., Rivers, T., and Ryan, A. B., eds., *Mid-Proterozoic Laurentia-Baltica*, Volume 38, Geological Association of Canada, Special Paper, p. 1-20.
- Hanchar, J. M., and Hoskin, P. W. O., 2003, Zircon, *in* Ribbe, P. H., and Rosso, J. J., eds., *Reviews in Mineralogy and Geochemistry*, Volume 53: Washington, DC, The Mineralogical Society of America, p. 500.
- Harlov, D. E., Wirth, R., and Hetherington, C. J., 2011, Fluid-mediated partial alteration in monazite: the role of coupled dissolution-reprecipitation in element redistribution and mass transfer: *Contributions to Mineralogy and Petrology*, v. 162, p. 329-348.
- Henderson, I. H. C., and Ihlen, P. M., 2004, Emplacement of polygeneration pegmatites in relation to Sveco-Norwegian contractional tectonics: examples from southern Norway: *Precambrian Research*, v. 133, no. 3-4, p. 207-222.
- Hermans, G. A. E. M., Tobi, A. C., Poorter, R. P. E., and Maijer, C., 1975, The high-grade metamorphic Precambrian of the Sirdal-Ørdsdal area, Rogaland/Vest-Agder, south-west Norway: *Norges geologiske undersøkelse*, v. 318, p. 51-74.
- Högdahl, K., Andersson, U. B., and Eklund, O., 2004, Geological Survey of Finland Special paper: The Transscandinavian Igneous Belt: A review of its character and evolution Volume 37, p. 1-125.
- Högdahl, K., Majka, J., Sjöström, H., Nilsson, K. P., Claesson, S., and Konečný, P., 2012, Reactive monazite and robust zircon growth in diatexites and leucogranites from a hot, slowly cooled orogen: implications for the Palaeoproterozoic tectonic evolution of the central Fennoscandian Shield, Sweden.: *Contributions to Mineralogy and Petrology*, v. 163, p. 167-188.
- Horstwood, M. S. A., 2008, Data reduction strategies, uncertainty assessment and resolution of LA-(MC-)ICP-MS isotope data., Vancouver, Mineralogical Association of Canada, Short Course Series.
- Jackson, S. E., Pearson, N. J., Griffin, W. L., and Belousova, E. A., 2004, The application of laser ablation-inductively coupled plasma-mass spectrometry to in situ U-Pb zircon geochronology: *Chemical Geology*, v. 211, p. 47-69.
- Jaffey, A. H., Flynn, K. F., Glendenin, W. C., Bentley, W. C., and Essling, A. M., 1971, Precision measurements of half-lives and specific activities of ^{235}U and ^{238}U : *Physical Reviews C: Nuclear Physics*, v. 4, p. 1889-1906.
- Jensen, E., and Corfu, F., 2016, The U-Pb age of the Finse batholith, a composite bimodal Sveconorwegian intrusion: *Norwegian Journal of Geology*, v. 96, no. 3.
- Johansson, L., Möller, C., and Söderlund, U., 2001, Geochronology of eclogite facies metamorphism in the Sveconorwegian Province of SW Sweden: *Precambrian Research*, v. 106, p. 261-275.
- Karlstrom, K. E., and Williams, M. L., 1998, Heterogeneity of the middle crust: Implications for strength of continental lithosphere: *Geology*, v. 26, p. 815-818.

- Kelly, N. M., Harley, S. L., and Möller, A., 2012, Complexity in the behavior and recrystallization of monazite during high-T metamorphism and fluid infiltration: *Chemical Geology*, v. 322–323, p. 192-208.
- Kelsey, D. E., Clark, C., and Hand, M., 2008, Thermobarometric modelling of zircon and monazite growth in melt-bearing systems: examples using model metapelitic and metapsammitic granulites: *Journal of Metamorphic Geology*, v. 26, p. 199-212.
- Kosler, J., and Sylvester, P. J., 2003, Present Trends and the Future of Zircon in Geochronology: Laser Ablation ICPMS: *Reviews in Mineralogy and Geochemistry* p. 243-275.
- Kylander-Clark, A. R. C., and Cottle, J. M., 2014, Short Course: Laser Ablation Split Stream (LASS), Geochronology and Petrochronology.: US Santa Barbara Earth Science.
- Loehn, C. W., 2011, Investigation of the monazite chemical dating technique [Doctor of Philosophy: Virginia Polytechnic Institute and State University, 85 p.
- Ludwig, K. R., 2003, Isoplot 3.00, A Geochronological Toolkit for Microsoft Excel: Berkley Geochronology Center, Special Publication, v. 4, p. 1-74.
- Mattinson, J. M., 2010, Analysis of the relative decay constants of ²³⁵U and ²³⁸U by multi-step CA-TIMS measurements of closed-system natural zircon samples: *Chemical Geology*, v. 275, no. 3–4, p. 186-198.
- McFarlane, C. R. M., and Harrison, T. M., 2006, Pb-diffusion in monazite: Constraints from a high-T contact aureole setting: *Earth and Planetary Science Letters*, v. 250, p. 376-384.
- Möller, A., O'Brien, P. J., Kennedy, A., and Kröner, A., 2003, Linking growth episodes of zircon and metamorphic textures to zircon chemistry: An example from the ultrahigh-temperature granulites of Rogaland (SW Norway), *in* Vance, D., Müller, W., and Villa, I. M., eds., *Geochronology: Linking the Isotopic Record with Petrology and Textures*. Geological Society of London, Special Publication, Volume 220, p. 65-81.
- Möller, C., 1998, Decompressed eclogites in the Sveconorwegian (-Grenvillian) orogen of SW Sweden: petrology and tectonic implications: *Journal of Metamorphic Geology*, v. 16, p. 641-656.
- Möller, C., Andersson, J., Dyck, B., and Antal Lundin, I., 2015, Exhumation of an eclogite terrane as a hot migmatitic nappe, Sveconorwegian orogen: *Lithos*, v. 226, no. 0, p. 147-168.
- Mueller, P. A., and Vervoort, J. D., 2012, Secondary Ion Mass Spectrometer (SIMS), Volume 2015: Carleton College, Science Education Resource Center.
- Passarelli, C. R., Basei, M. A. S., Siga, J. R. O., Sato, K., Sproesser, W. M., and Loios, V. A. P., 2009, Dating minerals by ID-TIMS geochronology at times of in situ analysis: selected case studies from CPGeo-IGc-USP laboratory: *Anais da Academia Brasileira de Ciencias*, v. 81, no. 1, p. 73-97.
- Roberts, N. M. W., 2010, From crystal to crust: the Proterozoic crustal evolution of southwest Norway PhD]: University of Leicester.

- Roberts, N. M. W., and Slagstad, T., 2015, Continental growth and reworking on the edge of the Columbia and Rodinia supercontinents; 1.86–0.9 Ga accretionary orogeny in southwest Fennoscandia: *International Geology Review*, v. 57, no. 11-12, p. 1582-1606.
- Salli, I., 1983, Pielaveden karta-alueen kallioperä.: *Kallioperan selitykset*, v. 3314, p. 1-31.
- Scheiber, T., Viola, G., Bingen, B., Peters, M., and Solli, A., 2015, Multiple reactivation and strain localization along a Proterozoic orogen-scale deformation zone: The Kongsberg-Telemark boundary in southern Norway revisited: *Precambrian Research*, v. 265, p. 78-103.
- Scherer, E., Münker, C., and Mezger, K., 2001, Calibration of the lutetium-hafnium clock: *Science*, v. 293, p. 683-687.
- Schoene, B., 2014, 4.10 U-Th-Pb Geochronology: *Treatise on Geochemistry*, p. 341-378.
- Skår, Ø., 2002, U-Pb geochronology and geochemistry of early Proterozoic rocks of the tectonic basement windows in central Nordland, Caledonides of north-central Norway: *Precambrian Research*, v. 116, p. 265-283.
- Slagstad, T., 2006, Chemical (U–Th–Pb) dating of monazite: Analytical protocol for a LEO 1450VP scanning electron microscope and examples from Rogaland and Finnmark, Norway: *Norges geologiske undersøkelse Bulletin*, v. 446, p. 11-18.
- Slagstad, T., Roberts, N. M. W., Marker, M., Røhr, T. S., and Schiellerup, H., 2013a, A non-collisional, accretionary Sveconorwegian orogen: *Terra Nova*, v. 25, no. 1, p. 30-37.
- , 2013b, A non-collisional, accretionary Sveconorwegian orogen – Reply: *Terra Nova*, v. 25, no. 2, p. 169-171.
- Smith, H. A., and Barreiro, B., 1990, Monazite U-Pb dating of staurolite grade metamorphism in pelitic schists: *Contributions to Mineralogy and Petrology*, v. 105, no. 5, p. 602-615.
- Smith, H. A., and Giletti, B. J., 1997, Lead diffusion in monazite: *Geochimica et Cosmochimica Acta*, v. 61, no. 5, p. 1047-1055.
- Söderlund, U., Möller, C., Andersson, J., Johansson, L., and Whitehouse, M., 2002, Zircon geochronology in polymetamorphic gneisses in the Sveconorwegian orogen, SW Sweden: Ion microprobe evidence for 1.46-1.42 and 0.98-0.96 Ga reworking: *Precambrian Research*, v. 113, p. 193-225.
- Stacey, J. S., and Kramers, J. D., 1975, Approximation of terrestrial lead isotope evolution by a two-stage model: *Earth and Planetary Science Letters*, v. 26, p. 207-221.
- Stormoen, M. A., 2015, Synkinematic intrusion of granitoid sheets, with implications for molybdenite deposits in the Knaben Zone [Master: Norwegian University of Science and Technology 131 p.
- Tera, F., and Wasserburg, G. J., 1972, U-Th-Pb systematics in three Apollo 14 basalts and the problem of initial Pb in lunar rocks: *Earth and Planetary Science Letters*, v. 14, no. 3, p. 281-304.
- Van Achterbergh, E., Ryan, C., Jackson, S., and Griffin, W. L., 2001, Laser-ablation-ICPMS in the Earth Sciences - Appendix 3 data reduction software for LA-ICP-MS. In: P. Sylvester (Editor): *Mineralogical Association of Canada Short Course*, v. 29, p. 239-243.

- Vander Auwera, J., Bogaerts, M., Liégeois, J.-P., Demaiffe, D., Wilmart, E., Bolle, O., and Duchesne, J.-C., 2003, Derivation of the 1.0.0.9 Ga ferro-potassic A-type granitoids of southern Norway by extreme differentiation from basic magmas: *Precambrian Research*, v. 124, p. 107-148.
- Vander Auwera, J., Bolle, O., Bingen, B., Liégeois, J.-P., Bogaerts, M., Duchesne, J.-C., De Waele, B., and Longhi, J., 2011, Sveconorwegian massif-type anorthosites and related granitoids result from post-collisional melting of a continental arc root: *Earth Science Reviews*, v. 107, p. 375-397.
- Viola, G., Henderson, I. H. C., Bingen, B., and Hendriks, B. W. H., 2011, The Grenvillian-Sveconorwegian orogeny in Fennoscandia: Back-thrusting and extensional shearing along the "Mylonite Zone": *Precambrian Research*, v. 189, p. 368-388.
- Weaver, S. G., Bruce, R., Nelson, E. P., BRUECKNER, H. K., and LeHuray, A. P., 1990, The Patagonian batholith at 48°S latitude, Chile; Geochemical and isotopic variations, *in* Kay, S. M., and Rapela, C. W., eds., *Plutonism from Antarctica to Alaska*, Volume 241: Boulder, Colorado, p. 33-50.
- Westphal, M., Schumacher, J. C., and Boschert, S., 2003, High-temperature metamorphism and the role of magmatic heat sources at the Rogaland Anorthosite Complex in southwestern Norway: *Journal of Petrology*, v. 44, p. 1145-1162.
- Wetherill, G. W., 1956, Discordant U-Pb ages: *Transactions of the American Geophysical Union*, v. 37, p. 320-326.
- Whitney, D. L., and Evans, B. W., 2010, Abbreviations for names of rock-forming minerals: *American Mineralogist*, v. 95, p. 185-187.
- Wiedenbeck, M., Allé, P., Corfu, F., Griffin, W. L., Meier, M., Oberli, F., Von Quadt, A., Roddick, J. C., and Spiegel, W., 1995, Three natural zircon standards for U-Th-Pb, Lu-Hf, trace element and REE analyses: *Geostandards Newsletter*, v. 19, p. 1-23.
- Williams, M. L., Jercinovic, M. J., Harlov, D. E., Budzyn, B., and Hetherington, C. J., 2011, Resetting monazite ages during fluid-related alteration: *Chemical Geology*, v. 283, p. 218-225.
- Winter, J. D., 2001, *Principles of Igneous and Metamorphic Petrology*, New Jersey, Peason Education, Inc.
- Wolf, R. E., 2005, *Introduction to ICP-MS*, Volume 2015: U.S. Geological Survey.
- Wu, Y., and Zheng, Y., 2004, Genesis of zircon and its constraints on interpretation of U-Pb age: *Chinese Science Bulletin*, v. 49, no. 15, p. 1554-1569.

Appendix

Appendix A – Samples

Appendix B – Zircon geochronological data

Appendix C – Monazite geochronological data

Appendix A – Samples

Samples taken from Gyadalen, Lysefjorden and the Kvås-Konsmo area

Sample	Locality	Zone+N/S	East (m)	North (m)	Rocktype	Rock forming minerals	Accessory minerals
IH128051	Kvås/Konsmo	32	395363	6459671	Leucosome in metapelite	Qz, pl	Grt, bt, zrn
IH128052	Kvås/Konsmo	32	395395	6459675	Leucosome and melanosome in metapelite	Qz, pl, bt	Grt, zrn, ap
IH128053	Kvås/Konsmo	32	395887	6459642	Granite	Kfs, Qz, bt, pl, hbl	Spn, opq, zrn, ap
IH128056	Kvås/Konsmo	32	396017	6459582	Amphibolite	Hbl, pl, bt	Chl, ap
IH128057	Kvås/Konsmo	32	396991	6459698	Granite	Qz, kfs, bt	Opq, zrn, ap
IH128058	Kvås/Konsmo	32	397261	6459640	Diorite	Hbl, opx, pl, bt	Opq, zrn, ap
IH128059	Kvås/Konsmo	32	399743	6464701	Granite	Hbl, bt, qz, ksf	Opq, spn, zrn, ap, chl
IH128060	Kvås/Konsmo	32	393564	6457540	Amphibolite	Chl, hbl, qz, pl	Ep, ap
IH128061	Kvås/Konsmo	32	395379	6459660	Metapelite	Bt, qz, pl, grt, kfs	Zrn, mnz, opq
IH128062	Kvås/Konsmo	32	395400	6459674	Pegmatite	Qz, bt, kfs, pl	Grt, opq, ap, zrn
IH128063	Kvås/Konsmo	32	395988	6459604	Amphibolite	Hbl, bt, pl	Ap, opq
IH128064	Kvås/Konsmo	32	403000	6461183	Granite	Kfs, qz, bt	Opq, zrn, ep
IH128065a	Kvås/Konsmo	32	403000	6461183	Migmatite, mesosome	Bt, qz, ksp, pl	Opq, zrn, chl, ep, ap
IH128065b	Kvås/Konsmo	32	403000	6461183	Migmatite, leucosome	Kfs, qz, bt	Chl, zrn, ms, opq
IH128066	Kvås/Konsmo	32	403000	6461183	Pegmatite	Kfs, qz	Opq, ep
IH128067	Kvås/Konsmo	32	399578	6466420	Deformed porphyritic granite	Hbl, bt, qz, kfs	Opq, spn, zrn
IH128068	Kvås/Konsmo	32	400453	6465027	Deformed porphyritic granite	Hbl, bt, kfs, qz	Opq, spn, zrn
IH128069	Kvås/Konsmo	32	401737	6465730	Foliated granite	Ksp, qz, bt, hbl, pl	Opq, spn, zrn
IH128070	Kvås/Konsmo	32	401687	6465410	Foliated granite	No thin section	No thin section
IH128071	Kvås/Konsmo	32	402170	6464883	Foliated granite	Bt, qz, ksp	Opq, zrn
IH128072	Kvås/Konsmo	32	402995	6461179	Migmatite	Bt, qz, hbl, pl	Opq, zrn, ap
IH128073	Kvås/Konsmo	32	400091	6460789	Porphyritic granite	Kfs, qz, bt	Opq, ap, zrn
IH128074	Kvås/Konsmo	32	398980	6460798	Porphyritic granite	Kfs, qz, bt	Opq, ap, zrn
ROG092326	Lysefjorden	32	334213	6532806	Metapelite	Crd, pl, bt, qz, grt, sil	Spl (green), opq, pinnite, zrn, mnz, ap
ROG092322	Lysefjorden	32	335928	6538186	Foliated granitoid	Kfs, qz	Zrn, mnz, ap, opq
VAG084396	Gyadalen	32	356101	6502651	Granitic gneiss	Qz, kfs, bt	Chl, ap, zrn, opq
VAG084397	Gyadalen	32	357625	6503462	Quartz dioritic migmatitic gneiss	Qz, hbl, pl, cpx, bt, ap	Zrn, opq
VAG084399	Gyadalen	32	359379	6504170	Porphyritic foliated hbl bt granite	Kfs, pl, hbl, bt	Ap, opq, zrn

Appendix B – Zircon geochronological data

IH128061 (metapelite, Kvås)

[illegible]

IH128065A (mesosome), IH128065B (leucosome), IH128058 (diorite), IH128068 (granite)

[illegible]

IH128070 (folded granite), IH128072 (migmatite) and IH128074 (porphyritic granite)

Isotope ratios										Age estimates (ma)										Concentrations																																																																																																																																																																																																																																																																																																																																																																																																																																																																																																																																																																																																																																																																																																																																																																																																																																																											
Concordia output					Terra-Wasserburg output					Pb207/Pb206					Pb207/235U					Pb206/238U					Th/U					U*					Th*					Photo*																																																																																																																																																																																																																																																																																																																																																																																																																																																																																																																																																																																																																																																																																																																																																																																																																																							
Analysis_#		Pb207/Pb206		Is %		Pb206/238U		Is %		207Pb/206		Is %		Pb207/235U		Is %		Pb206/238U		Is %		Pb207/235U		Is %		Pb206/238U		Is %		Pb207/235U		Is %		Pb206/238U		Is %		Pb207/235U		Is %		Pb206/238U		Is %		Pb207/235U		Is %		Pb206/238U		Is %		Pb207/235U		Is %		Pb206/238U		Is %		Pb207/235U		Is %		Pb206/238U		Is %		Pb207/235U		Is %		Pb206/238U		Is %		Pb207/235U		Is %		Pb206/238U		Is %		Pb207/235U		Is %		Pb206/238U		Is %		Pb207/235U		Is %		Pb206/238U		Is %		Pb207/235U		Is %		Pb206/238U		Is %		Pb207/235U		Is %		Pb206/238U		Is %		Pb207/235U		Is %		Pb206/238U		Is %		Pb207/235U		Is %		Pb206/238U		Is %		Pb207/235U		Is %		Pb206/238U		Is %		Pb207/235U		Is %		Pb206/238U		Is %		Pb207/235U		Is %		Pb206/238U		Is %		Pb207/235U		Is %		Pb206/238U		Is %		Pb207/235U		Is %		Pb206/238U		Is %		Pb207/235U		Is %		Pb206/238U		Is %		Pb207/235U		Is %		Pb206/238U		Is %		Pb207/235U		Is %		Pb206/238U		Is %		Pb207/235U		Is %		Pb206/238U		Is %		Pb207/235U		Is %		Pb206/238U		Is %		Pb207/235U		Is %		Pb206/238U		Is %		Pb207/235U		Is %		Pb206/238U		Is %		Pb207/235U		Is %		Pb206/238U		Is %		Pb207/235U		Is %		Pb206/238U		Is %		Pb207/235U		Is %		Pb206/238U		Is %		Pb207/235U		Is %		Pb206/238U		Is %		Pb207/235U		Is %		Pb206/238U		Is %		Pb207/235U		Is %		Pb206/238U		Is %		Pb207/235U		Is %		Pb206/238U		Is %		Pb207/235U		Is %		Pb206/238U		Is %		Pb207/235U		Is %		Pb206/238U		Is %		Pb207/235U		Is %		Pb206/238U		Is %		Pb207/235U		Is %		Pb206/238U		Is %		Pb207/235U		Is %		Pb206/238U		Is %		Pb207/235U		Is %		Pb206/238U		Is %		Pb207/235U		Is %		Pb206/238U		Is %		Pb207/235U		Is %		Pb206/238U		Is %		Pb207/235U		Is %		Pb206/238U		Is %		Pb207/235U		Is %		Pb206/238U		Is %		Pb207/235U		Is %		Pb206/238U		Is %		Pb207/235U		Is %		Pb206/238U		Is %		Pb207/235U		Is %		Pb206/238U		Is %		Pb207/235U		Is %		Pb206/238U		Is %		Pb207/235U		Is %		Pb206/238U		Is %		Pb207/235U		Is %		Pb206/238U		Is %		Pb207/235U		Is %		Pb206/238U		Is %		Pb207/235U		Is %		Pb206/238U		Is %		Pb207/235U		Is %		Pb206/238U		Is %		Pb207/235U		Is %		Pb206/238U		Is %		Pb207/235U		Is %		Pb206/238U		Is %		Pb207/235U		Is %		Pb206/238U		Is %		Pb207/235U		Is %		Pb206/238U		Is %		Pb207/235U		Is %		Pb206/238U		Is %		Pb207/235U		Is %		Pb206/238U		Is %		Pb207/235U		Is %		Pb206/238U		Is %		Pb207/235U		Is %		Pb206/238U		Is %		Pb207/235U		Is %		Pb206/238U		Is %		Pb207/235U		Is %		Pb206/238U		Is %		Pb207/235U		Is %		Pb206/238U		Is %		Pb207/235U		Is %		Pb206/238U		Is %		Pb207/235U		Is %		Pb206/238U		Is %		Pb207/235U		Is %		Pb206/238U		Is %		Pb207/235U		Is %		Pb206/238U		Is %		Pb207/235U		Is %		Pb206/238U		Is %		Pb207/235U		Is %		Pb206/238U		Is %		Pb207/235U		Is %		Pb206/238U		Is %		Pb207/235U		Is %		Pb206/238U		Is %		Pb207/235U		Is %		Pb206/238U		Is %		Pb207/235U		Is %		Pb206/238U		Is %		Pb207/235U		Is %		Pb206/238U		Is %		Pb207/235U		Is %		Pb206/238U		Is %		Pb207/235U		Is %		Pb206/238U		Is %		Pb207/235U		Is %		Pb206/238U		Is %		Pb207/235U		Is %		Pb206/238U		Is %		Pb207/235U		Is %		Pb206/238U		Is %		Pb207/235U		Is %		Pb206/238U		Is %		Pb207/235U		Is %		Pb206/238U		Is %		Pb207/235U		Is %		Pb206/238U		Is %		Pb207/235U		Is %		Pb206/238U		Is %		Pb207/235U		Is %		Pb206/238U		Is %		Pb207/235U		Is %		Pb206/238U		Is %		Pb207/235U		Is %		Pb206/238U		Is %		Pb207/235U		Is %		Pb206/238U		Is %		Pb207/235U		Is %		Pb206/238U		Is %		Pb207/235U		Is %		Pb206/238U		Is %		Pb207/235U		Is %		Pb206/238U		Is %		Pb207/235U		Is %		Pb206/238U		Is %		Pb207/235U		Is %		Pb206/238U		Is %		Pb207/235U		Is %		Pb206/238U		Is %		Pb207/235U		Is %		Pb206/238U		Is %		Pb207/235U		Is %		Pb206/238U		Is %		Pb207/235U		Is %		Pb206/238U		Is %		Pb207/235U		Is %		Pb206/238U		Is %		Pb207/235U		Is %		Pb206/238U		Is %		Pb207/235U		Is %		Pb206/238U		Is %		Pb207/235U		Is %		Pb206/238U		Is %		Pb207/235U		Is %		Pb206/238U		Is %		Pb207/235U		Is %		Pb206/238U		Is %		Pb207/235U		Is %		Pb206/238U		Is %		Pb207/235U	

VAG084396 (granitic gneiss), VAG084397 (quartz dioritic gneiss) VAG084399 (foliated granite)

▼	Isotope ratios										Age estimates (ma)										Concentrations					Pb com. >LLD (%)		
	Concordia output					Terra-Wasserburg output					Pb207 U235					Pb206 U238					Th/U						Th *	U* conc
	Pb207 U235	Is %	Pb206 U238	Is %	roh	238/206	Is %	207/206	Is %	238/206	Is %	Pb207 U235	Is	Pb206 U238	Is	Th/U	Th *	U*										
Analysis #	84396_01	1.77274	1.01	0.17799	0.96	0.43	5.618293	0.96	0.07223	1.05	992.5	21.27	1035.5	6.55	1056	9.34	106.4	0.1233	1488	183	293	0						
	84396_02	1.73155	1.02	0.17031	0.96	0.42	5.871646	0.96	0.07373	1.07	1034.2	21.12	1020.3	6.57	1013.8	9.01	98.0	0.43012	506	218	103	1						
	84396_03	1.72495	1.05	0.17143	0.96	0.41	5.833285	0.96	0.07297	1.10	1034.2	22.07	1017.9	6.76	1020	9.09	100.7	0.39292	278	109	57	-						
	84396_04	1.78638	1.00	0.17264	0.96	0.44	5.7924	0.96	0.07504	1.04	1069.7	20.87	1040.5	6.51	1026.6	9.10	96.0	0.27872	1972	550	394	1						
	84396_05	1.79684	1.01	0.17636	0.96	0.42	5.67022	0.96	0.07389	1.06	1038.4	20.78	1044.3	6.57	1047.1	9.27	100.8	0.4163	1327	553	279	0						
	84396_06	1.88114	1.01	0.18143	0.96	0.43	5.511768	0.96	0.07519	1.05	1073.7	21.02	1074.5	6.68	1074.8	9.49	100.1	0.33777	1432	484	305	1						
	84396_07	1.78104	1.00	0.17541	0.96	0.43	5.700929	0.96	0.07364	1.05	1031.5	21.04	1038.6	6.52	1041.8	9.22	101.0	0.15945	1839	293	362	0						
	84396_08	1.78412	1.01	0.17792	0.96	0.42	5.620504	0.96	0.07272	1.06	1006.3	21.26	1039.7	6.57	1055.6	9.34	104.9	0.28498	982	280	201	0						
	84396_09	1.82086	1.01	0.17939	0.96	0.42	5.574447	0.96	0.07361	1.06	1030.9	21.14	1053	6.60	1063.6	9.40	103.2	0.33255	1169	389	244	0						
	84396_10	1.71005	1.00	0.17015	0.96	0.44	5.877167	0.96	0.07288	1.04	1010.8	21.12	1012.3	6.43	1013	8.98	100.2	0.16121	1979	319	377	0						
	84396_11	1.85316	1.01	0.17994	0.96	0.42	5.557408	0.96	0.07469	1.06	1060.2	21.02	1064.6	6.64	1066.6	9.42	100.6	0.34962	1364	477	289	1						
	84396_12	1.72828	1.02	0.16991	0.96	0.42	5.885469	0.96	0.07377	1.07	1035.1	21.16	1019.1	6.58	1011.6	8.99	97.7	0.45323	561	254	115	0						
	84397_01	1.77656	1.11	0.17508	0.97	0.39	5.71167	0.97	0.07359	1.16	1030.2	23.21	1036.9	7.22	1040.1	9.31	101.0	0.92882	127	118	30	3						
	84397_02	1.77573	1.16	0.17506	0.98	0.38	5.71233	0.98	0.07356	1.20	1029.5	23.77	1036.6	7.51	1039.9	9.35	101.0	0.34233	143	49	29	2						
	84397_03	1.79211	1.36	0.17464	1.00	0.32	5.72607	1.00	0.07442	1.41	1052.9	28.16	1042.6	8.88	1037.6	9.58	98.5	0.28897	73	21	15	-						
	84397_04	1.74757	1.44	0.17271	1.01	0.29	5.79005	1.01	0.07338	1.50	1024.5	29.61	1026.3	9.33	1027	9.59	100.2	0.3452	64	22	13	4						
	84397_05	1.75005	1.17	0.1714	0.97	0.37	5.83431	0.97	0.07405	1.22	1042.8	24.4	1027.2	7.58	1019.8	9.20	97.8	0.7718	95	74	21	4						
	84397_06	1.73884	1.13	0.17271	0.97	0.38	5.79005	0.97	0.07301	1.18	1014.4	23.73	1023	7.31	1027	9.22	101.2	0.80323	125	100	28	2						
	84397_07	1.74308	1.08	0.17134	0.96	0.40	5.83635	0.96	0.07378	1.12	1035.4	22.28	1024.6	6.97	1019.5	9.10	98.5	0.91352	178	163	41	1						
	84397_08	1.71574	1.12	0.17104	0.97	0.38	5.84659	0.97	0.07275	1.17	1007	23.52	1014.4	7.20	1017.8	9.13	101.1	0.81272	120	98	27	-						
	84397_09	1.76103	1.29	0.1735	0.99	0.34	5.76369	0.99	0.07361	1.33	1030.8	26.47	1031.2	8.34	1031.4	9.42	100.1	0.27741	60	17	12	3						
	84397_10	1.73297	1.27	0.17007	0.99	0.34	5.87993	0.99	0.0739	1.31	1038.7	26.34	1020.9	8.16	1012.5	9.24	97.5	0.2504	67	17	13	8						
	84397_11	1.64164	1.34	0.16138	1.00	0.32	6.19655	1.00	0.07377	1.40	1035.2	27.83	986.3	8.46	964.5	8.91	93.2	0.24316	58	14	11	6						
	84397_12	1.79567	1.13	0.17455	0.97	0.38	5.72902	0.97	0.07461	1.18	1057.6	23.93	1043.9	7.40	1037.1	9.30	98.1	0.88448	123	109	28	-						
	84399_01	1.82206	1.05	0.17748	0.96	0.41	5.634438	0.96	0.07445	1.09	1053.4	22.19	1063.4	6.85	1053.2	9.33	100.0	0.24681	399	99	81	1						
	84399_02	1.84945	1.04	0.17933	0.96	0.41	5.576312	0.96	0.07479	1.08	1063	21.64	1063.2	6.83	1063.3	9.41	100.0	0.26503	573	152	118	1						
	84399_03	1.8006	1.05	0.17782	0.96	0.40	5.623664	0.96	0.07343	1.10	1026	22.07	1045.7	6.87	1055.1	9.35	102.8	0.39465	662	261	140	1						
	84399_04	1.7564	1.17	0.17207	0.98	0.37	5.811588	0.98	0.07403	1.22	1042.2	24.34	1029.5	7.56	1023.5	9.22	98.2	0.55812	91	51	19	5						
	84399_05	1.76163	1.06	0.17413	0.96	0.39	5.742836	0.96	0.07337	1.12	1024.1	22.33	1031.4	6.89	1034.8	9.19	101.0	0.40908	579	237	120	1						
	84399_06	1.72017	1.04	0.16979	0.96	0.41	5.889628	0.96	0.07347	1.09	1027	21.93	1016.1	6.70	1010.9	8.98	98.4	0.40897	632	258	128	1						
	84399_07	1.78006	1.04	0.17424	0.96	0.40	5.73921	0.96	0.07409	1.09	1043.9	21.78	1038.2	6.76	1035.4	9.17	99.2	0.54313	772	419	165	1						
	84399_08	1.82955	1.10	0.17635	0.96	0.39	5.670542	0.96	0.07524	1.14	1074.9	22.84	1066.1	7.21	1047	9.33	97.4	1.55807	286	445	76	1						
	84399_09	1.72429	1.04	0.17092	0.96	0.41	5.85069	0.96	0.07316	1.09	1018.4	21.96	1017.6	6.71	1017.2	9.03	99.9	0.40786	660	269	134	1						
	84399_10	1.7659	1.06	0.17372	0.96	0.40	5.75639	0.96	0.07372	1.11	1033.7	21.98	1033	6.88	1032.6	9.17	99.9	0.3777	416	157	86	1						
	84399_11	1.78636	1.12	0.17644	0.97	0.38	5.667649	0.97	0.07342	1.17	1025.7	23.4	1040.5	7.27	1047.5	9.35	102.1	1.35339	147	199	38	3						
	84399_12	1.74272	1.05	0.17201	0.96	0.40	5.813615	0.96	0.07347	1.10	1027	22.04	1024.5	6.77	1023.2	9.08	99.6	0.42546	583	248	120	0						

ROG092326 (metapelite, Lysefjorden)

Analysis #	Isotope ratios					Terra-Wasserburg output											Age estimates (ma)					Concentrations					Ph com. >1LD (%)
	Concordia output					Terra-Wasserburg output																					
	Pb207 U235	1s%	Pb206 U238	1s%	rob	238/206	1s%	207/206	1s%	Pb207 Pb206	Is	Pb207 U235	Is	Pb206 U238	Is	conc	Th/U	U*	Th*	Phot*							
ROG092326_31	3.41465	1.16	0.26209	1.05	0.48	3.815483	1.05	0.09451	1.13	1518.3	21.21	1507.8	9.09	1500.5	14.03	98.8	0.51	55	28	0.0	-						
ROG092326_32	3.04566	1.10	0.23867	1.04	0.50	4.189886	1.04	0.09257	1.07	1478.9	20.18	1419.1	8.37	1379.8	12.91	93.3	1.58	218	346	0.1	0						
ROG092326_33	1.72167	1.12	0.16907	1.04	0.50	5.91471	1.04	0.07387	1.08	1037.9	21.8	1016.6	7.16	1007	9.71	97.0	0.01	216	2	0.1	-						
ROG092326_34	3.72703	1.11	0.2697	1.04	0.50	3.707824	1.04	0.10024	1.08	1628.6	19.93	1577.2	8.87	1539.3	14.26	94.5	0.29	124	35	0.1	-						
ROG092326_35	2.9958	1.26	0.20907	1.07	0.43	4.783087	1.07	0.10394	1.25	1695.7	22.82	1406.6	9.62	1223.9	11.88	72.2	0.44	80	35	0.1	-						
ROG092326_36	4.45805	1.11	0.30475	1.04	0.50	3.281378	1.04	0.10612	1.08	1733.7	19.76	1723.2	9.24	1714.8	15.71	98.9	0.50	96	48	0.1	0						
ROG092326_37	1.72089	1.11	0.16948	1.04	0.49	5.900401	1.04	0.07366	1.09	1032.1	21.42	1016.4	7.15	1009.3	9.73	97.8	0.10	166	16	0.1	-						
ROG092326_38	3.20528	1.18	0.2514	1.05	0.47	3.977725	1.05	0.09249	1.16	1477.3	21.94	1458.4	9.16	1445.7	13.63	97.9	0.47	68	32	0.0	-						
ROG092326_39	3.14005	1.13	0.24407	1.04	0.50	4.097185	1.04	0.09333	1.09	1494.6	20.6	1442.6	8.67	1407.8	13.21	94.2	0.63	90	57	0.0	-						
ROG092326_40	3.49925	1.13	0.26728	1.04	0.49	3.741395	1.04	0.09497	1.10	1527.5	20.49	1527	8.89	1527	14.21	100.0	0.30	95	28	0.2	1						
ROG092326_41	1.77597	1.15	0.17625	1.04	0.48	5.673759	1.04	0.0731	1.12	1016.6	22.61	1036.7	7.48	1046.4	10.11	102.9	0.19	135	25	0.0	0						
ROG092326_42	1.79032	1.13	0.17093	1.05	0.49	5.850348	1.05	0.07598	1.11	1094.6	21.97	1041.9	7.39	1017.2	9.83	92.9	0.06	150	9	0.1	0						
ROG092326_43	3.42231	1.19	0.25188	1.06	0.47	3.970145	1.06	0.09856	1.17	1597.1	21.58	1509.5	9.35	1448.2	13.68	90.7	0.70	52	36	0.3	2						
ROG092326_44	3.30858	1.13	0.25109	1.05	0.49	3.982636	1.05	0.09559	1.11	1539.7	20.62	1483.1	8.84	1444.1	13.54	93.8	0.31	89	27	0.2	1						
ROG092326_45	2.12273	1.15	0.19211	1.05	0.49	5.205351	1.05	0.08016	1.11	1200.8	21.84	1156.2	7.90	1132.8	10.87	94.3	0.23	102	23	0.1	-						
ROG092326_46	3.35735	1.19	0.26041	1.06	0.47	3.840098	1.06	0.09553	1.17	1498.5	21.91	1494.5	9.34	1491.9	14.05	99.6	0.41	50	21	0.1	-						
ROG092326_47	3.37937	1.15	0.25518	1.05	0.49	3.918802	1.05	0.09607	1.11	1549.1	20.85	1499.6	8.99	1465.1	13.74	94.6	0.33	87	29	0.0	-						
ROG092326_48	3.7721	1.15	0.27622	1.05	0.49	3.620303	1.05	0.09906	1.12	1606.5	20.8	1586.8	9.26	1572.3	14.65	97.9	0.89	72	65	0.0	-						
ROG092326_49	1.7261	1.21	0.15441	1.06	0.46	6.476264	1.06	0.08109	1.18	1223.7	23.05	1018.3	7.76	925.6	9.09	75.6	0.04	190	7	0.3	1						
ROG092326_50	1.74112	1.15	0.1728	1.05	0.48	5.787037	1.05	0.07309	1.12	1016.5	22.43	1023.9	7.39	1027.5	9.95	101.1	0.16	151	25	0.1	-						
ROG092326_51	5.5231	1.15	0.33392	1.05	0.48	2.994729	1.05	0.11999	1.13	1956	19.94	1904.2	9.93	1857.4	16.96	95.0	0.56	98	55	0.1	0						
ROG092326_52	4.28732	1.16	0.2964	1.05	0.48	3.373819	1.05	0.10493	1.12	1713.1	20.57	1690.9	9.53	1673.4	15.48	97.7	0.76	78	59	0.1	-						
ROG092326_53	3.65069	1.16	0.27428	1.05	0.48	3.645909	1.05	0.09655	1.13	1558.6	21.03	1560.7	9.25	1562.5	14.58	100.3	0.24	100	24	0.0	-						
ROG092326_54	0.77012	67.00	0.12592	10.24	0.02	7.94155	10.24	0.04436	67.61	0.1	1051.1	579.8	295.97	764.6	73.80	764600.0	0.77	38	30	1.6	30						
ROG092326_55	3.45776	1.21	0.2602	1.06	0.46	3.843198	1.06	0.0964	1.18	1555.6	21.96	1517.6	9.51	1490.9	14.08	95.8	0.68	54	36	0.0	-						
ROG092326_56	5.95418	1.19	0.34452	1.06	0.47	2.902589	1.06	0.12537	1.16	2034.1	20.32	1969.2	10.32	1908.4	17.46	93.8	0.57	98	56	0.2	0						
ROG092326_57	3.14526	1.19	0.2481	1.06	0.48	4.030633	1.06	0.09197	1.15	1466.6	21.94	1443.8	9.15	1428.6	13.51	97.4	0.03	128	4	0.1	0						
ROG092326_58	5.60761	1.17	0.35028	1.05	0.48	2.854859	1.05	0.11613	1.15	1897.5	20.4	1917.3	10.12	1935.9	17.62	102.0	0.49	87	43	0.0	-						
ROG092326_59	1.67099	1.17	0.16446	1.05	0.48	6.080506	1.05	0.07371	1.14	1033.4	22.64	997.6	7.46	981.5	9.57	95.0	0.23	192	44	0.1	-						
ROG092326_60	3.6473	1.21	0.26994	1.06	0.47	3.704527	1.06	0.09801	1.17	1586.7	21.81	1559.9	9.60	1540.5	14.49	97.1	0.45	74	33	0.0	-						
ROG092326_61	3.94721	1.01	0.28343	0.98	0.47	3.528208	0.98	0.10106	1.03	1643.6	18.98	1623.4	8.16	1608.6	14.01	97.9	0.51	343	176	0.3	-						
ROG092326_62	12.71105	1.01	0.46709	0.99	0.47	2.140915	0.99	0.19747	1.03	2805.4	16.68	2658.5	9.46	2470.8	20.26	88.1	0.53	260	137	0.0	-						
ROG092326_63	2.97385	1.01	0.23798	0.98	0.47	4.202034	0.98	0.09068	1.03	1439.8	19.44	1401	7.64	1376.2	12.18	95.6	0.16	473	77	0.4	-						
ROG092326_64	3.74627	1.00	0.25896	0.98	0.47	3.8616	0.98	0.10498	1.02	1713.9	18.69	1581.3	8.02	1484.5	13.03	86.6	0.04	1013	40	1.3	0						
ROG092326_65	3.3916	1.01	0.25788	0.98	0.46	3.877773	0.98	0.09544	1.04	1536.7	19.37	1502.5	7.96	1479	13.01	96.2	0.38	512	193	0.7	0						
ROG092326_66	3.22192	1.00	0.24188	0.98	0.47	4.134281	0.98	0.09666	1.02	1560.6	19.12	1462.4	7.78	1396.4	12.34	89.5	0.27	497	133	1.4	1						
ROG092326_67	3.53466	1.01	0.2656	0.98	0.46	3.76506	0.98	0.09657	1.04	1558.9	19.25	1535	7.80	1518.4	13.31	97.4	0.16	344	56	0.3	-						
ROG092326_68	7.56455	0.99	0.37059	0.98	0.47	2.6984	0.98	0.14812	1.01	2324.3	17.26	2180.7	8.90	2032.2	17.12	87.4	0.26	606	157	0.1	-						
ROG092326_69	1.7877	1.04	0.17539	0.99	0.46	5.701579	0.99	0.07396	1.05	1040.4	21.26	1041	6.76	1041.8	9.48	100.1	0.23	319	75	0.0	-						
ROG092326_70	5.1714	1.01	0.3294	0.98	0.46	3.035823	0.98	0.11392	1.04	1862.9	18.53	1847.9	8.60	1835.5	15.73	98.5	0.56	401	225	0.0	-						
ROG092326_71	2.43699	1.00	0.20224	0.98	0.46	4.94462	0.98	0.08744	1.03	1370.2	19.59	1253.6	7.22	1187.3	10.65	86.7	0.14	702	102	0.8	1						
ROG092326_72	3.25072	1.01	0.24471	0.98	0.46	4.08647	0.98	0.09639	1.04	1555.5	19.25	1469.3	7.85	1411.2	12.47	90.7	0.43	482	207	0.1	-						

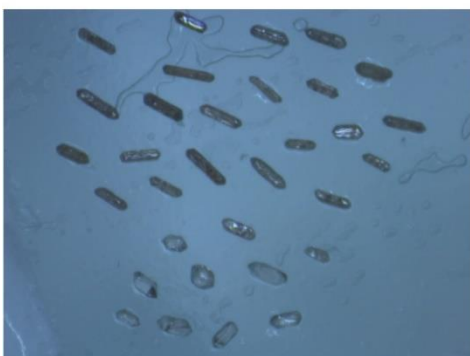
Zircons on tape



IH128058



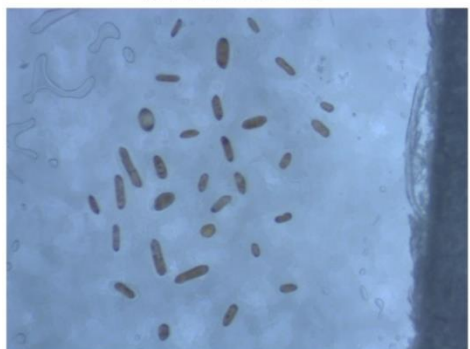
IH128065A



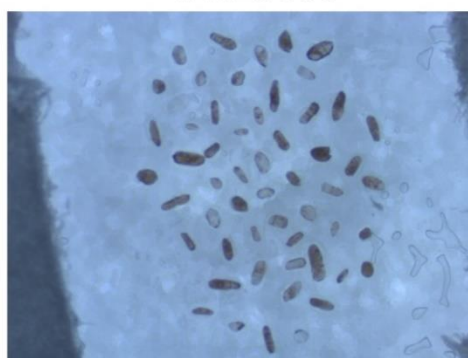
IH128065B



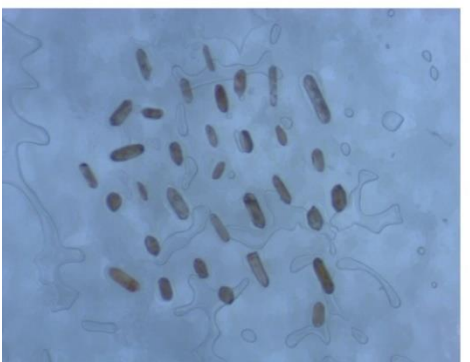
IH128068



IH128070



IH128072



IH128074

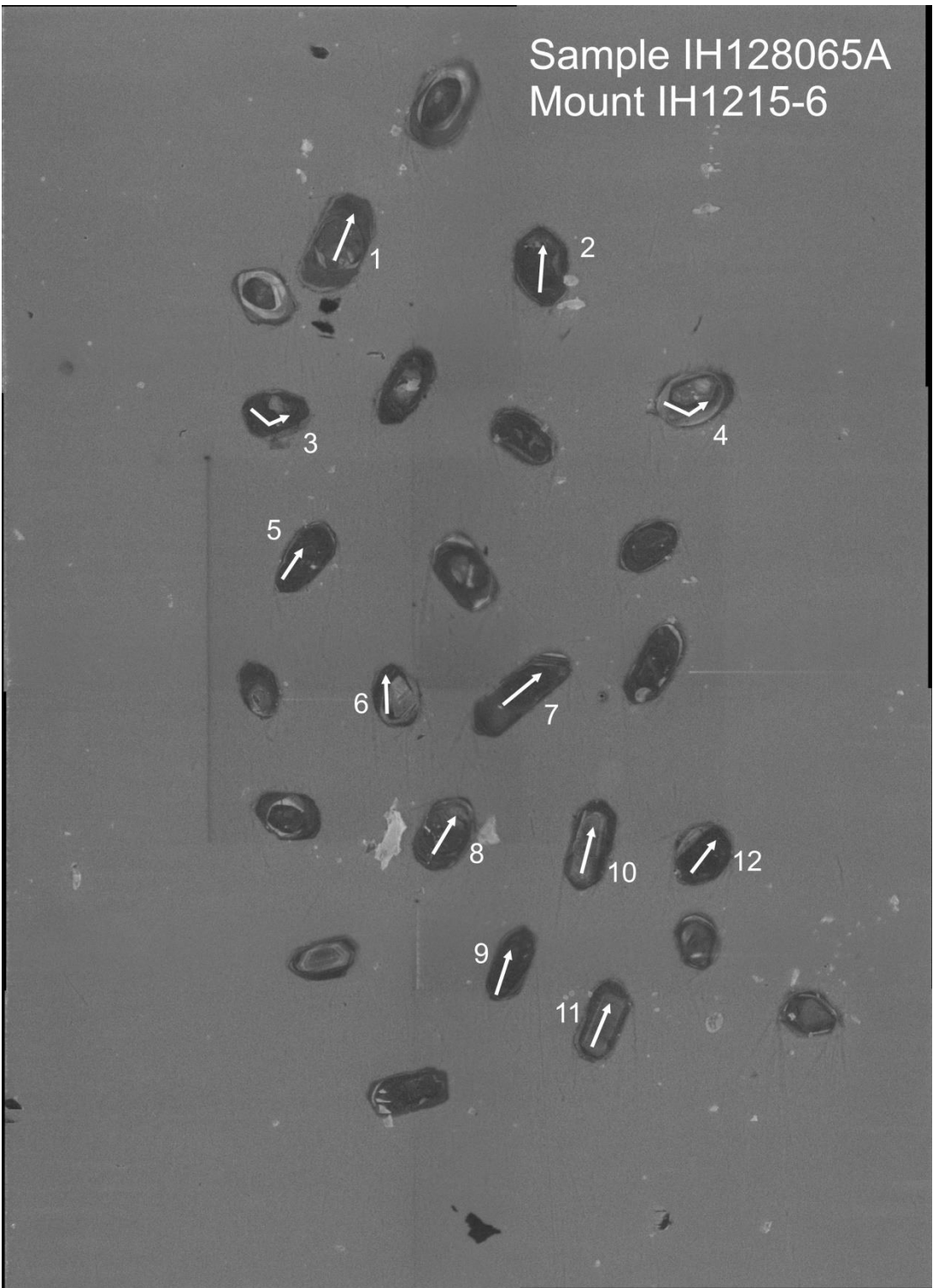
Only sample no. IH128058, 65A & B, 68, 70, 72 and 74 were captured when mounted on tape.




IH128061:The CL image is of poor quality.

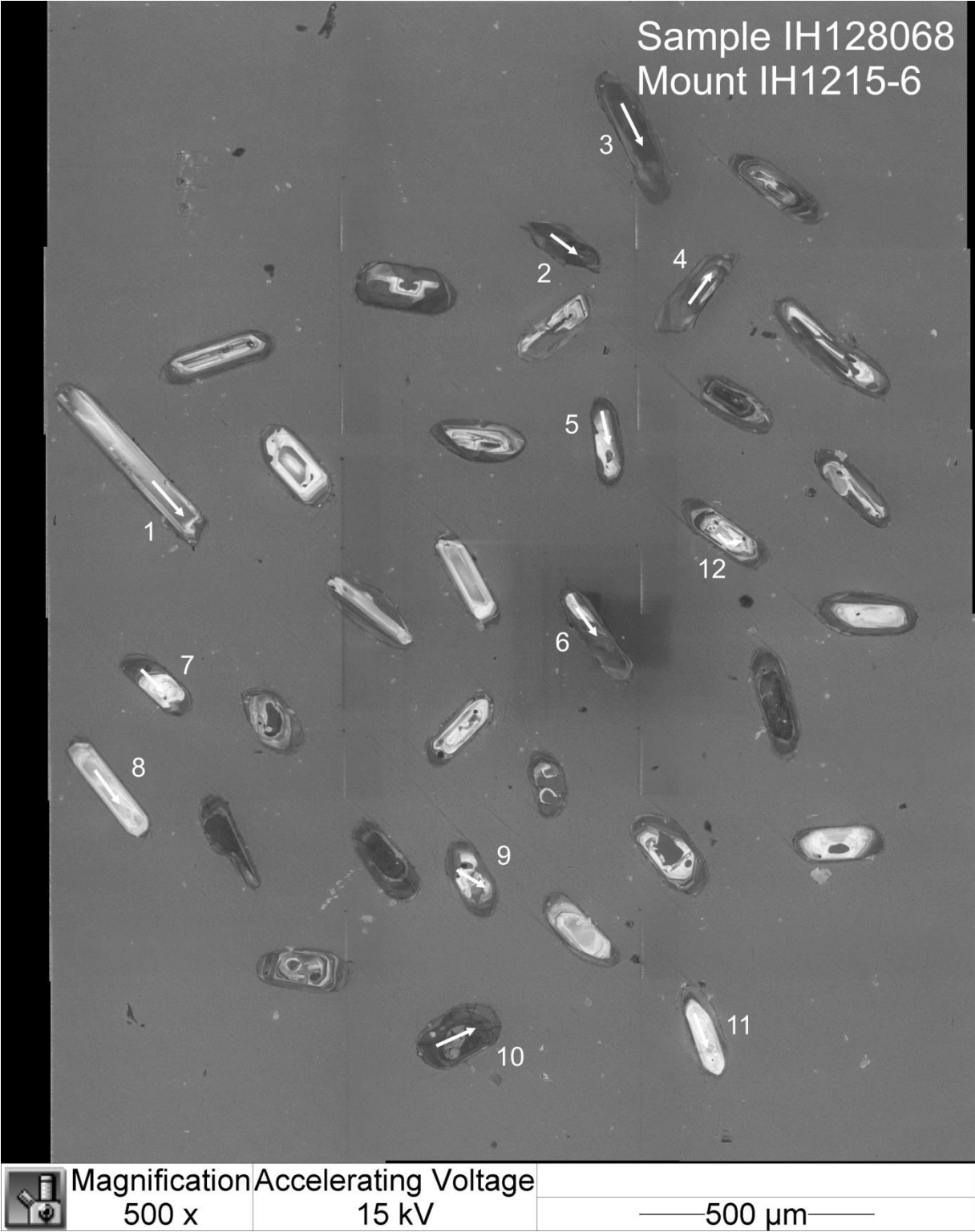


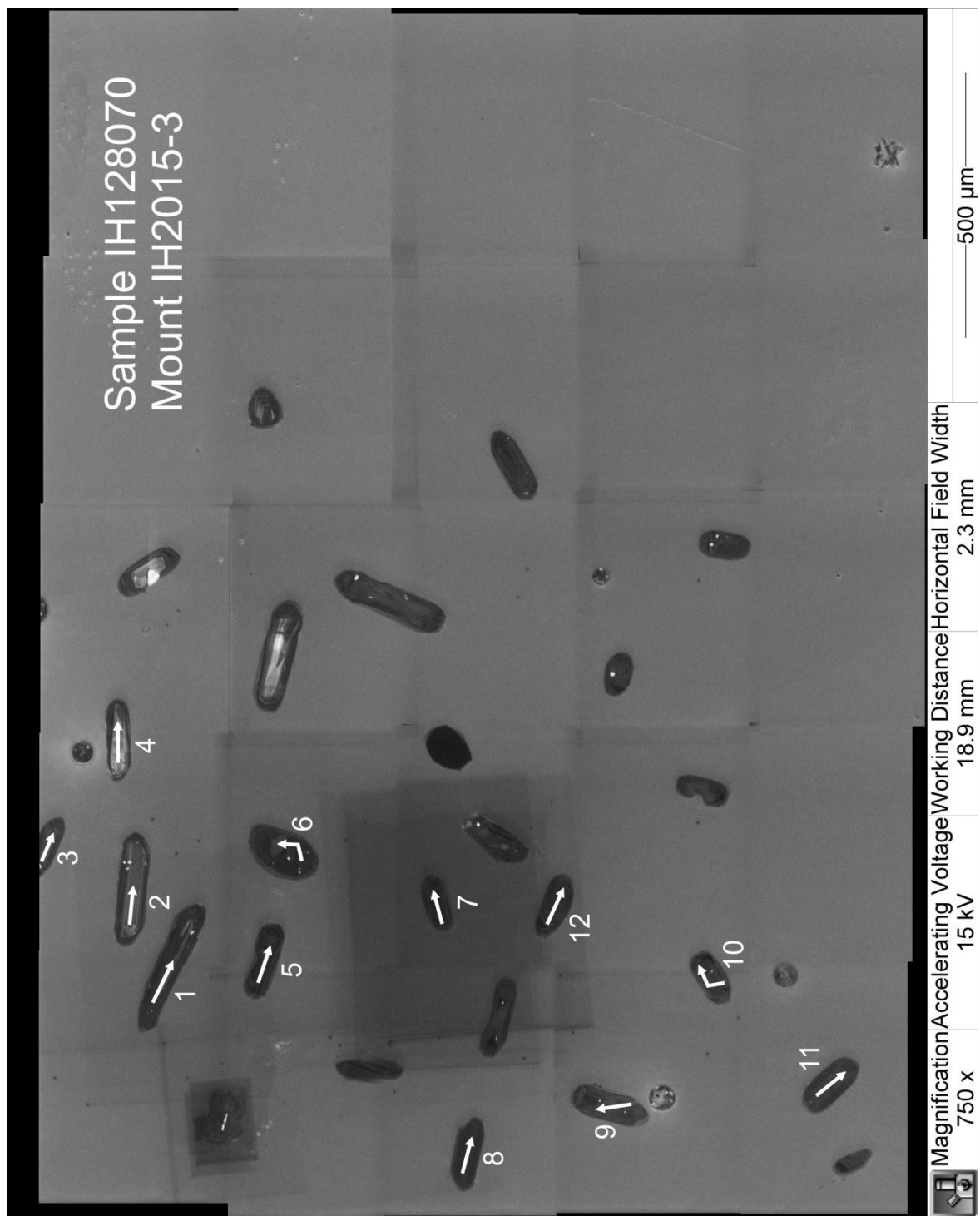
Sample IH128065A
Mount IH1215-6

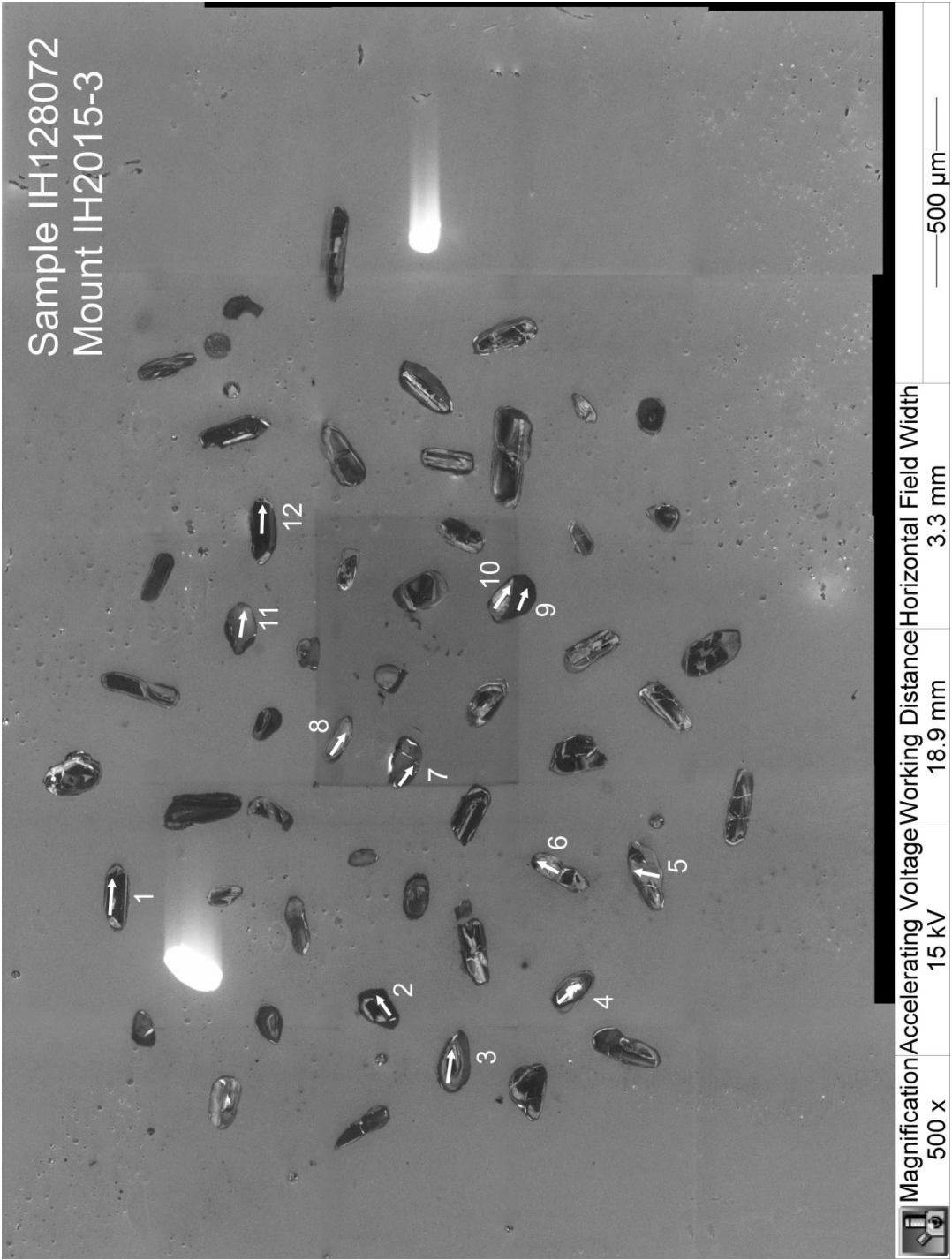


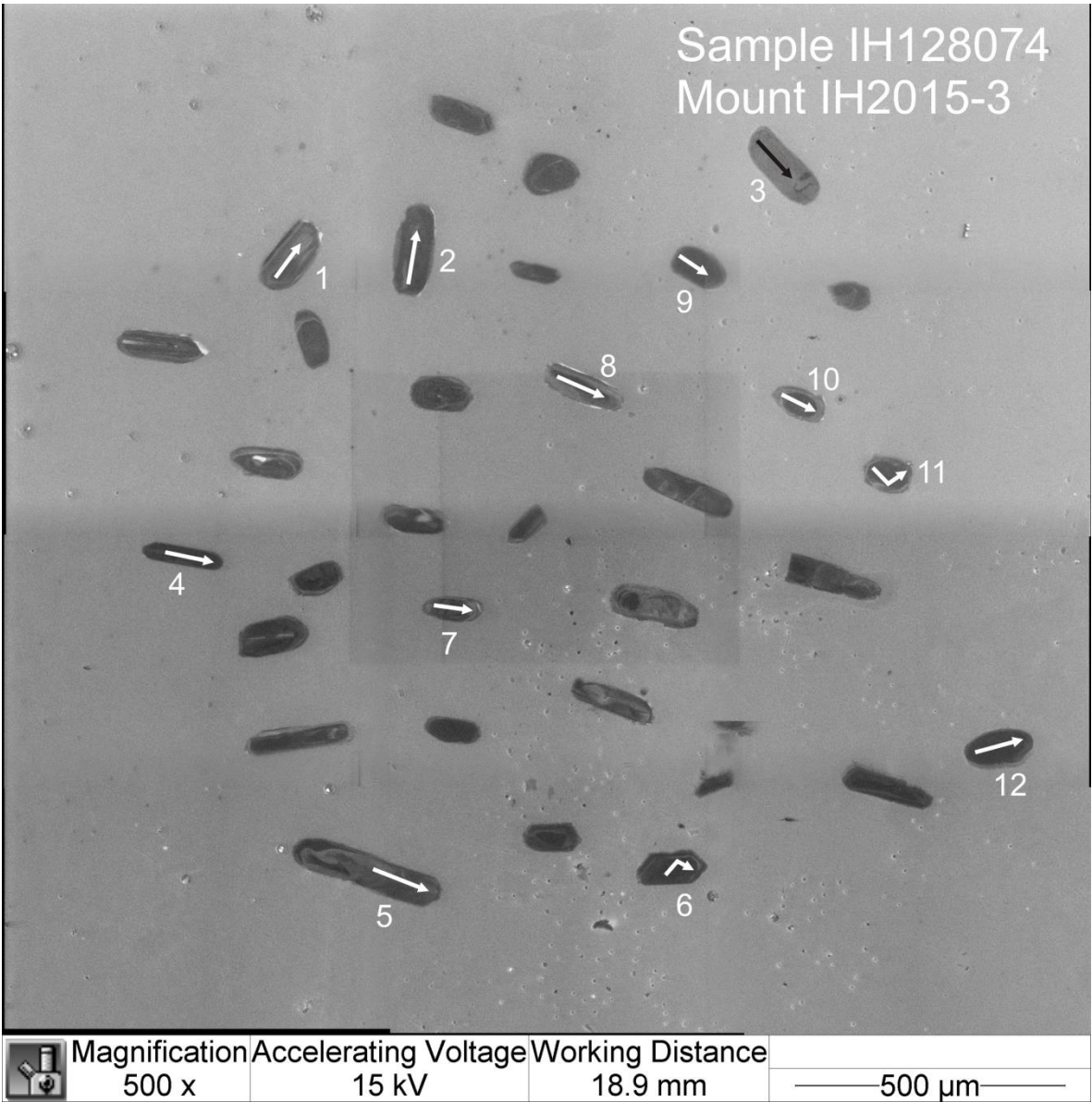
	Magnification	Accelerating Voltage	
	500 x	15 kV	-200 μ m-

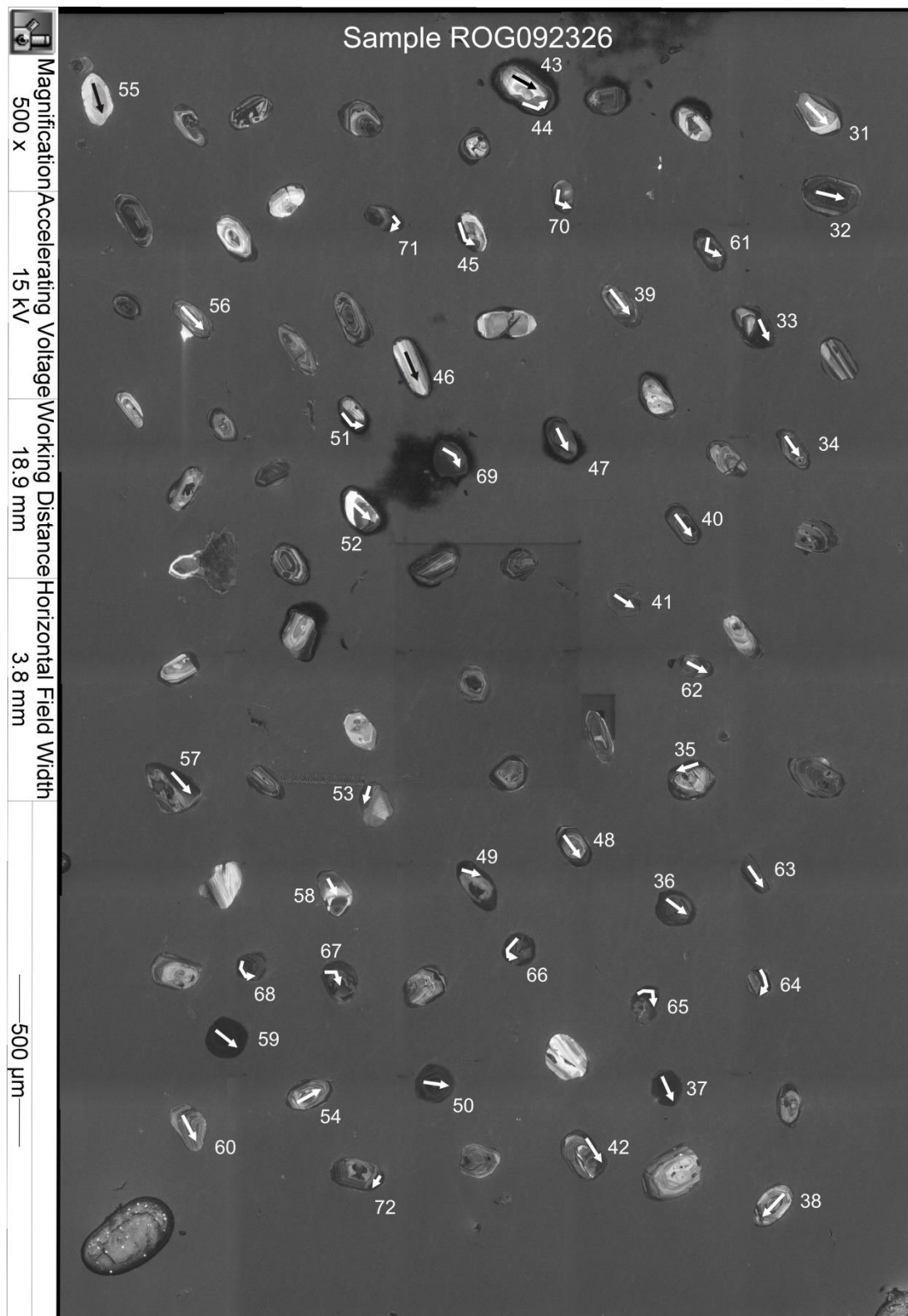


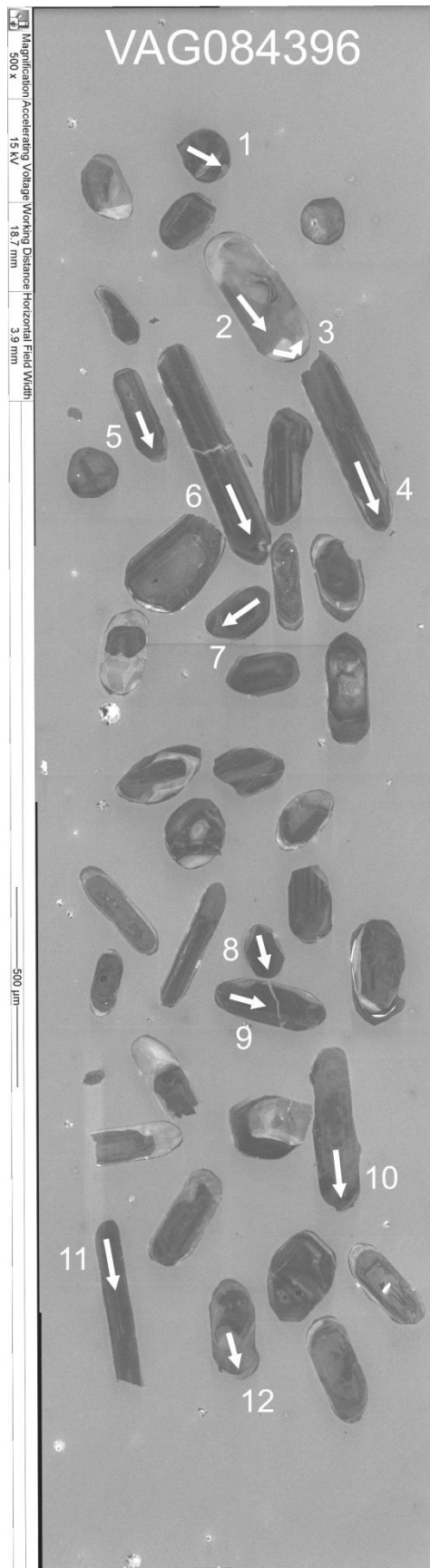






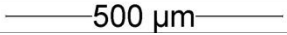




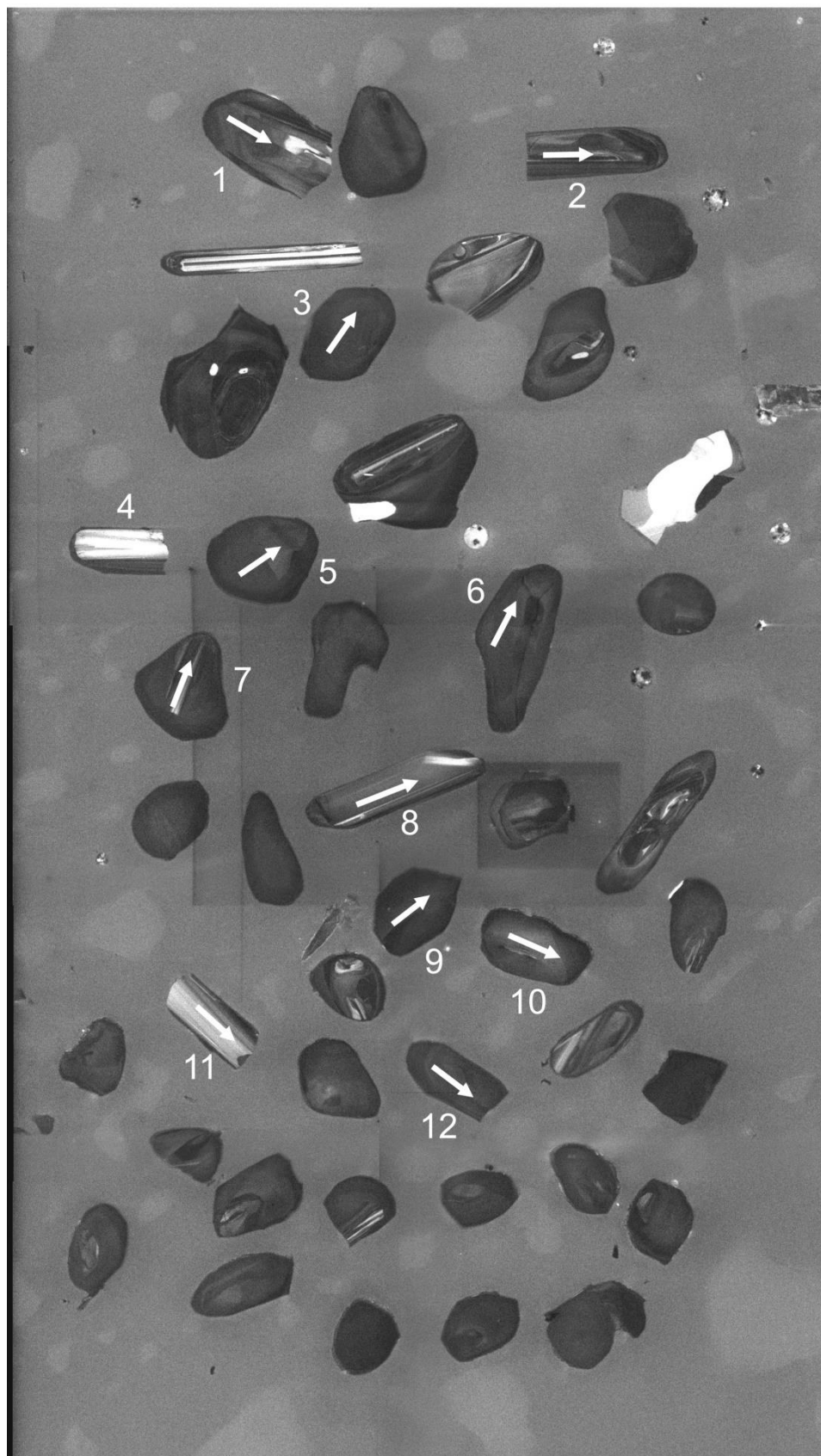


VAG084397



	Magnification	Accelerating Voltage	Working Distance	
	500 x	15 kV	18.7 mm	

VAG084399



	Magnification	Working Distance	
	500 x	18.7 mm	200 μ m

Appendix C – Monazite geochronological data

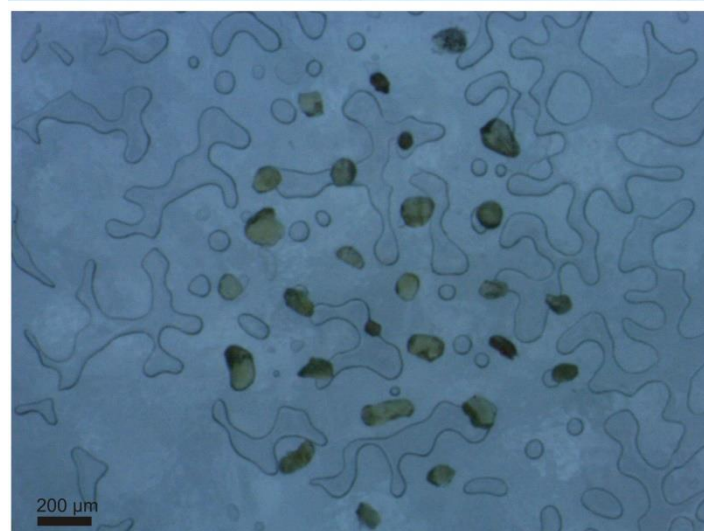
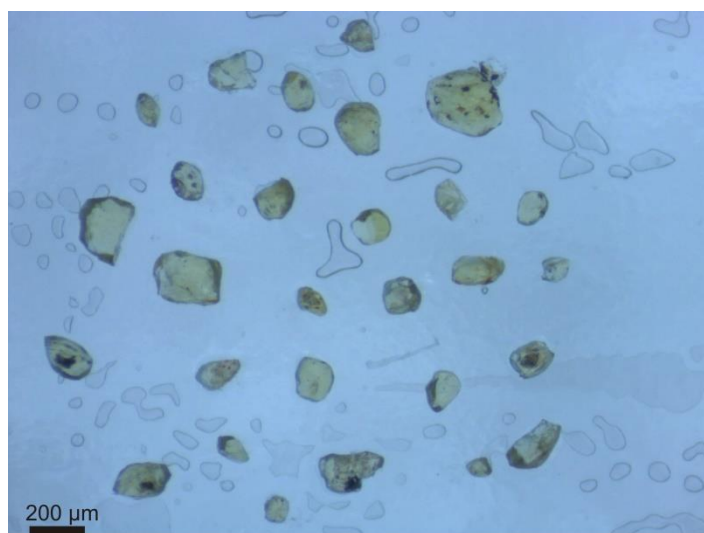
IH128061 (metapelite, Kvås)

▼	Isotope ratios										Age estimates (ma)							
	Concordia output					Terra-Wasserburg output												
	Pb207 U235	Is%	Pb206 U238	Is%	roh	238/206	Is%	207/206	Is%	Pb207 Pb206	Is	Pb207 U235	Is	Pb206 U238	Is	conc		
Analysis_#1	1.5351	0.83	0.16027	0.80	0.22	6.239471	0.80	0.0693	1.02	907.8	20.98	944.5	5.12	958.3	7.16	105.6		
128061_1-02	1.5173	0.83	0.15607	0.80	0.21	6.407381	0.80	0.07034	1.02	938.4	20.87	937.4	5.09	934.9	7.00	99.6		
128061_1-03	1.57386	0.83	0.16221	0.80	0.21	6.164848	0.80	0.0702	1.03	934.3	20.78	960	5.13	969.1	7.23	103.7		
128061_1-04	1.62692	0.83	0.16656	0.80	0.22	6.003842	0.80	0.07068	1.02	948	20.74	980.7	5.20	993.1	7.39	104.8		
128061_1-05	1.6162	0.83	0.16467	0.80	0.20	6.072752	0.80	0.07101	1.03	957.8	20.74	976.5	5.19	982.7	7.32	102.6		
128061_1-06	1.48449	0.83	0.15402	0.81	0.22	6.492663	0.81	0.06974	1.02	920.7	20.84	924.1	5.01	923.4	6.91	100.3		
128061_1-07	1.50158	0.84	0.15713	0.80	0.21	6.364157	0.80	0.06914	1.03	903	21.08	931	5.09	940.8	7.03	104.2		
128061_1-08	1.48649	0.83	0.15518	0.81	0.22	6.444129	0.81	0.06931	1.02	908	21.02	924.9	5.06	929.9	6.95	102.4		
128061_1-09	1.61555	0.83	0.16479	0.80	0.20	6.068329	0.80	0.07093	1.03	955.5	20.79	976.3	5.20	983.3	7.32	102.9		
128061_1-10	1.5674	0.83	0.15956	0.80	0.21	6.267235	0.80	0.07107	1.03	959.6	20.8	957.4	5.14	954.3	7.12	99.4		
128061_1-11	1.4987	0.84	0.15528	0.80	0.21	6.439979	0.80	0.06983	1.03	923.4	21.05	929.9	5.10	930.5	6.96	100.8		
128061_1-12	1.49403	0.83	0.15589	0.80	0.21	6.41478	0.80	0.06934	1.02	908.9	20.9	928	5.02	933.9	6.97	102.8		
128061_1-13	1.43533	0.83	0.14837	0.80	0.20	6.739907	0.80	0.06999	1.03	928.2	20.9	903.8	4.96	891.8	6.68	96.1		
128061_1-14	1.46984	0.83	0.1509	0.80	0.21	6.626905	0.80	0.07048	1.02	942.3	20.81	918.1	4.99	906	6.77	96.1		
128061_1-15	1.56648	0.83	0.15625	0.80	0.21	6.4	0.80	0.07254	1.02	1001.1	20.65	957	5.12	935.9	6.98	93.5		
128061_1-16	1.47207	0.83	0.15174	0.80	0.22	6.59022	0.80	0.07019	1.03	934	20.99	919	5.04	910.7	6.81	97.5		
128061_1-17	1.49983	0.83	0.15612	0.80	0.21	6.405329	0.80	0.06951	1.02	913.9	20.95	930.3	5.04	935.2	6.97	102.3		
128061_1-18	1.49922	0.84	0.15557	0.80	0.21	6.427975	0.80	0.06973	1.03	920.3	21.06	930.1	5.09	932.1	6.95	101.3		
128061_1-19	1.54429	0.84	0.15933	0.80	0.22	6.276282	0.80	0.07013	1.03	932.1	21.03	948.2	5.15	953	7.10	102.2		
128061_1-20	1.49432	0.84	0.15447	0.80	0.22	6.473749	0.80	0.06999	1.03	928.1	21.12	928.1	5.11	926	6.92	99.8		
128061_13-01	1.56572	0.83	0.16072	0.80	0.20	6.222001	0.80	0.07048	1.04	942.5	20.99	956.7	5.16	960.8	7.14	101.9		
128061_13-02	1.57994	0.84	0.15988	0.80	0.20	6.254691	0.80	0.0715	1.03	971.7	20.93	962.3	5.20	956.1	7.11	98.4		
128061_13-03	1.5831	0.83	0.15987	0.80	0.20	6.255082	0.80	0.07165	1.03	975.9	20.85	963.6	5.17	956.1	7.10	98.0		
128061_13-04	1.66266	0.83	0.16757	0.80	0.20	5.967655	0.80	0.07179	1.03	980	20.84	994.4	5.27	998.7	7.40	101.9		
128061_13-05	1.66207	0.84	0.16398	0.80	0.20	6.098305	0.80	0.07333	1.04	1023.2	20.77	994.2	5.29	978.9	7.26	95.7		
128061_13-06	1.44299	0.83	0.15265	0.80	0.21	6.550934	0.80	0.06839	1.02	880.5	21.16	907	4.98	915.8	6.82	104.0		
128061_13-07	1.6668	0.84	0.16397	0.80	0.20	6.098677	0.80	0.07355	1.03	1029.1	20.84	996	5.32	978.8	7.26	95.1		
128061_13-08	1.63941	0.84	0.16268	0.80	0.19	6.147037	0.80	0.07291	1.04	1011.6	20.87	985.5	5.28	971.7	7.21	96.1		
128061_13-09	1.61402	0.84	0.16012	0.80	0.19	6.245316	0.80	0.07293	1.04	1012.1	20.9	975.7	5.26	957.5	7.11	94.6		
128061_13-10	1.3938	0.83	0.14711	0.80	0.19	6.797634	0.80	0.06855	1.04	885.2	21.23	886.3	4.93	884.8	6.60	100.0		
128061_13-11	1.39551	0.83	0.14615	0.80	0.21	6.842285	0.80	0.06909	1.03	901.3	21.16	887	4.93	879.3	6.56	97.6		
128061_13-12	1.56799	0.83	0.15992	0.80	0.21	6.253127	0.80	0.07094	1.03	955.6	21.02	957.6	5.18	956.4	7.10	100.1		
128061_13-13	1.57278	0.84	0.15678	0.80	0.20	6.378365	0.80	0.07258	1.03	1002.3	20.93	959.5	5.20	938.9	6.98	93.7		
128061_13-14	1.44808	0.84	0.1521	0.80	0.18	6.574622	0.80	0.06888	1.05	895.2	21.31	909.1	5.04	912.8	6.79	102.0		
128061_13-15	1.66115	0.84	0.16434	0.80	0.20	6.084946	0.80	0.07313	1.04	1017.7	20.96	993.8	5.33	980.9	7.26	96.4		
128061_13-16	1.45748	0.84	0.15047	0.80	0.19	6.645843	0.80	0.07008	1.04	930.8	21.23	913	5.06	903.6	6.73	97.1		
128061_13-17	1.61775	0.84	0.16163	0.80	0.18	6.18697	0.80	0.07242	1.05	997.8	21.07	977.1	5.30	965.8	7.16	96.8		
128061_13-18	1.60637	0.84	0.16081	0.80	0.20	6.218519	0.80	0.07228	1.04	993.7	21.05	972.7	5.27	961.3	7.13	96.7		
128061_13-19	1.62227	0.85	0.16016	0.80	0.19	6.243756	0.80	0.07329	1.05	1021.9	21.03	978.9	5.31	957.7	7.10	93.7		
128061_13-20	1.60828	0.86	0.16079	0.80	0.18	6.219292	0.80	0.07237	1.06	996.4	21.38	973.4	5.40	961.2	7.14	96.5		
128061_2-01	1.44715	0.86	0.15081	0.81	0.21	6.63086	0.81	0.06942	1.05	911.3	21.37	908.7	5.15	905.5	6.83	99.4		
128061_2-02	1.51063	0.83	0.15781	0.80	0.21	6.336734	0.80	0.06925	1.03	906.2	20.84	934.7	5.05	944.6	7.08	104.2		
128061_2-03	1.52259	0.82	0.15631	0.81	0.22	6.397543	0.81	0.07047	1.02	942.1	20.71	939.5	5.06	936.2	7.01	99.4		
128061_2-04	1.49677	0.83	0.15753	0.81	0.22	6.347997	0.81	0.06874	1.02	890.9	20.93	929.1	5.04	943	7.06	105.8		
128061_2-05	1.5097	0.82	0.15813	0.80	0.22	6.323911	0.80	0.06907	1.01	900.7	20.81	934.3	5.02	946.4	7.08	105.1		
128061_2-06	1.55405	0.83	0.16023	0.81	0.21	6.241029	0.81	0.07016	1.03	933.1	20.81	952.1	5.12	958.1	7.16	102.7		
128061_2-07	1.48149	0.82	0.15405	0.80	0.21	6.491399	0.80	0.06957	1.02	915.7	20.85	922.8	4.99	923.6	6.88	100.9		
128061_2-08	1.46374	0.86	0.15225	0.80	0.21	6.568144	0.80	0.06955	1.05	915.2	21.53	915.5	5.20	913.6	6.84	99.8		
128061_2-09	1.50125	0.82	0.15423	0.80	0.20	6.483823	0.80	0.07042	1.02	940.5	20.78	930.9	5.01	924.7	6.88	98.3		
128061_2-10	1.51766	0.82	0.15663	0.80	0.20	6.384473	0.80	0.07091	1.03	931.2	20.86	937.5	5.05	938	6.98	100.7		
128061_2-11	1.52065	0.83	0.15739	0.80	0.20	6.353644	0.80	0.06989	1.03	925.3	20.96	938.7	5.08	942.3	7.01	101.8		
128061_2-12	1.53954	0.83	0.15936	0.80	0.20	6.2751	0.80	0.06989	1.03	925	21.05	946.3	5.14	953.2	7.08	103.0		
128061_2-13	1.4663	0.82	0.15429	0.80	0.21	6.481301	0.80	0.06875	1.02	891.3	20.9	916.6	4.94	925	6.87	103.8		
128061_2-14	1.54297	0.83	0.16048	0.80	0.19	6.231306	0.80	0.06956	1.04	915.3	21.13	947.7	5.13	959.4	7.09	104.8		
128061_2-15	1.51896	0.83	0.15975	0.79	0.19	6.259781	0.79	0.06879	1.03	892.4	21.13	938.1	5.07	955.4	7.06	107.1		
128061_2-16	1.4294	0.84	0.14945	0.80	0.19	6.691201	0.80	0.06919	1.04	904.5	21.22	901.3	4.99	897.9	6.66	99.3		
128061_2-17	1.46778	0.83	0.15147	0.79	0.20	6.601967	0.79	0.0701	1.03	931.4	20.98	917.2	4.99	909.2	6.73	97.6		

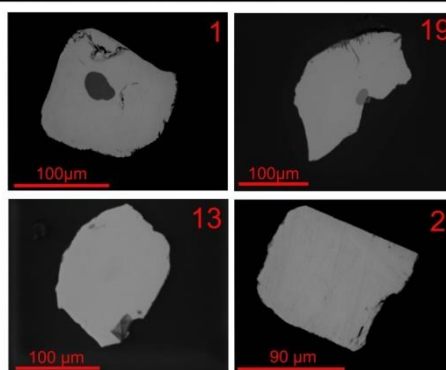
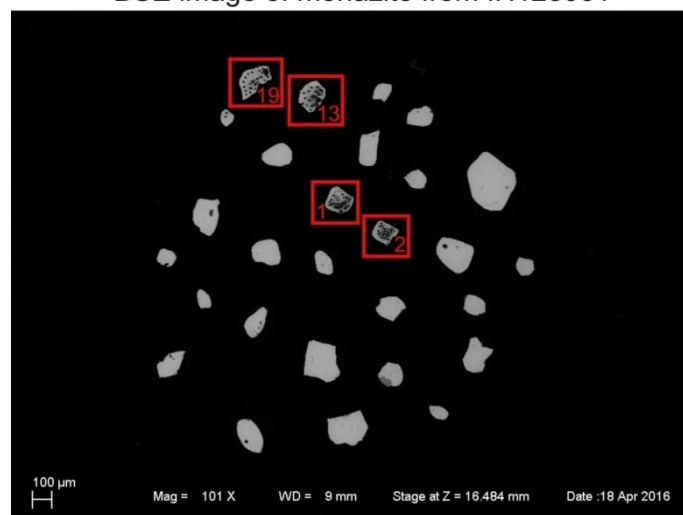
ROG092322 (granitic gneiss, Lysefjorden)

Analysis #	Isotope ratios										Age estimates (ma)						
	Concordia output					Terra-Wasserburg output											
	Pb207 U235	Is%	Pb206 U238	Is%	roh	238/206	Is%	207/206	Is%		Pb207 Pb206	Is	Pb207 U235	Is	Pb206 U238	Is	conc
92322_1-01	1.67119	0.90	0.16489	0.83	0.24	6.064649	0.83	0.0733	1.06		1022.3	21.32	997.6	5.69	983.9	7.58	96.2
92322_1-02	1.68074	0.91	0.16628	0.84	0.24	6.013952	0.84	0.0731	1.08		1016.8	21.63	1001.3	5.81	991.6	7.66	97.5
92322_1-03	1.69069	1.00	0.16783	0.85	0.23	5.95841	0.85	0.07286	1.15		1010	23.17	1005	6.37	1000.1	7.82	99.0
92322_1-04	1.71332	1.01	0.17429	0.84	0.23	5.737564	0.84	0.0711	1.15		960.2	23.51	1013.5	6.47	1035.7	8.10	107.9
92322_1-05	1.67576	1.03	0.16446	0.85	0.22	6.080506	0.85	0.07369	1.18		1033.1	23.3	999.4	6.54	981.5	7.73	95.0
92322_1-06	1.74958	1.00	0.17272	0.85	0.23	5.789717	0.85	0.07326	1.15		1021.3	23.07	1027	6.45	1027.1	8.04	100.6
92322_1-07	1.78928	1.02	0.17408	0.86	0.25	5.744485	0.86	0.07435	1.16		1050.9	23.19	1041.6	6.63	1034.5	8.19	98.4
92322_1-08	1.68706	0.91	0.16932	0.84	0.26	5.905977	0.84	0.07207	1.07		987.8	21.59	1003.7	5.81	1008.4	7.88	102.1
92322_1-09	1.73267	0.96	0.16974	0.85	0.25	5.891363	0.85	0.07383	1.11		1036.9	21.9	1020.7	6.20	1010.7	7.96	97.5
92322_1-10	1.87008	0.95	0.17858	0.85	0.26	5.599731	0.85	0.07575	1.10		1088.4	21.79	1070.6	6.27	1059.2	8.30	97.3
92322_2-01	1.73807	0.95	0.16638	0.85	0.25	6.010338	0.85	0.07556	1.10		1083.5	21.75	1022.7	6.10	992.1	7.82	91.6
92322_2-02	1.7448	1.02	0.17686	0.86	0.24	5.65419	0.86	0.07136	1.16		967.8	23.46	1025.2	6.58	1049.8	8.33	108.5
92322_2-03	1.76827	0.98	0.17424	0.86	0.25	5.73921	0.86	0.07341	1.13		1025.3	22.59	1033.9	6.38	1035.4	8.19	101.0
92322_2-04	1.79652	0.99	0.17668	0.87	0.27	5.65995	0.87	0.07355	1.13		1029.3	22.58	1044.2	6.46	1048.8	8.36	101.9
92322_2-05	1.76376	0.99	0.17202	0.87	0.26	5.813278	0.87	0.07417	1.13		1046.2	22.56	1032.2	6.44	1023.2	8.18	97.8
92322_2-06	1.81511	1.01	0.17803	0.87	0.27	5.617031	0.87	0.07376	1.14		1034.8	22.6	1050.9	6.62	1056.2	8.45	102.1
92322_2-07	1.66862	0.98	0.16948	0.87	0.27	5.900401	0.87	0.07122	1.12		963.8	22.63	996.7	6.25	1009.2	8.08	104.7
92322_2-08	1.84847	1.07	0.18084	0.88	0.25	5.52975	0.88	0.07394	1.20		1039.9	23.99	1062.9	7.07	1071.6	8.66	103.0
92322_2-09	1.747	1.01	0.17037	0.87	0.26	5.869578	0.87	0.07418	1.15		1046.4	22.8	1026.1	6.53	1014.1	8.16	96.9
92322_2-10	1.74388	1.02	0.17175	0.87	0.28	5.822416	0.87	0.07345	1.14		1026.5	23.08	1024.9	6.60	1021.7	8.24	99.5

Monazite on tape (IH128061(top) and ROG092322 (bottom))



BSE image of monazite from IH128061



BSE image of monazite from ROG092322

